(12) INTERNATIONAL APPLICATION PUBLISHED UNDER THE PATENT COOPERATION TREATY (PCT)

(19) World Intellectual Property Organization
International Bureau

(43) International Publication Date
17 April 2025 (17.04.2025)

WIPO | PCT

(10) International Publication Number
WO 2025/080651 A1

(51) International Patent Classification:
B09C 1/06 (2006.01) *B09C 1/08* (2006.01)

(21) International Application Number:
PCT/US2024/050478

(22) International Filing Date:
09 October 2024 (09.10.2024)

(25) Filing Language: English

(26) Publication Language: English

(30) Priority Data:
63/589,489 11 October 2023 (11.10.2023) US

(71) Applicant: **WILLIAM MARSH RICE UNIVERSITY** [US/US]; 6100 Main Street, Houston, Texas 77005 (US).

(72) Inventors: **TOUR, James M.**; 6100 Main Street, Houston, Texas 77005 (US). **CHENG, Yi**; 6100 Main Street, Houston, Texas 77005 (US). **DENG, Bing**; 6100 Main Street, Houston, Texas 77005 (US). **EDDY, Lucas John**; 6100 Main Street, Houston, Texas 77005 (US).

(74) Agent: **GARSSON, Ross Spencer**; DICKINSON WRIGHT PLLC, International Square, 1825 Eye St. N.W., Suite 900, Washington, District of Columbia 20006 (US).

(81) Designated States *(unless otherwise indicated, for every kind of national protection available)*: AE, AG, AL, AM, AO, AT, AU, AZ, BA, BB, BG, BH, BN, BR, BW, BY, BZ, CA, CH, CL, CN, CO, CR, CU, CV, CZ, DE, DJ, DK, DM, DO, DZ, EC, EE, EG, ES, FI, GB, GD, GE, GH, GM, GT, HN, HR, HU, ID, IL, IN, IQ, IR, IS, IT, JM, JO, JP, KE, KG, KH, KN, KP, KR, KW, KZ, LA, LC, LK, LR, LS, LU, LY, MA, MD, MG, MK, MN, MU, MW, MX, MY, MZ, NA, NG, NI, NO, NZ, OM, PA, PE, PG, PH, PL, PT, QA, RO, RS, RU, RW, SA, SC, SD, SE, SG, SK, SL, ST, SV, SY, TH, TJ, TM, TN, TR, TT, TZ, UA, UG, US, UZ, VC, VN, WS, ZA, ZM, ZW.

(84) Designated States *(unless otherwise indicated, for every kind of regional protection available)*: ARIPO (BW, CV, GH, GM, KE, LR, LS, MW, MZ, NA, RW, SC, SD, SL, ST, SZ, TZ, UG, ZM, ZW), Eurasian (AM, AZ, BY, KG, KZ, RU, TJ, TM), European (AL, AT, BE, BG, CH, CY, CZ, DE, DK, EE, ES, FI, FR, GB, GR, HR, HU, IE, IS, IT, LT, LU, LV, MC, ME, MK, MT, NL, NO, PL, PT, RO, RS, SE, SI, SK, SM, TR), OAPI (BF, BJ, CF, CG, CI, CM, GA, GN, GQ, GW, KM, ML, MR, NE, SN, TD, TG).

Declarations under Rule 4.17:
— *as to applicant's entitlement to apply for and be granted a patent (Rule 4.17(ii))*
— *as to the applicant's entitlement to claim the priority of the earlier application (Rule 4.17(iii))*

Published:
— *with international search report (Art. 21(3))*
— *before the expiration of the time limit for amending the claims and to be republished in the event of receipt of amendments (Rule 48.2(h))*

(54) **Title:** METHODS FOR REMEDIATION OF CONTAMINATED SOIL BY RAPID ELECTROTHERMAL MINERALIZATION

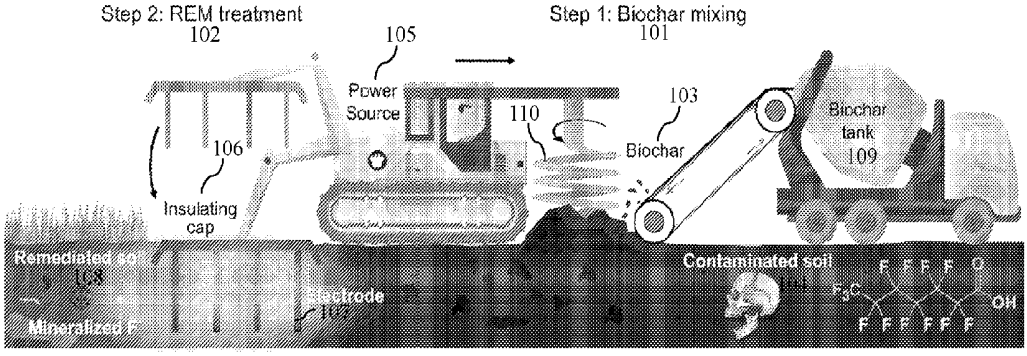

FIG. 1A

(57) **Abstract:** Methods for remediating soil having persistent and bioaccumulative pollutants, and. more particularly, methods for remediating soil having per- and polyfluorinated alkyl substances (PFAS) and other halogen-containing contaminates by rapid electrothermal mineralization.

WO 2025/080651 A1

METHODS FOR REMEDIATION OF CONTAMINATED SOIL BY RAPID ELECTROTHERMAL MINERALIZATION

CROSS-REFERENCED TO RELATED PATENT APPLICATIONS

[0001] The application claims priority to U.S. Patent Appl. Serial No. 63/589,489, to James Mitchell Tour, *et al.*, entitled "Methods For Remediation Of PFAS-Contaminated Soil By Rapid Electrothermal Mineralization," October 11, 2023, which patent application is commonly owned by the owner of the present invention and is incorporated herein in its entirety.

[0002] The application is related to PCT Patent Appl. Serial No. PCT/US24/033209, entitled "Methods Of Flash Joule Heating Per- And Polyfluorinated Alkyl Substances And Compositions Thereof, filed June 10, 2024, to James M. Tour, *et al* ("*Tour '209 PCT Application*"), claiming priority to U.S. Patent Appl. Serial No. 63/507,045, entitled "Methods Of Flash Joule Heating Per- And Polyfluorinated Alkyl Substances And Compositions Thereof," filed June 8, 2023, to James M. Tour, *et al*, all of which patent applications are commonly owned by the owner of the present invention. The *Tour '209 PCT Application* is incorporated herein in its entirety.

[0003] This application is also related to U.S. Patent Appl. Serial No. 18/263,831, entitled "Ultrafast Flash Joule Heating Synthesis Methods And Systems For Performing Same," filed August 1, 2023, to James M. Tour *et al.* ("*Tour '831 Application*"), which is the U.S. § 371 nationalization of PCT Patent Appl. Serial No. PCT/US22/14923, entitled "Ultrafast Flash Joule Heating Synthesis Methods And Systems For Performing Same," filed February 2, 2022, to James M. Tour *et al.*, claiming priority to U.S. Patent Appl. Serial No. 63/144,862, filed February 2, 2021, all of which patent applications are commonly owned by the owner of the present invention. The *Tour '831 Application* is incorporated herein in its entirety.

[0004] The application is also related to U.S. Patent Appl. Serial No. 18/246,460, entitled "Ultrafast Flash Joule Heating Synthesis Methods And Systems For Performing Same," filed

March 23, 2023, to James M. Tour, *et al.* ("*Tour '460 Application*"), which is the U.S. § 371 nationalization of PCT Patent Appl. Serial No. PCT/US21/52070, entitled "Ultrafast Flash Joule Heating Synthesis Methods And Systems For Performing Same," filed September 24, 2021, to James M. Tour *et al.,* claiming priority to U.S. Patent Appl. Serial No. 63/082,592, filed September 24, 2020 and U.S. Patent Appl. Seral No. 63/144,862, filed February 2, 2021. A copy of the *Tour '460 Application* is incorporated herein in its entirety.

[0005]

TECHNICAL FIELD

[0006] The present invention relates to methods for remediating soil having persistent and bioaccumulative pollutants, and, more particularly, methods for remediating soil having per- and polyfluorinated alkyl substances (PFAS) and other halogen-containing contaminates by rapid electrothermal mineralization.

GOVERNMENT INTEREST

[0007] This invention was made with government support under Grant No. FA9550-22-1-0526, awarded by the United States Air Force Office of Scientific Research, and Grant Nos. W912HZ-21-2-0050 and W912HZ-24-2-0027, awarded by the United States Engineer Research and Development Center for the United States Army Corp of Engineers. The government has certain rights in the invention.

BACKGROUND

[0008] Per- and polyfluoroalkyl substances (PFAS) are persistent and bioaccumulative pollutants that can easily accumulate in soil, posing a threat to environment and human health. PFAS include more than 10,000 man-made substances that all have tight chemical bonds between their carbon and fluorine atoms. PFAS are often referred to as "forever chemicals," in that they are recalcitrant in the environment and in biological organisms, including humans. They have entered the human food chain through freshwater fish and food grown on

contaminated fields. Current PFAS degradation processes suffer from low efficiency, high energy and water consumption, or lack of generality.

[0009] PFAS are a diverse class of anthropogenic chemicals that are extensively used in plastics, textiles, food wrapping materials, and fire-fighting foam. [*Evich 2022*; *Glüge 2020*]. PFAS can easily accumulate in soil through waste disposal and animal migration and has been proven to be bioaccumulative and toxic to humans and wildlife. [*Leeson 2021*; *Salvatore 2022*; *Schaefer 2022*; *Judy 2022*]. Due to the high bond energy of C-F (~485 kJ mol^{-1}) [*Huang 2016*] and resulting long half-lives (>100 years in soils) [*Washington 2015*], the efficient elimination of PFAS is difficult to realize by natural decomposition or microbiological treatment. [*Washington 2015*; *Maimaiti 2018*; *Duan 2020*].

[0010] Many efforts have been devoted to the remediation of PFAS-contaminated soil in the past decade, mainly including stabilization [*Hale 2017*; *Das 2013*; *Kupryianchyk 2016*], chemical oxidation [*Vecitis 2009*; *Dombrowski 2018*; *Mahinroosta 2020*] and thermal treatment [*Javaherian 2016*; *Sörengård 2020*; *Xiao 2020*]. The stabilization method involves mixing sorbents, such as activated carbon or clay, with the contaminated soil to sorb PFAS and reduces PFAS mobility and bioavailability [*Hale 2017*; *Das 2013*; *Kupryianchyk 2016*]. However, this method does not degrade PFAS in soil and sorbed PFAS could still pose long-term environmental damage. Chemical treatment uses strong oxidants to oxidize PFAS. [*Vecitis 2009*; *Dombrowski 2018*; *Mahinroosta 2020*]. The residual oxidants need to be washed out with a large amount of water to avoid its damage to the soil, where the wastewater could lead to secondary pollution to the environment. Traditional thermal treatment requires furnace heating for PFAS desorption and degradation, which often lasts for hours at 400-1100 °C. [*Javaherian 2016*; *Sörengård 2020*; *Xiao 2020*; *Vargette 2023*]. Some toxic short-chain fluorocarbon compounds, such as CF_4, C_2F_6, and C_2F_4, could be generated and emitted to the environment during this process. This is due to inadequate decomposition of C-

F bonds, which will cause secondary pollution [*Vargette 2023*; *Alinezhad 2022*] and the extended heating also degrades soil properties [*Zhao 2019*]. Therefore, developing an efficient, economical and general method for remediation of PFAS-contaminated soil is highly desirable, but remains challenging yet.

[0011] Converting PFAS into non-toxic metal fluoride with the aid of alkali or alkaline earth metal ions like calcium ions (Ca^{2+}) under thermal treatment, termed as mineralization, is promising for PFAS degradation. [*Wang 2011*; *Wang 2013*; *Wang 2015*; *Fournie 2023*]. However, traditional furnace heating often lasts hours, consuming large amounts of energy and the PFAS mineralization ratios are typically < 80%. Moreover, additional calcium compounds are always required for PFAS mineralization, leading to high material consumption. [*Wang 2011*; *Wang 2013*; *Wang 2015*; *Fournie 2023*].

[0012] Hence, developing an efficient, economical and general thermal process for remediation of PFAS-contaminated soil is highly desirable, especially if the soil can remain in place and need not be excavated or transported. Accordingly, a need remains for PFAS remediation processes that do not suffer from low efficiency, high energy and water consumption, and lack of generality.

SUMMARY OF THE INVENTION

[0013] The present invention relates to methods for remediating soil having persistent and bioaccumulative pollutants, and. more particularly, methods for remediating soil having per- and polyfluorinated alkyl substances (PFAS) and other halogen-containing contaminates by rapid electrothermal mineralization.

[0014] The present invention relates to a rapid electrothermal mineralization (REM) process to remediate PFAS-contaminated soil. With environmentally compatible biochar as the conductive additive, the soil temperature increases to >1000 °C within seconds by current pulse input, converting PFAS to calcium fluoride with inherent calcium compounds in soil This

process is applicable for remediating various PFAS contaminants in soil, with high removal efficiencies (>99%) and mineralization ratios (>90%). While retaining soil particle size, composition, water infiltration rate, and cation exchange, REM facilitates an increase of exchangeable nutrient supply and arthropod survival in soil, rendering it superior to the time-consuming calcination approach that severely degrades soil properties. REM is scaled up to remediate soil at two kilograms per batch and promising for large-scale, on-site soil remediation. Life-cycle assessment and techno-economic analysis demonstrate REM as an environmentally friendly and economic process, with a significant reduction of energy consumption, greenhouse gas emission, water consumption, and operation cost, when compared to existing soil remediation practices.

[0015] The present invention also relates to a REM process to remediate contaminated soil by mineralizing other halogen-containing contaminates, including tetrachloroethylene (PCE), trichloroethylene (TCE), polychlorinated biphenyls (PCB), tribromophenol (TBP), brominated flame retardants (BFR), and halogen-containing antibiotics, like ciprofloxacin, chloramphenicol, and iodoquinol.

[0016] In general, in one embodiment, the invention features a method that includes mixing a PFAS-contaminated soil with a conductive additive to form a PFAS-contaminated soil mixture. The PFAS-contaminated soil is soil that includes a pollutant selected from the group consisting of per- and polyfluorinated alkyl substances (PFAS). The method further includes performing a rapid electrothermal mineralization (REM) process utilizing the PFAS-contaminated soil mixture to remediate the PFAS-contaminated soil.

[0017] Implementations of the invention can include one or more of the following features:

[0018] The PFAS can be selected from the group consisting of perfluorooctane acid (PFOA), perfluorooctane sulfonate (PFOS), perfluorohexane sulfonate (PFH_xS), perfluorobutane sulfonate (PFBS), polytetrafluoroethylene (PTFE), and combinations thereof.

[0019] The PFAS can include exactly one per- and polyfluorinated alkyl substance selected from the group of the pollutant.

[0020] The PFAS can include two or more per- and polyfluorinated alkyl substances selected from the group of the pollutant.

[0021] The step of performing the REM process can include subjecting the PFAS-contaminated soil mixture to a flash Joule heating process.

[0022] The conductive additive can be selected from the group consisting of graphene, flash graphene, turbostratic graphene, anthracite coal, coconut shell-derived carbon, higher temperature-treated biochar, biochar, activated charcoal, calcined petroleum coke, metallurgical coke, coke, shungite, carbon nanomaterials, carbon nanotubes, asphaltenes, acetylene black, carbon black, ash, carbon fiber, and mixtures thereof.

[0023] The REM process can remediate the PFAS-contaminated soil by removing more than 90 wt% of the PFAS from the PFAS-contaminated soil.

[0024] The REM process can remediate the PFAS-contaminated soil by removing more than 99 wt% of the PFAS from the PFAS-contaminated soil.

[0025] The REM process can remediate the PFAS-contaminated soil by removing more than 99.9 wt% of the PFAS from the PFAS-contaminated soil.

[0026] 'The REM process can remediate the PFAS-contaminated soil by removing more than 99.99 wt% of the PFAS from the PFAS-contaminated soil.

[0027] The REM process can provide a fluorine mineralization ratio of more than 90% for the remediated PFAS-contaminated soil.

[0028] The method further can further include removing the PFAS-contaminated soil from the ground before the step of performing the REM process.

[0029] The step of removing the PFAS-contaminated soil from the ground can be performed before the step of mixing the PFAS-contaminated soil with the conductive additive.

[0030] The step of removing the PFAS-contaminated soil from the ground can be performed during the step of mixing the PFAS-contaminated soil with the conductive additive.

[0031] The step of removing the PFAS-contaminated soil from the ground can be performed after the step of mixing the PFAS-contaminated soil with the conductive additive.

[0032] The step of performing the REM process can be performed at an on-site location. The on-site location is a location at or near where the PFAS-contaminated soil was removed from the ground.

[0033] The REM process can be performed utilizing a REM reactor located at the on-site location.

[0034] The REM reactor can be a mobile REM reactor that can be transported to the on-site location.

[0035] The method can further include the step of transporting the REM reactor to the on-site location.

[0036] The step of performing the REM process can be performed at an off-site location. The off-site location is a location that is not at or near where the PFAS-contaminated soil was removed from the ground.

[0037] The method can further include transporting the PFAS-contaminated soil to the off-site location.

[0038] The REM process can be performed utilizing a REM reactor located at the off-site location.

[0039] The PFAS-contaminated soil can be ground soil located on the ground (PFAS-contaminated ground soil). The step of mixing the PFAS-contaminated soil with the conductive additive can include mixing the conductive additive to the PFAS-contaminated ground soil on-site in the ground. The step of performing the REM process can include utilizing electrodes inserted in the ground.

[0040] There can be a cover positioned over the PFAS-contaminated soil mixture when the REM process is performed.

[0041] The cover can be positioned over the PFAS-contaminated soil mixture after the step of mixing the PFAS-contaminated soil with the conductive additive.

[0042] The cover can form a seal about the PFAS-contaminated soil mixture.

[0043] The pressure about the PFAS-contaminated soil mixture can be at a low vacuum pressure during the REM process.

[0044] The method can further include inserting one or more evacuation tubes into the ground soil. The evacuation tubes can be utilized to assist in capturing one or more volatile components formed during the REM process.

[0045] The step of performing the REM process can include utilizing two or more electrode arrays. The two or more electrode arrays can include the electrodes inserted in the ground.

[0046] During the step of performing the REM process, the two or more electrode arrays can be utilized by independently discharging each of the two or more electrode arrays.

[0047] The independent discharging of each of the two or more electrode arrays can uniformly heat the soil around the two or more electrodes.

[0048] The two or more electrode arrays can be independently discharged in a predetermined pattern.

[0049] The conductive additive can be injected between the electrodes inserted in the ground.

[0050] The conductive additive can be injected in a predetermined pattern between the electrodes inserted in the ground.

[0051] The conductive additive can be injected as granules or as a slurry.

[0052] The conductive additive can be biochar.

[0053] The REM process can be performed under a vacuum.

[0054] The method can further include that, after the REM process, separating at least some of

the conductive carbon additive from the remediated PFAS-contaminated soil.

[0055] The step of separating can be based upon grain size of the conductive carbon additive and particle size of the remediated PFAS-contaminated soil.

[0056] The step of separating can include sieving to separate the at least some of the conductive carbon additive from the remediated PFAS-contaminated soil.

[0057] The step of separating can be based upon difference in densities between the conductive carbon additive and the remediated PFAS-contaminated soil.

[0058] The step of separating can include utilizing water to separating the at least some of the conductive carbon additive from the remediated PFAS-contaminated soil.

[0059] The at least some of the conductive carbon additive can float at or near the top surface of the water utilized for separating.

[0060] The step of separating can include decanting and/or skimming the at least some of the conductive carbon additive from the remediated PFAS-contaminated soil.

[0061] At least some of the PFAS can be mineralized into a fluoride salt.

[0062] The fluoride salt can be selected from the group consisting of calcium fluoride (CaF_2), magnesium fluoride (MgF_2), sodium fluoride (NaF), and potassium fluoride (KF).

[0063] Graphene can be formed during the step of performing the REM process.

[0064] The method can further include separating the graphene from the remediated PFAS-contaminated soil.

[0065] The method can further include collecting the graphene after the step of separating.

[0066] In general, in another embodiment, the invention features a method that includes mixing a contaminated soil with a conductive additive to form a contaminated soil mixture. The contaminated soil is soil that includes a pollutant selected from the group consisting of halogen-containing contaminates. The method further includes performing a rapid electrothermal mineralization (REM) process utilizing the contaminated soil mixture to remediate the

contaminated soil.

[0067] Implementations of the invention can include one or more of the following features:

[0068] The pollutant can be selected from the group consisting of tetrachloroethylene (PCE), trichloroethylene (TCE), polychlorinated biphenyls (PCB), brominated flame retardants (BFR), and halogen-containing antibiotics.

[0069] The pollutant can include halogen-containing antibiotics. The halogen-containing antibiotics can be selected from the group consisting of ciprofloxacin, chloramphenicol, and iodoquinol.

[0070] The pollutant can be tribromophenol (TBP).

[0071] In general, in another embodiment, the invention features an apparatus that performs any of the above-described methods.

[0072] Implementations of the invention can include one or more of the following features:

[0073] The apparatus can include a REM reactor.

[0074] In general, in another embodiment, the invention features graphene made any of the above-described methods.

BRIEF DESCRIPTION OF THE DRAWINGS

[0075] **FIGS. 1A-1G** show schematics rapid electrothermal mineralization (REM) process for the remediation of PFOA-contaminated soil. **FIG. 1A** is a conceptional schematic of REM process for soil remediation. **FIG. 1B** are pictures of the sample before (top) and during (bottom) the REM reaction. A spring coiled around the quartz tube is used to increase the mechanical integrity of the tube. **FIG. 1C** is a current curve with an input voltage of 100 V and a duration time of 1 s. **FIG. 1D** is a real-time temperature curve at an electric input of 100 V for 1 s recorded by an infrared thermometer. The temperature detection range of the thermometer is 200 to 1500 °C. **FIG. 1E** shows concentrations of organic fluorine and mineralized fluorine ion in PFOA-contaminated soil varied with input voltages. **FIG. 1F** shows

residual PFOA concentrations in soil after repetitive electric pulses, with voltage of 100 V and duration of 1 s each time. The error bars in **FIGS. 1E-1F** denote standard deviations, where $N = 3$. **FIG. 1G** is ^{19}F NMR spectra of the PFOA-contaminated soil extractant before (top) and after (bottom) REM. Inset of **FIG. 1G** shows the molecular structure of PFOA.

[0076] FIGS. 2A-2H show generality of REM process for various PFAS. **FIGS. 2A-2C** show concentrations of organic fluorine and mineralized fluorine ion varied with input voltages for, respectively, (a) PFOS-contaminated soil, (b) PFH_xS-contaminated soil and (c) PFBS-contaminated soil. **FIGS. 2D-2F** show ^{19}F NMR spectra of, respectively, the (d) PFOS, (e) PFH_xS and (f) PFBS -contaminated soil extractant before (top) and after (bottom) REM process. Inset in **FIGS. 2D-2F** are the molecular structure of PFOS, PFH_xS and PFBS, respectively. (The dots denote the F peaks and corresponding F-attached C atoms. **FIG. 2G** shows removal efficiencies of different kinds of PFASs. **FIG. 2H** shows mineralization ratios of different kinds of PFASs. The error bars in **FIGS 2A-2C** and **2G-2H** denote standard deviations, where $N = 3$.

[0077] FIGS. 3A-3H show mechanism of PFAS mineralization during the REM process. **FIG. 3A** shows XRD patterns of PFOA/biochar before (red) and after (blue) REM. **FIG. 3B** shows C 1*s* XPS fine spectra of PFOA/biochar before (top) and after (bottom) REM. **FIG. 3C** shows F 1*s* XPS fine spectra of PFOA/biochar before (top) and after (bottom) REM. **FIG. 3D** shows IR spectra of PFOA/biochar before (red) and after (blue) REM. **FIG. 3E** shows the Gibbs free energy change (ΔG) of each PFOA degradation step with (solid line) and without (dash line) Ca^{2+} varied with temperature. The dash line denotes $\Delta G = 0$ kJ mol^{-1}. **FIG. 3F** shows simulated variation of C-F bond ratio during REM process with calcium and without calcium. **FIG. 3G** shows optimized structure snapshots after simulated heating treatment with calcium (left, F105Ca96) or without calcium (right). **FIG. 3H** shows the relationship between C-F bond ratio after REM and the input atomic ratio of calcium and fluorine. Insets are the original

structure of PFOA (top right) and mineralized CaF_2 (bottom left).

[0078] FIGS. 4A-4H show soil properties after REM treatment. **FIG. 4A** is a picture of raw soil (left), REM soil (middle), and calcined soil (right). **FIG. 4B** shows particle size distribution of raw soil, REM soil, and calcined soil. The shadows denote standard deviations, where $N = 5$. **FIG. 4C** shows XRD patterns of raw soil, REM soil, and calcined soil. The powder diffraction file (PDF) reference card for quartz, 01-086-1629 (triangle). **FIG. 4D** shows XRF of raw soil, REM soil and calcined soil. **FIG. 4E** shows water penetration liquid level varied with time for raw soil, REM soil and calcined soil. **FIG. 4F** shows exchangeable soil nutrient content change after REM and calcination processes. c_0 and c are the concentrations of nutrients in raw soil and REM-treated soil, respectively. The error bars in **FIGS. 4E-4F** denote standard deviations, where $N = 3$. **FIG. 4G** shows survival ratio of springtail cultured in different soil samples. **FIG. 4H** shows survival ratio of isopod cultured in different soil samples. The error bars in **FIG. 4G-4H** denote standard deviations, which are calculated from model-predicted values from the generalized linear models with $N = 7$ and $N = 8$, respectively.

[0079] FIGS. 5A-5H show scalability, LCA and TEA for the remediation of PFAS-contaminated soil. **FIG. 5A** is a picture of the kilogram-scale REM process. **FIG. 5B** shows simulated distribution of current density on the soil surface with external voltage input. **FIG. 5C** shows the 3D mapping of PFOA removal efficiency. The mapping was sampled from 52 positions of 4 plane depths with an interval of 2 cm. **FIG. 5D** shows a materials flow analysis of REM. The dash rectangle denotes the system boundary. **FIG. 5E** shows comparison of cumulative energy demand. **FIG. 5F** shows comparison of cumulative GHG emission, **FIG. 5G** shows comparison of operating cost. **FIG. 5H** shows comprehensive comparison of different soil-remediation methods.

[0080] FIGS. 6A-6C show flow chart representation and boundary conditions for different LCA scenarios of (**FIG. 6A**) thermal treatment, (**FIG. 6B**) ball milling, and (**FIG. 6C**)

chemical oxidation. The dash rectangles denote the system boundaries.

[0081] FIGS. 7A-7E show TGA results for five different contaminates: (**FIG. 7A**) trichloroethylene (TCE); (**FIG. 7B**) tetrachloroethylene (PCE), (**FIG. 7C**) 2,4,6-tribromophenol (TBP), (**FIG. 7D**) 3-chlorobiphenyl (PCB 2), and (**FIG. 7A**) decachlorobiphenyl (PCB 209).

[0082] FIGS. 8A-8B show concentration of residue PCE in flash soil under different parameters. **FIG. 8A** shows PCE concentrations versus input voltage. **FIG. 8B** shows PCE concentrations versus flash times with different flash times. The error bars indicate the standard deviations, where $N = 3$.

[0083] FIG. 9 shows total Cl and Cl^- concentration in PCE-contaminated soil versus input voltage. The error bars indicate the standard deviations, where $N = 3$.

[0084] FIG. 10 shows total Cl and Cl^- concentration in TCE-contaminated soil versus input voltage. The error bars indicate the standard deviations, where $N = 3$.

[0085] FIG. 11 shows total Br and Br^- concentration in TBP-contaminated soil versus input voltage. The error bars indicate the standard deviations, where $N = 3$.

DETAILED DESCRIPTION

[0086] The present invention relates to methods for remediating soil having persistent and bioaccumulative pollutants, and more particularly, methods for remediating soil having per- and polyfluorinated alkyl substances (PFAS) and other halogen-containing contaminates by rapid electrothermal mineralization.

[0087] The emerging electric heating techniques, possessing the merits of rapid heating and cooling rates, short treatment duration and thus ultralow energy consumption, energy-efficient thermal treatment in material synthesis

[0088] The emerging direct electric heating techniques, possessing the merits of rapid heating and cooling rates, short treatment duration and thus ultralow energy consumption, can provide

a promising opportunity for PFAS mineralization. [*Jiang 2021*; *Luong 2020*; *Deng 2022*; *Deng I 2023*; *Deng II 2023*; Wyss *I 2023*; *Jia 2022*; *Dong 2023*; *Cheng 2021*; *Yu 2023*; *Sun 2023*].

[0089] The present invention relates to a rapid electrothermal mineralization (REM) method for the effective remediation of PFAS-contaminated soil. Using environmentally compatible biochar [*Yang 2023*; *Luo 2021*; *Lin 2022*] as the conductive additive, the temperature of contaminated soil rapidly escalates to >1000 °C within seconds through a direct current pulse input, with an ultrafast heating (~10^4 °C s^{-1}) and cooling rate (~10^3 °C s^{-1}). During REM, by virtue of the high Ca content inherent in soil and biochar, PFAS can be mineralized into calcium fluoride (CaF_2), a naturally occurring and non-toxic mineral.

[0090] In embodiments, this REM process conducted in a sealed system produces negligible harmful fluorocarbon gas emissions. High removal efficiencies (>99%) and fluorine mineralization ratios (>90%) for various PFAS were simultaneously realized, demonstrating the broad applicability of the REM process. REM facilitates an increased exchangeable nutrient supply of the treated soil, while maintaining soil particle size, composition, and water infiltration rate, rendering it superior to the time-extended calcination approach that severely degrades soil properties.

[0091] When further used for arthropod culture, REM soil exhibits a comparable arthropod survival ratio with the clean raw soil, while the arthropods die rapidly in the PFAS-contaminated soil. Remediation of soil on kilogram scale per batch has been accomplished here, suggesting the potential applicability of REM for large-scale deployment. Furthermore, life-cycle assessment shows that REM exhibits low energy consumption (~420 kWh ton^{-1}), no-water consumption, and, minimal greenhouse gas emission, making it an environmentally attractive alternative over existing remediation techniques.

REM For The Remediation Of PFOA-Contaminated Soil

[0092] In an embodiment of the REM process of the present invention, a design of on-site

REM is shown in **FIG. 1A**, which leverages mature agricultural techniques and soil remediation practices. In the first step (biochar mixing **101**), contaminated soil **104** is premixed with conductive additives, such as biochar **103** (from biochar tank **109**), to ensure appropriate electrical conductivity. As shown in **FIG. 1A**, the biochar mixing **101** can be performed using auger **110**). In the second step (REM treatment **102**), the electrodes **107** fixed in an insulating cap **106** are inserted into the soil. Using power source **105**, a high-voltage pulse input within seconds controllably brings the soil to a typical temperature of >1000°C, facilitating the rapid mineralization of toxic PFAS, with existing Ca compounds in soil and biochar into the nontoxic natural mineral, CaF_2, resulting in remediated soil **108**.

[0093] The REM process was performed on a bench scale. **FIG. 1B**. Raw soil was collected from the Rice University campus, which contained undetectable content of PFAS (<1 ppb) by liquid chromatography-mass spectrometry (LC-MS). The raw soil was separately spiked with different kinds of PFAS with the content of ~100 ppm. *See* **TABLE I**.

TABLE I
Physical Properties Of Different Kinds Of PFAS Utilized

Precursors	Formula	Molecular weight ($g\ mol^{-1}$)	F mass ratio (%)	Mixed concentration in the soil (ppm)
PFOA	$C_8HF_{15}O_2$	414.1	68.8	146.5
PFOS	$C_{24}H_{36}F_{17}NO_3S$	741.6	43.6	223.2
PFH_xS	$C_6HF_{13}O_3SK$	438.2	56.4	155.0
PFBS	$C_4F_9O_3SK$	338.2	50.6	119.2
PTFE	$-CF_2CF_2-$	/	76.0	105.2

[0094] PFAS-contaminated soil was mixed with appropriate amounts of biochar, and then loaded into a quartz tube reactor. No additional Ca-containing compound was added, considering there are sufficient Ca species inherent in the soil for PFAS mineralization. The sample resistance was regulated by compressing the graphite electrodes inserted at the end of the quartz tube, which were connected to a capacitor bank.

[0095] In a typical experiment, with an input voltage of 100 V, discharging time of 1 s, and sample resistance of 3.5 Ω (**TABLE II**), the peak current reached ~140 A (**FIG. 1C**) and the

peak temperature was ~1370 °C (**FIG. 1D**). The heating and cooling rates during REM were calculated to be ~10^4 °C s^{-1} and ~10^3 °C s^{-1}, respectively, using an infrared thermometer.

TABLE II
Parameters For REM Of Soil

Precursors	Mass Ratio	Mass (mg) **	Res (Ω)	Voltage (V)	Time (s)	Mass after REM (mg) ***
c-Soil(PFOA):biochar	2:1	300	3.5	40	1	271
c-Soil(PFOA):biochar	2:1	300	3.5	60	1	253
c-Soil(PFOA):biochar	2:1	300	3.5	80	1	245
c-Soil(PFOA):biochar	2:1	300	3.5	100	1	238
c-Soil(PFOA):biochar	2:1	300	3.5	120	1	227
c-Soil(PFOA):biochar	2:1	300	3.5	150	1	223
c-Soil(PFOA):biochar	1:1	300	2.5	100	1	221
c-Soil(PFOA):biochar	3:1	300	10.5	100	1	249
c-Soil(PFOA):biochar	4:1	300	18.5	100	1	282
c-Soil(wet, PFOA): biochar	2:1	300	4.5	100	1	192
c-Soil(PFOA): biochar (4 mm inner diameter tube)	2:1	108	2.1	60	1	76
c-Soil(PFOA):recycled biochar	2:1	300	3.5	100	1	247
c-Soil(PFOA):carbon black	2:1	300	1.0	100	1	241
c-Soil(PFOA):metcoke	2:1	302	1.5	100	1	236
c-Soil(PFOA):recycled metcoke	2:1	305	1.0	100	1	243
c-Soil(PFOA):metcoke	1:1	300	1.0	100	1	219
c-Soil(PFOA):metcoke	3:1	300	1.5	100	1	238
c-Soil(PFOA):metcoke	4:1	300	1.5	100	1	247
SiO_2(PFOA):metcoke	2:1	300	1.5	100	1	265
c-Soil(PFOA):flash graphene	2:1	305	1.0	100	1	249
c-Soil(PFOS):biochar	2:1	300	3.5	120	1	242
c-Soil(PFH_xS):biochar	2:1	300	3.5	120	1	248
c-Soil(PFBS):biochar	2:1	300	3.5	120	1	241
c-Soil(PTFE):biochar	2:1	300	3.5	80	1	252
c-Soil(PTFE):biochar	2:1	300	3.5	100	1	229
c-Soil(PTFE):biochar	2:1	300	3.5	120	1	212
c-Soil(PTFE):biochar	2:1	300	3.5	150	1	206

*c-Soil is abbreviation of contaminated soil. **The total mass includes c-Soil and carbon additives; ***The total mass includes residual carbon additives.

[0096] By tailoring the input voltage from 40 to 150 V, the REM temperature was tunable ranging from 300 to 2500°C, which meets the required temperature of PFAS degradation, as determined by thermogravimetric analysis (TGA). After REM, the residual PFAS content was quantified by high-performance liquid chromatography with a diode array detector (HPLC-

DAD) and QQQ LC-MS. The detecting limits of each PFAS characterization methods are listed in **TABLE III**. The mineralized fluorine ion (F^-) content was tested by ion chromatography (IC).

TABLE III
Detecting Limits of Different PFAS Characterization Methods

Characterization methods	Detecting limit
FT-IR	1 wt% [*Gorrochategui 2016*]
XRD	0.5 wt% [*Hillier 1999*]
^{19}F-NMR	50 ppb [*Camdzic 2023*]
HPLC-DAD	500 ppb
QQQ LC-MS	0.1 ppb

[0097] The degradation process of perfluorooctanoic acid (PFOA), a representative type of PFAS was first tested. REM was initially conducted in an open system without O-rings to seal the quartz tube. With the increase of input voltage, the PFOA content decreased, benefitting from a higher reaction temperature. However, the total fluorine content significantly decreased with the increase of input voltage, with only half of the organic fluorine mineralized into fluorine ions, which can be ascribed to the emission of PFOA-degraded short-chain species.

[0098] To avoid the emission of short-chain fluorocarbon species, a sealed reactor was constructed with two O-rings on each electrode to seal the reacting tube during REM (**FIG. 1B**). With the increase of input voltage, the PFOA content progressively decreased, benefiting from a higher reacting temperature. Consequently, the F^- content increased with an increase of input voltage from 0 to 100 V and an optimal mineralization ratio of 94% was obtained (**FIG. 1E** with plots **141-143** for organic F, F ion, and sum, respectively). By virtue of the sealing design, REM soil showed a much higher mineralization ratio (94%) compared with the furnace-calcined soil (0.34%), while keeping a high and comparable PFOA removal efficiency of >99%. The gaseous byproduct was collected and tested by gas chromatography mass spectrometry (GC-MS).

[0099] Compared to the clean raw soil as the control, no additional peaks corresponding to known PFOA degradation products were observed. On the contrary, some PFOA-degraded

fluorinated compounds, such as CF_4, CH_3F, C_2F_6, C_2F_4, and C_6H_5F, were observed when replacing soil with SiO_2. This indicated that REM in the presence of Ca effectively mineralizes F from soil contaminated with PFAS and avoids the emission of PFAS-degraded short-chain fluorocarbon species. Thus, the total fluorine mass was calculated by adding the organic fluorine in residual PFOA and the mineralized F^-. **FIG. 1E**. The slight decrease of mineralization ratio and quantifiable total fluorine mass when the REM voltage increases from 100 V to 150 V (**FIG. 1E**), may be attributed to the increased amount of insoluble F-containing compounds deposited on the quartz tube with the increase of REM temperature.

[0100] The PFOA content in the soil can be reduced to below the residential soil remediation standards (130 ppb, the New Jersey Department of Environmental Protection, "Residential soil remediation standards for the ingestion-dermal exposure"), after 2 electric pulses and further to an ultralow value of ~1.1 ppb after 4 electric pulses. **FIG. 1F**. ^{19}F NMR spectra were conducted using deuteroxide to extract PFOA and F^- in the soil before and after REM. **FIG. 1G**. The ^{19}F NMR spectrum of contaminated soil has several peaks, all of which fit well with PFOA standard. [*Camdzic 2021*; *Trang 2022*]. On the contrary, the REM-treated soil had a single peak at -128 ppm, corresponding to hydrated fluoride ions [*Camdzic 2021*], further proving the PFOA can be effectively converted into fluorine ions in the soil by the REM process.

REM For Soil Remediation

[0101] For generality of REM for PFAS degradation, other than PFOA, the mineralization behaviors were investigated of various PFAS, including heptadecafluorooctanesulfonic acid tetraethylammonium salt (PFOS), tridecafluorohexane-1-sulfonic acid potassium salt (PFH_xS), and nonafluorobutane-1-sulfonic acid potassium salt (PFBS). The trends of PFAS mineralization versus input voltage are similar to that of PFOA, where higher input voltages often facilitate higher degradation ratios of C-F bonds. **FIGS. 2A-2C** (plots **201-203** in **FIG.**

2A for organic F, F ion, and sum, respectively; plots **211-213** in **FIG. 2B** for organic F, F ion, and sum, respectively; and plots **221-223** in **FIG. 2C** for organic F, F ion, and sum, respectively).

[0102] In the ^{19}F NMR spectra, only the -128 ppm peak that assigned to hydrated F^- [*Camdzic 2021*] was observed for all REM treated soil samples (**FIGS. 2D-2F**), indicating the effective removal of PFAS by REM. The removal efficiencies of all the tested PFAS were calculated to be higher than 99% (**FIG. 2G**) and >90% mineralized fluorine ratios were quantified with a single electric pulse (**FIG. 2H**). In addition to short-chain PFAS, REM is also applicable to mineralize F-containing polymers, such as polytetrafluoroethylene (PTFE) with a high mineralization ratio of ~95%. Trace amounts of PTFE degradation compounds, including tetrafluoroethylene and trifluoromethanol, were detected in the gaseous phase during REM, while none of the fluorinated compounds were detected in the REM soil.

[0103] In addition to biochar, other carbon materials with sufficient conductivity, including carbon black, metallurgical coke (metcoke) and flash graphene [*Luong 2020*], were also used as the conductive additives for the REM process. Taking PFOA as an example, all tested carbon conductive additives can achieve a high mineralization ratio of >90%, proving the broad applicability of carbon additives. The used carbon additive can be optionally separated from the soil mixture and then reused for next-batch soil remediation. For example, biochar was separated from soil by dispersion and centrifugation with a recycling ratio of ~85 wt%, and reused in a second REM process with a comparable PFAS mineralization performance.

[0104] Similarly, when metcoke was used as the conductive additives, ~91 wt% can be recycled after REM by simply sieving and then reused with similar performance. This significantly reduces materials consumption of the REM process while requiring greater processing. The optimal ratio between soil and different carbon additives was also investigated, where sufficient carbon additive content (>33 wt%) was required to ensure REM temperature

for PFAS mineralization. For deployed applications, the choice of carbon additives depended on the specific scenarios and requirements.

Mechanism of PFAS Mineralization

[0105] Ca^{2+} is suggested to be a critical counterion for PFAS mineralization under thermal treatment. [*Wang 2013*; *Wang 2015*]. To confirm the influence of Ca on PFAS mineralization, mineralization performance of Ca^{2+} was compared with other alkali and alkaline earth metal ions, such as Mg^{2+} and Na^{+}, where calcium carbonate ($CaCO_3$, a representative calcium species in soil [*Pilbeam 2016*]), magnesium carbonate ($MgCO_3$) and sodium carbonate (Na_2CO_3), were separately mixed with PFOA and the metal counterion content is 1.2 mole equivalent compared with F. *See* **TABLE IV**.

TABLE IV
Parameters For REM By Mixing Metal Salt With PFOA*

Metal salts	Mass (mg)**	PFAS type	Mass (mg)	Mass of metcoke (mg)	Resistance (Ω)	Mass after REM (mg)***
$CaCO_3$	137	PFOA	63	100	2.5	212
$CaCO_3$	116	PFOS	84	99	2.5	216
$CaCO_3$	128	PFH_xS	72	100	2.5	208
$CaCO_3$	123	PFBS	77	102	2.5	205
$CaCO_3$	140	PTFE	59	101	3.0	220
$MgCO_3$	131	PFOA	70	100	2.6	197
Na_2CO_3	139	PFOA	61	100	2.2	221

* The input voltage was set as 100 V, REM time was set as 1 s and total mass for each REM is ~300 mg. **Metal counterion content was 1.2 mole equivalents compared with the F mole content in PFAS. ***The total mass included residual carbon additives.

[0106] After REM treatment, X-ray diffraction (XRD) patterns showed the loss of PFOA peaks and the appearance of metal fluoride peaks, indicating that all these alkaline and alkaline earth metal ions can be used for PFAS mineralization. However, Ca achieved a highest PFOA removal efficiency (~99.7%) over Mg (~94.2%) and Na (~98.5%, proving that Ca has the best mineralization performance for PFAS, greater than Mg and Na. Meanwhile, Ca-F bond has the highest bond energy among different metal-fluorine bonds. *See* **TABLE V**.

TABLE V
Metal-Fluorine Bond Energy

M-F type	Bond energy (kJ mol^{-1})
Na-F	477
Mg-F	463
K-F	489
Ca-F	529

[0107] Theoretical calculation revealed that once other metal fluorides (like MgF_2 or NaF) were formed, these fluoride compounds were thermodynamically favorable to convert to CaF_2 during REM under the temperature higher than 400 °C. The above analysis evinces that Ca dominates the PFAS mineralization process. Then, $CaCO_3$ was mixed with other kinds of PFAS and the same mineralization phenomena was observed, explicitly demonstrating the critical role of Ca^{2+} in PFAS mineralization.

[0108] When biochar was used as the conductive additive, a slightly higher mineralization ratio of ~94% was observed, compared to that of other carbon additives (90 - 91%). The composition of these carbon additives was examined by XPS, and it was found that Ca content is highest in biochar (~4 at%), while undetectable by XPS in the other carbon additives.

[0109] To verify that the Ca^{2+} in biochar can benefit PFAS mineralization, PFOA (5 wt%) and biochar (95 wt%) were mixed and REM was conducted. After the treatment, the peaks of PFOA diminished while CaF_2 peak appeared in the XRD patterns. **FIG. 3A**. The same phenomenon pertains to other PFAS. *See* **TABLE I**. The X-ray photoelectron spectroscopy (XPS) spectra show that the C 1*s* peak at ~292 eV (assigned to C-F) and the F 1*s* peak at ~689 eV (assigned to F-C) of PFOA disappeared after the REM process, while the new F 1*s* at ~684 eV (assigned to F-Ca) appeared. **FIGS. 3B-3C** (circles **311a-311b** in **FIG. 3B** for C 1*s*; areas **312a-312b**, **313a-313b**, and **314a** in **FIG. 3B** for C-C, C-O, and C-F, respectively; circles **321a-321b** in **FIG. 3C** for F 1*s*; areas **322** and **323** in **FIG. 3C** for F-C and F-Ca, respectively). In the infrared (IR) spectrum of initial PFOA, the peaks in the range of 1100-1200 cm^{-1} and 650-750 cm^{-1} correspond to stretching and rocking vibrations of C-F bonds [*Huang 2018*], respectively (**FIG.**

3D, with plots **331-332** for biochar+PFOA and after REM, respectively), disappeared after REM. The IR spectra for other PFAS exhibited the same behaviors, demonstrating that Ca in biochar facilitates effective mineralization of PFOA.

[0110] Theoretical analysis was further conducted to clarify the PFAS mineralization mechanism assisted by Ca^{2+}. Thermodynamically, the Gibbs free energy change (ΔG) was calculated for each degradation step of C_7F_{16}, which is the first-step degradation product of PFOA after decarboxylation. [*Trang 2022*]. Without Ca^{2+}, the thermal pyrolysis of the perfluorinated species required a high temperature >1500 °C (**FIG. 3E**, dashed lines **341**). In contrast, ΔG turns negative (favorable) with the existence of Ca^{2+} under broad temperature range (**FIG. 3E**, solid lines **342**), indicating that the PFOA mineralization reaction is spontaneous.

[0111] Molecular dynamic (MD) simulations were further performed to reveal the kinetics of PFOA mineralization. Since the cleavage of C-F bonds occurs for PFOA mineralization, the C-F bond ratio is used as an indicator to evaluate the mineralization efficiency. With Ca, F is more favorable to ionically bond with the Ca atom than forming a covalent bond with the C atom. The reaction barrier of C-F bond cleavage was calculated to be 0.67 eV and the total energy was lowered by 1.24 eV in the presence of Ca, indicating that the mineralization process is an energy-favorable reaction step. On the contrary, without Ca, the F atom spontaneously returned to its original position in the PFOA and reformed a covalent bond with the C atom.

[0112] Without Ca^{2+}, ~80% of C-F bonds in PFOA were maintained after thermal treatment in the temperature range of 1500 to 2500 K, and PFOA tends to degrade into short-chain perfluorinated species. **FIGS. 3F-3G** (with plots **351-352** in **FIG. 3F** for with Ca^{2+} and without Ca^{2+}, respectively. In contrast, with the presence of Ca^{2+}, >90% of C-F bonds in PFOA cleaved and the F were affiliated to Ca. **FIGS. 3F-3G**. With the increase of atomic ratio of Ca and F, more C-F bonds tended to cleave (**FIG. 3H**), demonstrating that more Ca^{2-} can facilitate a

higher mineralization ratio of PFAS. The Ca^{2+} content in both soil and biochar, as tested by X-ray fluorescence (XRF) and XPS, was in the range of 4 to 5 at%, which is hundreds of times excess relative to the reaction stoichiometry. PFAS can thus be effectively mineralized using the inherent Ca^{2+} in soil and biochar, without additional Ca^{2+} consumption, further reducing the materials expense of the REM process.

Soil Properties After REM

[0113] The soil properties after REM were investigated, which are significant for the soil reuse in the ecosystem. The soil after REM treatment and carbon additive removal (denoted as REM soil) was compared with raw soil and calcined soil as a control, since calcination has been reported to be an effective method to remove PFAS from the contaminated soil. [*Javaherian 2016*; *Sörengård 2020*].

[0114] The soil physical properties were first examined. The REM soil **402** exhibited a darker contrast than raw soil **401**, due to the trace residual biochar. **FIG. 4A**. The calcined soil **403** showed a brick-red contrast, indicating possible composition or structure change during the calcination process. **FIG. 4A**. The REM soil exhibited a similar fine powder feature with that of raw soil, while the calcined soil particle was severely aggregated. Laser particle size analysis results also revealed comparable size distributions between raw soil and REM soil, but a significant increase of particle sizes with much lower clay and silt ratio [*Faé 2019*; *Barman 2020*] after calcination. **FIG. 4B** (plots **411-413** for raw soil, REM soil, and calcined soil, respectively). Consequently, the calcined soil showed a drastically decreased surface area compared with raw soil and REM soil. The main crystalline composition was quartz for all tested soil samples (**FIG. 4C**), and XRF results showed that no obvious change for various oxides in the soil after treatment (**FIG. 4D** with bars **431-433** for raw soil, REM soil, and calcined soil, respectively).

[0115] Additionally, the soil water infiltration rates were assessed. **FIG. 4E** with plots **441-**

443 for raw soil, REM soil, and calcined soil, respectively. REM soil showed a slightly higher infiltration rate (~34 cm h^{-1}) than raw soil (~28 cm h^{-1}). Considering a larger porosity of biochar to soil, the small amounts of residual biochar in REM soil could contribute to the higher water infiltration rate. In contrast, the infiltration rate of calcined soil (~455 cm h^{-1}) was >10 times higher, probably due to its severely enlarged particle size (**FIG. 4B**), as water flows faster through the enlarged pores between soil particles. [*Weil 2017*]. The excessively high infiltration rate would lead to degradation of soil fertility by eluviation. [*Zhang 2004*].

[0116] Moreover, soil pH, cation exchange capacity (CEC), soil carbon and nutrients contents were analyzed. REM soil exhibited a pH of 7.58, which was slightly higher than that of raw soil (pH = 7.19). CEC of REM soil was 15.45 cmol kg^{-1}, which is comparable to that of raw soil (15.25 cmol kg^{-1}, **TABLE VI**). On the contrary, the pH of calcined soil increased to 10.63 and its CEC decreases to 4.08 cmol kg^{-1} (**TABLE VI**), indicating the inapplicability for its reuse.

TABLE VI
pH And Cation Exchange Capacity (CEC) Of Different Soil Samples

Soil types	pH	CEC (cmol kg^{-1})
Raw soil	7.19 ± 0.02	15.25 ± 0.81
REM soil	7.58 ± 0.03	15.45 ± 1.04
Calcined soil	10.63 ± 0.08	4.08 ± 0.37

[0117] Soil carbon content measurement showed that REM soil had a slightly higher carbon content (4.3 wt%) than raw soil (3.7 wt%,), possibly due to the existence of small amount of residual biochar. On the contrary, the calcined soil had a carbon content of <0.1 wt%. The contents of extractable organic compounds, including humic acid and fulvic acid, were quantified by the Walkley–Black method [*Baglieri 2007*], where <1 wt% of these compounds remained in the REM soil, indicating the decomposition of these compounds during REM process. The exchangeable nutrient content, including P, Ca, K, Mg, Mn, Fe, and N, is a critical parameter to evaluate soil fertility and directly related to soil biodiversity. [*Sicilaiano 2014*; *Inkotte 2023*]. The contents of most exchangeable nutrients in REM soil increased by 10% to

102%, except a ~5% decrease of Fe content. **FIG. 4F** (bars **451-452** for REM soil and calcined soil, respectively).

[0118] The influence of different carbon additives on soil nutrient contents was also evaluated and it was found that nutrient-rich biochar can facilitate higher exchangeable nutrient contents of REM soil, comparing with those of the REM soil using metcoke as carbon additive. Therefore, the increase of nutrient contents in REM soil can be attributed to the ion-exchange from biochar (**TABLE VII**) to the soil, and/or the mineralization of soil organic matter during REM. [*Bahureksa 2022*; *Chungu 2020*]. However, most of these nutrient contents dramatically decreased for the calcined soil.

TABLE VII
Soil Nutrient Concentrations

Nutrients	Raw soil (ppm)	Calcinated soil (ppm)	REM soil (ppm) **	Biochar (ppm)
P	68 ± 1	50 ± 2	137 ± 14	328 ± 69
Mg	255 ± 20	139 ± 9	406 ± 9	1189 ± 92
K	280 ± 11	71 ± 3	423 ± 7	3232 ± 195
Ca	2605 ± 109	1281 ± 569	3230 ± 275	3942 ± 168
Mn	133 ± 3	265 ± 40	156 ± 17	265 ± 40
N*	16 ± 3	0.74 ± 0.08	17 ± 2	0.23 ± 0.05
Fe	311 ± 12	432 ± 138	294 ± 64	307 ± 64

*The nutrient N refers to nitrate nitrogen; **REM soil tested here is the soil after removing the biochar inside.

[0119] Further, the arthropod culture was conducted to evaluate the applicability of REM soil in ecosystems. Springtail and isopod were used as two representative arthropods. The survival ratios were compared of four kinds of soil samples, including PFOA-contaminated soil (denoted as PFOA soil), raw soil, REM soil, and calcined soil. Because of the toxicity of PFOA [*Whitacre 2010*; *Labine 2022*], both springtails and isopods underwent rapid mortality in PFOA soil within the initial 1 to 2 weeks. **FIGS. 4G-4H** (plots **461-464** in **FIG. 4G** for PFOA soil, raw soil, REM soil, and calcined soil, respectively; plots **471-474** in **FIG. 4H** for PFOA soil, raw soil, REM soil, and calcined soil, respectively); **TABLES VIII-IX**.

TABLE VIII
Results From The Generalized Linear Models Testing For The Main And Interactive Effects Of Soil Types And Culture Time On Springtail Survival

	Survival ratio	
Predictors	*CI*	*p*
(Intercept)	0.18 – 1.44	0.203
Soil Type [Raw soil]	0.29 – 4.83	0.819
Soil Type [REM soil]	0.46 – 6.26	0.430
Soil Type [PFOA soil]	0.00 – Inf.	0.997
Week [Week_2]	0.00 – Inf.	0.997
Week [Week_3]	0.00 – Inf.	0.997
Soil Type [Raw soil] × Week [Week_2]	0.00 – Inf.	0.997
Soil Type [REM soil] × Week [Week_2]	0.00 – Inf.	0.997
Soil Type [PFOA soil] × Week [Week_2]	0.00 – Inf.	0.998
Soil Type [Raw soil] × Week [Week_3]	0.00 – Inf.	1.000
Soil Type [REM soil] × Week [Week_3]	0.00 – Inf.	0.998
Soil Type [PFOA soil] × Week [Week_3]	0.00 – Inf.	0.998
Observations	84	

TABLE IX
Results From The Generalized Linear Models Testing For The Main And Interactive Effects Of Soil Types And Culture Time On Isopod Survival

	Survival ratio		
Predictors	*Odds Ratios*	*CI*	*p*
(Intercept)	7.00	1.25 – 130.85	0.069
Soil Type [Raw soil]	1.00	0.03 – 28.82	1.000
Soil Type [REM soil]	1.00	0.03 – 28.82	1.000
Soil Type [PFOA soil]	0.05	0.00 – 0.49	0.024
Week [Week_2]	0.43	0.02 – 5.61	0.529
Week [Week_3]	0.14	0.01 – 1.39	0.129
Soil Type [Raw soil] × Week [Week_2]	1.44	0.03 – 84.59	0.850
Soil Type [REM soil] × Week [Week_2]	1.44	0.03 – 84.59	0.850
Soil Type [PFOA soil] × Week [Week_2]	1.00	0.02 – 52.84	1.000
Soil Type [Raw soil] × Week [Week_3]	1.00	0.02 – 45.26	1.000
Soil Type [REM soil] × Week [Week_3]	1.00	0.02 – 45.26	1.000
Soil Type [PFOA soil] × Week [Week_3]	0.00	0.00 – Inf.	0.995
Observations	96		

[0120] In contrast, REM soil exhibited a comparable arthropod survival ratio with raw soil (**FIGS. 4G-4H**), demonstrating the effective elimination of toxic substances and the restoration of soil properties. The calcined soil displayed a lessening in arthropods survival ratio compared with raw soil (**FIGS. 4G-4H**), which could originate from the nutrient loss and soil structure change. These results reveal that apart from the PFAS mineralization, REM maintains soil

morphology, particle size, crystal components and water infiltration rate, while promoting soil nutrients and biodiversity. This is in striking contrast to the calcination process, which leads to soil degradation. This difference can be attributed to the short duration of the REM process that lasts only seconds with rapid heating and cooling rates.

Scaling-Up REM Process

[0121] To outline the practical applicability of REM for PFAS-contaminated soil remediation, an initial scale-up study was first conducted. The PFAS mineralization efficiency depends mainly on the peak temperature and reaction duration during REM. Therefore, maintaining a constant temperature can be critical for the scale-up, which can be realized by increasing the input voltage or capacitance of the REM system.

[0122] For the REM process, the PFAS mineralization in the soil mostly depends on the treating temperature and the time. *See* **FIG. 1D**; **FIGS 2A-2C**. Hence, the REM temperature across the soil sample has import when scaling up the process. For REM process, the input heat (Q) can be calculated by Eq. (1),

$$Q = I^2Rt \qquad (1),$$

where I is the current passing through the sample, R is the sample resistance, and t is the discharging time.

[0123] The heat amount per volume (Q_v) is calculated by Eq. (2),

$$Q_v = j^2\rho_e t \qquad (2),$$

where j is the current density, and ρ_e is the electrical resistivity. For a specific sample, the electrical resistivity (ρ_e) is constant.

[0124] The temperature difference (ΔT) is proportional to the heat amount by Eq. (3),

$$Q = C_p m\Delta T \quad (3),$$

where C_p is heat capacity and m is the mass of the sample.

[0125] Eq. (3) could be reformulated per volume to Eq. (4),

$$Q_v = C_p \rho_m \Delta T \qquad (4),$$

where ρ_m is the density of the sample. For a specific sample, the C_p and ρ_m were constant; hence, maintaining a constant Q_v is proportional to ΔT.

[0126] The charge amount (q) in the capacitor bank could be calculated by Eq. (5),

$$q = CV \qquad (5),$$

where C is the capacitance of the capacitor bank, and V is the voltage of the capacitor bank.

[0127] Assuming that all the charges in the capacitor bank are discharged within the time of t, the current density (j) could be calculated by Eq. (6),

$$j = \frac{I}{S} = \frac{CV}{St} \qquad (6),$$

where S is the cross-sectional area of the sample.

[0128] Since the cylinder-shaped sample is typically used, the mass (m) could be calculated by Eq. (7),

$$m = \rho_m SL \qquad (7),$$

where ρ_m is the density of the sample, S is the cross-sectional area of the sample, and L is the length of the sample.

[0129] For a specific type of sample, such as soil and biochar, the density (ρ_m) is the same.

[0130] To summarize, Eq. (8) was obtained that determines the current density,

$$j = \frac{CV\rho_m L}{mt} \qquad (8).$$

[0131] Hence, ΔT can be calculated following the Eq. (9).

$$\Delta T = \frac{C^2 V^2 L^2 \rho_m \rho_e}{m^2 t C_p} \qquad (9).$$

[0132] As aforementioned, to scale up the REM process, increasing the mass (m) of the sample is required, while a constant temperature difference (ΔT) should be maintained. Two routes can be adopted: (1) increasing the input voltage (V), and/or (2) increasing the capacitance (C) of the REM system.

[0133] In a first-generation REM setup, a capacitor bank composed of 10 aluminum electrolytic capacitors (450 V, 6 mF, Mouser #80-PEH200YX460BQU2) was used with a total capacitance of C_0 = 0.06 F. In a small-scale experiment, the input voltage (V_0) of 100 V and capacitance (C_0) of 0.06 F were used for the sample mass of m_0 = 0.30 g. The scaling up of the REM process was demonstrated to a mass of m_1 = 10 g based on a second-generation setup with larger capacitance of C_1 = 0.624 F. Thus, the below formula of Eq. (10) was obtained,

$$\frac{m_1}{m_0} = \frac{C_1 V_1}{C_0 V_0} \qquad (10).$$

[0134] For the mass of m_1 = 11 g and C_1 = 0.624 F, a REM voltage of $V_1 \approx$ 300 V was used, which basically fits with Eq. (10). The peak temperature during this REM process was ~1600 °C, similar to small-batch temperature (**FIG. 1C**), proving the efficiency of the scale-up.

[0135] Utilizing the REM system (developed with a larger capacitance of C = 0.624 F), with an input voltage of 300 V, the sample temperature can ramp to 1700 °C, and ~7 g of contaminated soil per batch can be remediated within 6 s.

[0136] Furthermore, an alternating current (AC) source with better scalability was integrated into a subsequent REM system, which directly converted commercial AC into DC output instead of using capacitors. 2 kg of PFOA-contaminated soil was mixed with 500 g of metcoke in a 10-inch-diameter clay pot **501** with a plastic cap **502**, where four graphite rods **503** were applied as the electrodes. **FIG. 5A**. During REM, bright light emission was observed through cap **502** (**FIG. 5A**), with a steady current of ~18 A and the temperature of ~1000 °C. Afterwards, the soil samples from different positions in the pot were collected for the PFOA quantification. The average PFOA removal efficiency of the kilogram-scale REM reached ~97% with high uniformity both radically and axially (**FIG. 5B**), comparable to that of small-scale samples. Numeric simulation of the current density across the soil under external voltage input were further conducted.

[0137] Electric field simulation. The simulation was conducted based on the finite element method using the COMSOL Multiphysics 5.5 software. The Electric Currents interface under the AC/DC module was used as the model. The geometric configuration and materials parameters are shown in **TABLE X**.

TABLE X
Parameters Of Electric Field Simulation

Parameters	Soil	Graphite electrode
Shape	Cyclinder	Cyclinder
Size	15 cm (diameter), 6 cm (height)	6.36 mm (diameter), 8 cm (height)
Electrical conductivity	0.83 S m^{-1}	2×10^5 S m^{-1}
Relative permittivity	4	18
Boundary condition	200 V input	

[0138] The electrical conductivity of the mixed soil/carbon additive was calculated by measuring the resistance. Other material parameters were from the physical constant table. A simulated electric potential map showed the linear decrease of electric potential from the electrical potential electrodes to the ground electrodes. The simulated in-plane current density map is shown in **FIG 5C**. The maps were uniform, proving the homogeneous heating capability of the REM process. (The current density was uniform both in-plane (**FIG. 5C**) and in-depth, substantiating the homogeneous heating capability of the REM process for soil remediation).

[0139] Current density can have import for the Joule heating. According to $Q = I^2Rt$, since soil conductivity is the same, similar current density leads to a similar heating effect. In the kilogram-scale sample with 200 V input, the current density was ~1000 A m^{-2}.

[0140] To assess the practical applicability of the REM process, the simulation was further extended to a 1 m × 1 m × 1 m scale. The material properties and boundary conditions were the same as in the aforementioned small-scale sample. In this case, the voltage input with 1000 V was applied. The current density in the central position was calculated to be ~800 A m^{-2}, similar to that in the small-scale clay pot. According to the theoretical analysis as discussed

above, the current density determined the accessible temperature of the sample during the REM process. This indicated that a comparable temperature of ~1000 °C can be achieved under such a voltage input for the large-scale 1 m^3 sample.

[0141] To reveal the relationship of electrode surface area on the heating efficacy, a simulation was conducted on a 1 m × 1 m × 1 m volume sample with different electrode surface area. With the increase of each electrode surface area from 0.25 to 0.75 m^2, the current density at the center position increases from 730 to 870 A m^2, which indicated a higher REM temperature since the current density determines the temperature according to the analysis discussed above. Therefore, during REM, a higher electrode surface area can facilitate a higher REM temperature and thus a higher PFOA removal efficiency.

[0142] Again, the current density is uniform both in-plane (**FIG. 5C**) and in-depth, substantiating the homogeneous heating capability of the REM process for soil remediation. The field-scale application potential of REM was evaluated by simulation at a 1 m × 1 m × 1 m scale. Under the voltage input at 1000 V, the current density of the 1 m^3 scale soil sample was similar to that in the small-scale clay pot (**FIG. 5B**). Since, as discussed above, the current density mainly determines the accessible temperature, it is projected that a similar heating pattern can be achieved for the large-scale sample.

[0143] In addition, the current density of the large-scale soil sample uniformly distributes both in-plane and in-depth, confirming the homogenous heating capability of REM for on-site soil remediation. Meanwhile, based on the simulation results, the increase of electrode surface areas facilitates an increase of current density with a certain voltage input, leading to a higher REM temperature for PFAS mineralization. For the practical application, considering the moisture contained in field soil, it is assessed that REM is applicable for PFAS mineralization in wet soil. After REM, the wet soil with a moisture content of ~30 wt% achieved a PFOA mineralization ratio comparable to pre-dried soil, further suggesting the feasibility of REM for

practical deployment.

[0144] In certain embodiments, scalability in the field include a process by which the conductive additive (such as biochar) can be introduced, with or without an auger, at various (and strategic) locations relative to one or more electrode arrays. In such manner, this can reduce the conductive additive content to a lower weight percentage (such as 1 wt%) relative to the contaminated soil (as opposed to a higher wt% such 20 wt%). The electrode array can be inserted at strategic locations, and a desired depth. The electrodes can then be used to strategically flash the soil, such as by firing across several pairs, to heat the ground.

[0145] By way of example, such approach can be biochar added to the soil by solid or slurry injection at strategic locations between the inserted electrodes (or the biochar can be injected at strategic locations between where the electrodes will be inserted). The biochar can be injected before or after the insertion of the electrode array the soil, or even during the time when the electrodes are being inserted. The biochar can be injected at as little at 0.1 wt% relative to the soil weight to be flashed, and up to 25 wt%. Generally, this would be in amount of biochar at ~1 wt% of the contaminated soil to be treated. There can generally be between two electrodes and 120 electrodes inserted per electrode array insertion. Strategically firing can be performed across multiple electrode pairs over a timed sequence to heat the soil. The electrode arrays and biochar can be inserted to desired locations (such as within a 1 square meter area) based upon the contaminant concentration at a particular depth (such as 3 meters).

Life Cycle Assessment

[0146] The environmental impact of the REM process was thereafter assessed. The energy consumption of the REM process is calculated to be ~420 kWh ton^{-1}. This low energy consumption benefits from the short duration, ultrafast heating/cooling rates, and in-place soil treatment.

[0147] Furthermore, a comparative cradle-to-gate life cycle assessment (LCA) was conducted

to compare the environmental impact and cumulative energy demand of REM with existing remediation approaches. Four scenarios were considered in this study, including thermal treatment (**FIG. 6A**), ball milling (**FIG. 6B**) chemical oxidation (**FIG. 6C**), and REM (**FIG. 5D**). *See* **TABLS XI-XVI**.

TABLE XI
Materials Flow For Various Scenarios

Scenarios	Thermal treatment (tonne)	Chemical oxidation (tonne)	Ball milling (tonne)	REM by biochar (tonne)	REM by metcoke (tonne)
PFAS-contaminated soil	1	1	1	1	1
Biochar	0	0	0	0.075	0
Biochar pretreatment	0	0	0	0.075	0
Metcoke	0	0	0	0	0.035
Potassium permanganate	0	0.01	0	0	0
Water	0	10	0	0	0
Potassium hydroxide	0	0	0.0095	0	0
Excavation and transportation	1	1	1	0	0
Mixing	0	1.01	1.0095	1.5	1.5
Furnace heating	1	0	0	0	0
Water bath heating	0	11.01	0	0	0
Filtration	0	11.01	0	0	0
Ball milling	0	0	1.0095	0	0
Transportation and refilling	1	1	1	0	0
REM	0	0	0	1.5	1.5
Cyclone separation	0	0	0	1.5	0
Sieving	0	0	0	0	1.5

The material mass flows are normalized to treat 1 tonne of PFAS-contaminated soil. **PFAS concentration in the contaminated soil is set as 100 ppm. ***REM, rapid electrothermal mineralization.

TABLE XII
Life Cycle Inventory

Impact Category	Energy consumption (MJ)	GHG emission (kg)	Water consumption (kg)
Biochar	20025	5.04	4.7
Metcoke	28030	362.6	416.9
Potassium permanganate	19480	1891	8682
Potassium hydroxide	28000	1980	17221
Biochar pretreatment	360	46.8	241.2
Excavation and transportation	451.5	33.8	302.5
Mixing	9.43	1.23	6.3
Furnace heating	3874	504	2595.6
Water bath heating	1866	243	1260.2
Filtration	2.2	0.29	1.5
Ball milling	3456	449	2315.5
Transportation and refilling	466.6	35.7	312.6
REM	1000	130	670
Cyclone separation	6.75	19	4.5
Sieving	4.2	0.55	2.8

*The material mass flows are normalized to treat 1 tonne of PFAS-contaminated soil. **PFAS concentration in the contaminated soil is set as 100 ppm. ***REM, rapid electrothermal mineralization. ****GHG, greenhouse gas.

TABLE XIII
Energy Consumption For Various Scenarios

Scenarios	Thermal treatment (MJ)	Chemical oxidation (MJ)	Ball milling (MJ)	REM by biochar (MJ)	REM by metcoke (kg)
Biochar	0	0	0	1501.9	0
Metcoke	0	0	0	0	981.05
Potassium permanganate	0	194.8	0	0	0
Potassium hydroxide	0	0	266	0	0
SUM of Materials	0	194.8	266	1501.9	981.05
Excavation and transportation	451.5	451.5	451.5	0	0
Biochar pretreatment	0	0	0	27	0
Mixing	0	9.43	9.44	14.15	14.15
Furnace heating	3874	0	0	0	0
Water bath heating	0	1866	0	0	0
Filtration	0	24.2	0	0	0

Ball milling	0	0	3460	0	0
Transportation and refilling	466.6	466.6	466.6	0	0
REM	0	0	0	1500	1500
Cyclone separation	0	0	0	10.13	0
Sieving	0	0	0	0	6.30
SUM of Process	4792.1	2817.7	4387.5	1551.3	1520.45
SUM	**4792**	**3013**	**4654**	**3053**	**2502**

*The material mass flows are normalized to treat 1 tonne of PFAS-contaminated soil. **PFAS concentration in the contaminated soil is set as 100 ppm. ***REM, rapid electrothermal mineralization.

TABLE XIV
GHG Emissions For Various Scenarios

Scenarios	**Thermal treatment (kg)**	**Chemical oxidation (kg)**	**Ball milling (kg)**	**REM by biochar (kg)**	**REM by metcoke (kg)**
Biochar	0	0	0	0.38	0
Metcoke	0	0	0	0	12.69
Potassium permanganate	0	18.9	0	0	0
Potassium hydroxide	0	0	18.81	0	0
SUM of Materials	0	18.9	18.8	0.4	12.69
Excavation and transportation	33.79	33.79	33.79	0	0
Biochar pretreatment	0	0	0	3.51	0
Mixing	0	1.23	1.24	1.84	1.84
Furnace heating	504	0	0	0	0
Water bath heating	0	243	0	0	0
Filtration	0	3.19	0	0	0
Ball milling	0	0	453	0	0
Transportation and refilling	35.75	35.75	35.75	0	0
REM	0	0	0	195	195
Cyclone separation	0	0	0	1.32	0
Sieving	0	0	0	0	0.83
SUM of Process	573.5	317.0	523.8	201.7	197.7
SUM	**574**	**336**	**543**	**202**	**210**

*The material mass flows are normalized to treat 1 tonne of PFAS-contaminated soil. **PFAS concentration in the contaminated soil is set as 100 ppm. ***REM, rapid electrothermal mineralization. ****GHG, greenhouse gas.

TABLE XV
Water Consumption For Various Scenarios

Scenarios	Thermal treatment (kg)	Chemical oxidation (kg)	Ball milling (kg)	REM by biochar (kg)	REM by biochar (kg)
Biochar	0	0	0	0.35	0
Metcoke	0	0	0	0	145.9
Potassium permanganate	0	86.82	0	0	0
Potassium hydroxide	0	0	163.6	0	0
SUM of Materials	0	86.8	163.6	0.35	145.9
Excavation and transportation	302.5	302.5	302.5	0	0
Biochar pretreatment	0	0	0	27	0
Mixing	0	6.36	6.36	9.45	9.45
Furnace heating	2595.6	0	0	0	0
Water bath heating	0	1272.8	0	0	0
Filtration	0	16.52	0	0	0
Ball milling	0	0	2337.5	0	0
Transportation and refilling	312.6	312.6	312.6	0	0
REM	0	0	0	1005	1005
Cyclone separation	0	0	0	6.75	0
Sieving	0	0	0	0	4.22
SUM of Process	3210.7	1910.8	2959	1048.2	1018.67
SUM	**3211**	**1998**	**3123**	**1049**	**1165**

*The material mass flows are normalized to treat 1 tonne of PFAS-contaminated soil. **PFAS concentration in the contaminated soil is set as 100 ppm. ***REM, rapid electrothermal mineralization.

TABLE XVI
Materials And Energy Cost Inventory

Scenarios	Materials cost ($)	Energy cost ($)
Biochar	1400	0
Metcoke	150	0
Potassium permanganate	37700	0
Potassium hydroxide	31600	0
Water	1.085	0
Excavation and transportation	0	26.50
Biochar pretreatment	0	5.87
Mixing	0	0.15
Furnace heating	0	63.17
Water bath heating	0	30.43
Filtration	0	0.036

Ball milling	0	56.36
Transportation and refilling	0	27.39
REM	0	16.31
Cyclone separation	0	0.17
Sieving	0	0.068

Note: *The material mass flows are normalized to treat 1 tonne of PFAS-contaminated soil. **PFAS concentration in the contaminated soil is set as 100 ppm. ***REM, rapid electrothermal mineralization. ****The consumed energy is assumed to be from electricity, and the industrial price of electrical energy in Texas, USA is \$0.0587 kWh^{1}.

[0148] REM demonstrated a low cumulative energy demand (CED) of 3053 MJ $tonne^{-1}$. This value is comparable with that of the chemical oxidation process (3013 MJ $tonne^{-1}$), but 31% to 33% lower than traditional thermal treatment and ball milling methods. **FIG. 5E** (bars **541-542** for materials and process, respectively). REM also exhibited 40% to 65% reduction in greenhouse gas emission (GHG) (**FIG. 5F**, with bars **551-552** for materials and process, respectively), and 47% to 67% reduction in water consumption compared to other methods. REM also has no chemical waste generation because of no consumption of chemicals. Additionally, REM can realize >99% PFAS removal within seconds, achieving the best performance in overcoming the trade-off between removal efficiency and processing time among reported methods. [*Javaherian 2016*; *Sörengård 2020*].

Techno-Economic Assessment

[0149] Additionally, a techno-economic analysis (TEA) was conducted, since economic incentives play a vital role in utilization. It was shown that REM had an operating expense of \$130 $tonne^{-1}$ of soil treated, which is comparable to thermal treatment (\$117 $tonne^{-1}$), but much lower than ball milling (\$411 $tonne^{-1}$) and chemical oxidation (\$473 $tonne^{-1}$). **FIG. 5G** (bars **561-562** for materials and process, respectively); **TABLE XVII**. With the merits of low cost, high PFAS removal and degradation efficiency, rapid treating process, zero water use, and the preservation of soil properties (**FIG. 5H**, with areas **571-574** for thermal, ball milling, chemical oxidation, and REM, respectively), REM shows potential superiorities over existing thermal treatment and chemical oxidation methods toward practical applications.

TABLE XVII
Cost Evaluation Of Various Scenarios

Scenarios	Thermal treatment ($)	Chemical oxidation ($)	Ball milling ($)	REM by biochar ($)	REM by metcoke ($)
Biochar	0	0	0	105	0
Metcoke	0	0	0	0	5.25
Potassium permanganate	0	377	0	0	0
Potassium hydroxide	0	0	300.2	0	0
Water	0	10.85	0	0	0
SUM of Materials	0	388	300	105	5.25
Transportation and refilling	26.50	26.50	26.50	0	0
Biochar pretreatment	0	0	0	0.44	0.23
Mixing	0	0.15	0.15	0.23	0
Furnace heating	63.17	0	0	0	0
Water bath heating	0	30.43	0	0	0
Filtration	0	0.39	0	0	0
Ball milling	0	0	56.42	0	0
Transportation and refilling	27.39	27.39	27.39	0	0
REM	0	0	0	24.46	24.46
Cyclone separation	0	0	0	0.17	0
Sieving	0	0	0	0	0.10
SUM of Process	117	85	110	25	24.89
SUM	**117**	**473**	**411**	**130**	**30**

*REM, rapid electrothermal mineralization. **PFOA, perfluorooctanoic acid; PFOS, perfluorooctane sulfonates. ***Material price: industrial water ($1.085 per tonne), $KMnO_4$ ($37.7 per kg), KOH ($31.6 per kg) biochar ($1400 per tonne) and metcoke ($150 per tonne). ****The consumed amount of biochar during REM process is calculated by subscribing the recycled mass from the input mass.

Remediating Soil Contaminated With Other Halogen-Containing Contaminates

[0150] In addition to PFAS mineralization, REM can also be extended to remediation soil by mineralizing other halogen-containing contaminates, including tetrachloroethylene (PCE), trichloroethylene (TCE), polychlorinated biphenyls (PCB), tribromophenol (TBP), brominated flame retardants (BFR), and halogen-containing antibiotics, like ciprofloxacin, chloramphenicol, iodoquinol.

[0151] TGA results revealed that all these contaminates degrades under a temperature lower than 600 °C. *See* **FIGS. 1A-1E** for TCE, PCE, TBP, PCB 2m and PCB 209, respectively. (The TGA was conducted under 100 mL min-1 N2 gas with a heating rate of 10 °C min-1.) These

TGA indicate that all these contaminates can be easily degraded under flash temperature.

[0152] For the PCE-contaminated soil, the REM process was performed by flashing it under different input voltages in an O-ring sealed system, then extracted the residue PCE from the flash soil using 5× hexane, and then tested the residual PCE contents by GC-MS. GC results showed that with the increasing input voltage and flash times, the lower PCE residue contents in the soil. **FIGS. 8A-8B**. With an input voltage of 80 V, the residue PCE contents were lower than the safety limits for the residential soil (~5.5 ppm).

[0153] IC and combustion IC (CIC) were used to quantify the mineralized Cl^- and total Cl contents in the soil before and after flash, which can realize an 85% mineralization of organic Cl into Cl^-. *See* **FIG. 9** (plots **901-902** for total Cl and Cl^-, respectively). Considering initial raw soil has a high content of Cl^- with a distinct variation (30-70 ppm), the mineralization of Cl has a relatively large error bar.

[0154] Similar evaluations were performed for TCE-contaminated soil. The corresponding IC and CIC data also shows a >80% mineralization ratios of TCE after flash. *See* **FIG. 10** (plots **1001-1002** for total Cl and Cl^-, respectively).

[0155] Using the similar processes, the degradation process of 2,4,6-tribromophenol (TBP) (which is a typical BFR compound) in the contaminated soil was evaluated, using IC and CIC. **FIG. 11** ((plots **1001-1002** for total Br and Br^-, respectively). When conducted in the sealed system, ~93% Br can be effectively mineralized into Br^-, which proves the efficiency of REM process to mineralize any kind of halogen-contained contaminants.

Applications

[0156] A facile and versatile REM methods can be used for the effective remediation of PFAS-contaminated soil. Through a rapid reaction with inherent Ca^{2+} in soil as well as biochar additives, harmful PFAS can be converted into its naturally mineralized form, CaF_2, in seconds. REM demonstrates high removal efficiencies (>99.9%) and fluorine mineralization ratios

(>90%) for various kinds of PFAS. Distinguished from some existing PFAS removal processes that could degrade soil and are PFAS-type-specific, REM can destroy a host of PFAS types and it preserves most of the soil properties, which is crucial to maintain the overall health and function of the soil ecosystem. With low time- and energy-consumption, high efficiency, and potential scalability, REM provides a promising method to remediate soil from PFAS contamination.

[0157] In addition to soil, these REM methods can be utilized to remedy other PFAS-contaminated solid waste.

[0158] The REM method can also be utilized for the for the effective remediation of soil that has other halogen-containing contaminates, including tetrachloroethylene (PCE), trichloroethylene (TCE), polychlorinated biphenyls (PCB), tribromophenol (TBP), brominated flame retardants (BFR), and halogen-containing antibiotics, like ciprofloxacin, chloramphenicol, iodoquinol.

[0159] While embodiments of the invention have been shown and described, modifications thereof can be made by one skilled in the art without departing from the spirit and teachings of the invention. The embodiments described and the examples provided herein are exemplary only, and are not intended to be limiting. Many variations and modifications of the invention disclosed herein are possible and are within the scope of the invention. The scope of protection is not limited by the description set out above, but is only limited by the claims which follow, that scope including all equivalents of the subject matter of the claims.

[0160] The disclosures of all patents, patent applications, and publications cited herein are hereby incorporated herein by reference in their entirety, to the extent that they provide exemplary, procedural, or other details supplementary to those set forth herein.

[0161] Amounts and other numerical data may be presented herein in a range format. It is to be understood that such range format is used merely for convenience and brevity and should

be interpreted flexibly to include not only the numerical values explicitly recited as the limits of the range, but also to include all the individual numerical values or sub-ranges encompassed within that range as if each numerical value and sub-range is explicitly recited. For example, a numerical range of approximately 1 to approximately 4.5 should be interpreted to include not only the explicitly recited limits of 1 to approximately 4.5, but also to include individual numerals such as 2, 3, 4, and sub-ranges such as 1 to 3, 2 to 4, *etc*. The same principle applies to ranges reciting only one numerical value, such as "less than approximately 4.5," which should be interpreted to include all of the above-recited values and ranges. Further, such an interpretation should apply regardless of the breadth of the range or the characteristic being described.

[0162] Unless defined otherwise, all technical and scientific terms used herein have the same meaning as commonly understood to one of ordinary skill in the art to which the presently disclosed subject matter belongs. Although any methods, devices, and materials similar or equivalent to those described herein can be used in the practice or testing of the presently disclosed subject matter, representative methods, devices, and materials are now described.

[0163] Following long-standing patent law convention, the terms "a" and "an" mean "one or more" when used in this application, including the claims.

[0164] Unless otherwise indicated, all numbers expressing quantities of ingredients, reaction conditions, and so forth used in the specification and claims are to be understood as being modified in all instances by the term "about." Accordingly, unless indicated to the contrary, the numerical parameters set forth in this specification and attached claims are approximations that can vary depending upon the desired properties sought to be obtained by the presently disclosed subject matter.

[0165] As used herein, the term "about" and "substantially" when referring to a value or to an amount of mass, weight, time, volume, concentration or percentage is meant to encompass

variations of in some embodiments ±20%, in some embodiments ±10%, in some embodiments ±5%, in some embodiments ±1%, in some embodiments ±0.5%, and in some embodiments ±0.1% from the specified amount, as such variations are appropriate to perform the disclosed method.

[0166] As used herein, the term "substantially perpendicular" and "substantially parallel" is meant to encompass variations of in some embodiments within ±10° of the perpendicular and parallel directions, respectively, in some embodiments within ±5° of the perpendicular and parallel directions, respectively, in some embodiments within ±1° of the perpendicular and parallel directions, respectively, and in some embodiments within ±0.5° of the perpendicular and parallel directions, respectively.

[0167] As used herein, the term "and/or" when used in the context of a listing of entities, refers to the entities being present singly or in combination. Thus, for example, the phrase "A, B, C, and/or D" includes A, B, C, and D individually, but also includes any and all combinations and subcombinations of A, B, C, and D.

REFERENCES

[0168] Al Amin, M., *et al.*, "Recent Advances in the Analysis of Per- and Polyfluoroalkyl Substances (PFAS)—A Review," *Environ Technol Innov*, **2020**, *19*, 100879 ("*Al Amin 2020*").

[0169] Algozeeb, W. A., *et al.*, "Flash Graphene from Plastic Waste," *ACS Nano*, **2020**, *14*(11), 15595–15604 ("*Algoeeb 2020*").

[0170] Alinezhad, A., *et al.*, "An investigation of thermal air degradation and pyrolysis of per- and polyfluoroalkyl substances and aqueous film-forming foams in soil," *ACS EST Engg.*, **2022**, *2*, 198-209 ("*Alinezhad 2022*").

[0171] Aro, R., *et al.*, "Organofluorine Mass Balance Analysis of Whole Blood Samples in Relation to Gender and Age," *Environ Sci Technol*, **2021**, *55*(19), 13142–13151 ("*Aro 2021*").

[0172] Baglieri, A., *et al.*, "A method for isolating soil organic matter after the extraction of

humic and fulvic acids," *Org. Geochem.*, **2007**, *38*, 140-150 ("*Baglieri 2007*").

[0173] Bahureksa, W., *et al.*, "Nitrogen enrichment during soil organic matter burning and molecular evidence of maillard reactions," *Environ. Sci. Technol.*, **2022**, *56*, 4597-4609 ("*Bahureksa 2022*").

[0174] Barman, U., *et al.*, "Soil texture classification using multi class support vector machine," *Inf. Process. Agric.*, **2020**, *7*, 318-332 ("*Barman 2020*").

[0175] Blöchl, P. E., "Projector augmented-wave method," *Phys. Rev. B*, **1994**, *50*, 17953 ("*Blöchl 1994*").

[0176] Bolan, N., *et al.*, "Remediation of poly-and perfluoroalkyl substances (pfas) contaminated soils–to mobilize or to immobilize or to degrade?" *J. Hazard. Mater.*, **2021**, *401*, 123892 ("*Bolan 2021*").

[0177] Booker, I. D., *et al.*, "Chloride-based SiC growth on a-axis 4H–SiC substrates," *Physica B Condens. Matter*, **2016**, *480*, 23-25 ("*Booker 2016*").

[0178] Brusseau, M. L., *et al.*, "PFAS Concentrations in Soils: Background Levels versus Contaminated Sites," *Sci Total Environ*, **2020**, *740* ("*Brusseau 2020*").

[0179] Buck, R. C., *et al.*, "Perfluoroalkyl and Polyfluoroalkyl Substances in the Environment: Terminology, Classification, and Origins," *Integr Environ Assess Manag*, **2011**, *7*(4), 513–541 ("*Buck 2011*").

[0180] Camdzic, D., *et al.*, "Quantitation of total pfas including trifluoroacetic acid with fluorine nuclear magnetic resonance spectroscopy," *Anal. Chem.*, **2023**, *95*, 5484-5488 ("*Camdzic 2023*").

[0181] Camdzic, D., *et al.*, "Total and class-specific analysis of per-and polyfluoroalkyl substances in environmental samples using nuclear magnetic resonance spectroscopy," *J. Hazard. Mater. Lett.*, **2021**, *2*, 100023 ("*Camdzic 2021*").

[0182] Carter, M. R., *et al.*, *Soil sampling and methods of analysis*, CRC press, **2007** ("*Carter*

2007").

[0183] Chen, W., *et al.*, "Flash Recycling of Graphite Anodes," *Advanced Materials*, **2023**, *35*(8), 2207303 ("*Chen 2023*").

[0184] Chen, W., *et al.*, "Heteroatom-Doped Flash Graphene," *ACS Nano*, **2022**, *16*(4), 6646–6656 ("*Chen 2022*").

[0185] Chen, Y., *et al.*, "Ultra-fast self-assembly and stabilization of reactive nanoparticles in reduced graphene oxide films," *Nat. Commun.*, **2016**, *7*, 12332 ("*Chen 2016*").

[0186] Cheng, Y., *et al.*, "Electric current aligning component units during graphene fiber Joule heating," *Adv. Funct. Mater.*, **2021**, *32*, 2103493 ("*Cheng 2021*").

[0187] Chow, S. J., *et al.*, "Comparative Investigation of PFAS Adsorption onto Activated Carbon and Anion Exchange Resins during Long-Term Operation of a Pilot Treatment Plant," *Water Res*, **2022**, *226*, 119198 ("*Chow 2022*").

[0188] Chungu, D., *et al.*, "Fire alters the availability of soil nutrients and accelerates growth of eucalyptus grandis in Zambia," *J. Forest. Res.*, **2020**, *31*, 1637-1645 ("*Chungu 2020*").

[0189] Clavaguera-Mora, M. T., *et al.*, "Growth of SiC films obtained by LPCVD," *Diam. Relat. Mater.*, **1997**, *6*, 1306-1310 ("*Clavaguera-Mora 1997*").

[0190] Crosby, N. T., "Equilibria of Fluorosilicate Solutions with Special Reference to the Fluoridation of Public Water Supplies," *Journal of Applied Chemistry*, **1969**, *19*(4), 100–102 ("*Crosby 1969*").

[0191] Cui, B., *et al.*, "Waste to wealth: Defect-rich ni-incorporated spent lifepo4 for efficient oxygen evolution reaction," *Sci. China Mater.*, **2021**, *64*, 2710-2718 ("*Cui 2021*").

[0192] Das, P., *et al.*, "Remediation of perfluorooctane sulfonate in contaminated soils by modified clay adsorbent—a risk-based approach," *Water Air Soil Pollut.*, **2013**, *224*, 1-14 ("*Das 2013*").

[0193] Dastgheib, S. A., *et al.*, "Thermogravimetric Studies for the Incineration of an Anion

Exchange Resin Laden with Short- or Long-Chain PFAS Compounds Containing Carboxylic or Sulfonic Acid Functionalities in the Presence or Absence of Calcium Oxide," *Ind Eng Chem Res*, **2021**, *60*(47), 16961–16968 ("*Dastgheib 2021*").

[0194] Deng, B., *et al.*, "Heavy metal removal from coal fly ash for low carbon footprint cement," *Commun. Eng.*, **2023**, *2*, 13 ("*Deng I 2023*").

[0195] Deng, B., *et al.*, "High-temperature electrothermal remediation of multi-pollutants in soil," *Nat. Commun.*, **2023**, *14*, 6371 ("*Deng II 2023*").

[0196] Deng, B., *et al.*, "Rare earth elements from waste," *Sci. Adv.*, **2022**, *8*, eabm3132 ("*Deng 2022*").

[0197] Deng, B., *et al.*, "Urban mining by flash Joule heating," *Nat. Commun.*, **2021**, *12*, 5794 ("*Deng 2021*").

[0198] Dombrowski, P. M., *et al.*, "Technology review and evaluation of different chemical oxidation conditions on treatability of pfas.," *Remediation*, **2018**, *28*, 135-150 ("*Dombrowski 2018*").

[0199] Dong, P. A. V., *et al.*, "Economic and environmental assessment of recovery and disposal pathways for CFRP waste management," *Resour. Conserv. Recycl.*, **2018**, *133*, 63-75 ("*Dong 2018*").

[0200] Dong, Q., *et al.*, "Depolymerization of plastics by means of electrified spatiotemporal heating," *Nature*, **2023**, *616*, 488-494 ("*Dong 2023*").

[0201] Dong, Q., *et al.*, "Programmable heating and quenching for efficient thermochemical synthesis, *Nature*, **2022**, *605*, 470-476 ("*Dong 2022*").

[0202] Duan, L., *et al.*, "Efficient photocatalytic pfoa degradation over boron nitride," *Environ. Sci. Technol. Lett.*, **2020**, *7*, 613-619 ("*Duan 2020*").

[0203] Duchesne, A. L., *et al.*, "Remediation of PFAS-Contaminated Soil and Granular Activated Carbon by Smoldering Combustion," *Environ Sci Technol*, **2020**, *54*(19), 12631–

12640 ("*Duchesne 2020*").

[0204] Dudarev, S. L., *et al.*, "Electron-energy-loss spectra and the structural stability of nickel oxide: An LSDA+ U study," *Phys. Rev. B*, **1988**, *57*, 1505 ("*Dudarev 1998*").

[0205] Ellis, D. A., *et al.*, "Thermolysis of Fluoropolymers as a Potential Source of Halogenated Organic Acids in the Environment," *Nature*, **2001**, *412*(6844), 321–324 ("*Ellis 2001*").

[0206] Evich, M. G., *et al.*, "Per-and Polyfluoroalkyl Substances in the Environment," *Science*, **2022**, *375*, eabg9065 ("*Evich 2022*").

[0207] Faé, G. S., *et al.*, "Making soil particle size analysis by laser diffraction compatible with standard soil texture determination methods," *Soil Sci. Soc. Am. J.*, **2019**, *83*, 1244-1252 ("*Faé 2019*").

[0208] Feng, G., *et al.*, "Highly selective photoelectroreduction of carbon dioxide to ethanol over graphene/silicon carbide composites," *Angew. Chem. Int. Ed.*, **2023**, *135*, e202218664 ("*Feng 2023*").

[0209] Flores, C., *et al.*, "Occurrence of Perfluorooctane Sulfonate (PFOS) and Perfluorooctanoate (PFOA) in N.E. Spanish Surface Waters and Their Removal in a Drinking Water Treatment Plant That Combines Conventional and Advanced Treatments in Parallel Lines," *Sci Total Environ*, **2013**, *461 462*, 618–626 ("*Flores 2013*").

[0210] Fournie, T., *et al.*, "Smouldering to treat PFAS in sewage sludge," *Waste Management*, **2023**, *164*, 219-227 ("*Fournie 2023*").

[0211] Glüge, J., *et al.*, "An Overview of the Uses of Per-and Polyfluoroalkyl Substances (PFAS)," *Environ. Sci. Process. Impacts*, **2020**, *22*, 2345-2373 ("*Glüge 2020*").

[0212] Gorrochategui, E., *et al.*, "Perfluoroalkylated substance effects in Xenopus laevis A6 kidney epithelial cells determined by ATR-FTIR spectroscopy and chemometric analysis," *Chem. Res. Toxicol.*, **2016**, *29*, 924-932 ("*Gorrochategui 2016*").

[0213] Guin, J. P., *et al.*, "Challenges Facing Sustainable Visible Light Induced Degradation of Poly- and Perfluoroalkyls (PFA) in Water: A Critical Review," *ACS Engineering Au*, **2022**, *2*(3), 134–150 ("*Guin 2022*").

[0214] Guo, X., *et al.*, "Nonlinear optical properties of 6H-SiC and 4H-SiC in an extensive spectral range," *Opt. Mater. Express*, **2021**, *11*, 1080-1092 ("*Guo 2021*").

[0215] Guo, X., *et al.*, "Preparation of SiC powders by carbothermal reduction with bamboo charcoal as renewable carbon source," *J. Adv. Ceram.*, **2013**, *2*, 128-134 ("*Guo 2013*").

[0216] Hale, S. E., *et al.*, "Sorbent amendment as a remediation strategy to reduce pfas mobility and leaching in a contaminated sandy soil from a norwegian firefighting training facility," *Chemosphere*, **2017**, *171*, 9-18 ("*Hale 2017*").

[0217] Han, X., *et al.* "Epitaxial cubic silicon carbide photocathodes for visible-light-driven water splitting," *Chem. Eur. J.*, **2020**, *26*, 3586-3590 ("*Han 2020*").

[0218] Helalia, A. M., "The relation between soil infiltration and effective porosity in different soils," *Agr. Water Manage.*, **1993**, *24*, 39-47 ("*Helalia 1993*").

[0219] Henkelman, G., *et al.*, "A climbing image nudged elastic band method for finding saddle points and minimum energy paths," *J. Chem. Phys.*, **2000**, *113*, 9901-9904 ("*Henkelman 2000*").

[0220] Hillier, S., "Quantitative analysis of clay and other minerals in sandstones by X-ray powder diffraction (XRPD), *Clay mineral cements in sandstones*, **1999**, 213-251 ("*Hillier 1999*").

[0221] Huang, D., *et al.*, "Photoinduced hydrodefluorination mechanisms of perfluorooctanoic acid by the sic/graphene catalyst," *Environ. Sci. Technol.*, **2016**, *50*, 5857-5863 ("*Huang 2016*").

[0222] Huang, P.-J. *et al.*, "Reusable functionalized hydrogel sorbents for removing long-and short-chain perfluoroalkyl acids (PFAAs) and GenX from aqueous solution," *ACS omega*,

2018, *3*, 17447-17455 ("*Huang 2018*").

[0223] Hunter Anderson, R., *et al.*, "Partitioning of Poly- and Perfluoroalkyl Substances from Soil to Groundwater within Aqueous Film-Forming Foam Source Zones," *J Contam Hydrol*, **2019**, *220*, 59–65 ("*Hunter Anderson 2019*").

[0224] Inkotte, J., *et al.*, "Litter removal impacts on soil biodiversity and eucalypt plantation development in the seasonal tropics," *J. Forest. Res.*, **2023**, *34*, 735-748 ("*Inkotte 2023*").

[0225] Javaherian, M., *et. al.*, "Bench-scale veg research & development study: Implementation memorandum for ex-situ thermal desorption of perfluoroalkyl compounds (pfcs) in soils," Endpoint Consulting Technical Memorandum, **2016** ("*Javaherian 2016*").

[0226] Jha, H. S., *et al.*, "Highly crystalline silicon carbide thin films grown at low substrate temperature by HWCVD technique," *J. Mater. Sci: Mater. Electron.*, **2015**, *26*, 1381-1388 ("*Jha 2015*").

[0227] Jia, C., *et al.*, "Graphene environmental footprint greatly reduced when derived from biomass waste via flash Joule heating," *One Earth*, **2022**, *5*, 1394-1403 ("*Jia 2022*").

[0228] Jia, X., *et al.*, "Emerging and Legacy Per- and Polyfluoroalkyl Substances in an Elderly Population in Jinan, China: The Exposure Level, Short-Term Variation, and Intake Assessment," *Environ Sci Technol*, **2022**, *56*(12), 7905–7916 ("*Jia 2022*").

[0229] Jiang, R., *et al.*, "Ultrafast synthesis for functional nanomaterials," *Cell Rep. Phys. Sci.*, **2021**, *2* ("*Jiang 2021*").

[0230] Judy, J. D., *et al.*, "Trophic Transfer Of Pfas From Tomato (Solanum Lycopersicum) To Tobacco Hornworm (Manduca Sexta) Caterpillars," *Environ. Pollut.*, **2022**, *310*, 119814 ("*Judy 2022*").

[0231] Kresse, G., *et al.*, "Efficient iterative schemes for ab initio total-energy calculations using a plane-wave basis set," *Phys. Rev. B*, **1996**, *54*, 11169-11186 ("*Kresse 1996*").

[0232] Kupryianchyk, D., *et al.*, "Treatment of sites contaminated with perfluorinated

compounds using biochar amendment," *Chemosphere*, **2016**, *142*, 35-40 ("*Kupryianchyk 2016*").

[0233] Labine, L. M, *et al.*, "Comparison of sub-lethal metabolic perturbations of select legacy and novel perfluorinated alkyl substances (PFAS) in Daphnia magna," *Environ. Res.*, **2022**, *212*, 113582 ("*Labine 2022*").

[0234] Lee, M. C., *et al.*, "Efficient Destruction of CF_4 through in Situ Generation of Alkali Metals from Heated Alkali Halide Reducing Mixtures," *Environ Sci Technol*, **2002**, *36*(6), 1367–1371 ("*Lee 2002*").

[0235] Leeson, A., *et al.*, "Identifying and Managing Aqueous Film-Forming Foam-Derived Per- and Polyfluoroalkyl Substances in the Environment," *Environ. Toxicol. Chem.*, **2021**, *40*, 24-36 ("*Leeson 2021*").

[0236] Lin, L., *et al.*, "Copyrolysis of recycled plastics and biomass reduces biochar bioavailable silicon production and cadmium phytotoxicity," *ACS EST Engg.*, **2022**, *2*, 1356-1364 ("*Lin 2022*").

[0237] Liu, C. S., *et al.*, "Oxidative decomposition of perfluorooctanesulfonate in water by permanganate," *Sep. Purif. Technol.*, **2012**, *87*, 95-100 ("*Liu 2012*").

[0238] Liu, S., *et al.*, "Extreme environmental thermal shock induced dislocation-rich Pt nanoparticles boosting hydrogen evolution reaction," *Adv. Mater.*, **2022**, *34*, 2106973-2106979 ("*Liu 2022*").

[0239] Liu, Y. L., *et al.*, "Ion Exchange Removal and Resin Regeneration to Treat Per- and Polyfluoroalkyl Ether Acids and Other Emerging PFAS in Drinking Water," *Water Res*, **2021**, *207*, 117781 ("*Liu 2021*").

[0240] Liu, Y., *et al.*, "Method of recovering the fibrous fraction of glass/epoxy composites," *J. Reinf. Plast. Compos.*, **2006**, *25*, 1525-1533 ("*Liu 2006*").

[0241] Luo, J., *et al.*, "Waste plastics complement biochar: Innovative approach in curbing

toxicants (kcn/nacn) in n-containing biochar," *ACS Sustainable Chem. Eng.*, **2021**, *9*, 4617-4624 ("*Luo 2021*").

[0242] Luong, D. X., *et al.*, "Gram-Scale Bottom-up Flash Graphene Synthesis," *Nature*, **2020**, *577*, 647 ("*Luong 2020*").

[0243] Mahinroosta, R., *et al.*, "A review of the emerging treatment technologies for pfas contaminated soils," *J. Environ. Manage.*, **2020**, *255*, 109896 ("*Mahinroosta 2020*").

[0244] Maimaiti, A., *et al.*, "Competitive adsorption of perfluoroalkyl substances on anion exchange resins in simulated afff-impacted groundwater," *Chem. Eng. J.*, **2018**, *348*, 494-502 ("*Maimaiti 2018*").

[0245] Makuła, P., *et al.*, "How to correctly determine the band gap energy of modified semiconductor photocatalysts based on UV–Vis spectra," *J. Phys. Chem. Lett*, **2018**, *9*, 6814-6817 ("*Makula 2018*").

[0246] McCleaf, P., *et al.*, "Removal Efficiency of Multiple Poly- and Perfluoroalkyl Substances (PFASs) in Drinking Water Using Granular Activated Carbon (GAC) and Anion Exchange (AE) Column Tests," *Water Res*, **2017**, *120*, 77–87 ("*McCleaf 2017*").

[0247] Mehlich, A., "Mehlich 3 soil test extractant: A modification of mehlich 2 extractant," *Commun. Soil Sci. Plant Anal.*, **1984**, *15*, 1409-1416 ("*Mehlich 1984*").

[0248] Min, T. B., *et al.*, "Experimental Study on the Development of Compressive Strength of Early Concrete Age Using Calcium-Based Hardening Accelerator and High Early Strength Cement," *Constr Build Mater*, **2014**, *64*, 208–214 ("*Min 2014*").

[0249] Monkhorst, H. J., *et al.*, "Special points for Brillouin-zone integrations," *Phys. Rev. B*, **1976**, *13*, 5188 ("*Monkhorst 1976*").

[0250] Nath, P., *et al.*, "Use of OPC to Improve Setting and Early Strength Properties of Low Calcium Fly Ash Geopolymer Concrete Cured at Room Temperature," *Cem Concr Compos*, **2015**, *55*, 205–214 ("*Nath 2015*").

[0251] Perdew, J. P., *et al.*, "Generalized gradient approximation made simple," *Phys. Rev. Lett.*, **1996**, *77*, 3865-3868 ("*Perdew 1996*").

[0252] Pilbeam, D. J., *et al.*, *Handbook of plant nutrition*, CRC Press, **2016** ("*Pilbeam 2016*").

[0253] Salvatore, D., *et al.*, "Presumptive Contamination: A New Approach to PFAS Contamination Based on Likely Sources," *Environ. Sci. Technol. Lett.*, **2022**, *9*, 983-990 ("*Salvatore 2022*").

[0254] Schaefer, C. E., *et al.*, "Release Of Poly- And Perfluoroalkyl Substances From Finished Biosolids In Soil Mesocosms," *Water Res.*, **2022**, *217*, 118405 ("*Schaefer 2022*").

[0255] Scher, D. P., *et al.*, "Occurrence of Perfluoroalkyl Substances (PFAS) in Garden Produce at Homes with a History of PFAS-Contaminated Drinking Water," *Chemosphere*, **2018**, *196*, 548–555 ("*Scher 2018*").

[0256] Shin, Y., *et al.*, "Synthesis of SiC ceramics by the carbothermal reduction of mineralized wood with silica," *Adv. Mater.*, **2005**, *17*, 73-77 ("*Shin 2005*").

[0257] Siciliano, S. D., *et al.*, "Soil fertility is associated with fungal and bacterial richness, whereas pH is associated with community composition in polar soil microbial communities," *Soil Biol. Biochem.*, **2014**, *78*, 10-20 ("*Siciliano 2014*").

[0258] Sonmez Baghirzade, B., *et al.*, "Thermal Regeneration of Spent Granular Activated Carbon Presents an Opportunity to Break the Forever PFAS Cycle," *Environ Sci Technol*, **2021**, *55*(9), 5608–5619 ("*Sonmez Baghirzade 2021*").

[0259] Sörengård, M., Lindh, *et al.*, "Thermal desorption as a high removal remediation technique for soils contaminated with per-and polyfluoroalkyl substances (pfass)," *PloS one*, **2020**, *15*, e0234476 ("*Sörengård 2020*").

[0260] Stanford, M. G., *et al.*, "Flash graphene morphologies," *ACS Nano*, **2020**, *14*, 13691-13699 ("*Stanford 2020*").

[0261] Stoiber, T., *et al.*, "Disposal of Products and Materials Containing Per- and

Polyfluoroalkyl Substances (PFAS): A Cyclical Problem," *Chemosphere*, **2020**, *260*, 127659 ("*Stoiber 2020*").

[0262] Sun, C., *et al.*, "Interfacial coupled design of epitaxial graphene@SiC schottky junction with built-in electric field for high-performance anodes of lithium ion batteries," *Nano Energy*, **2020**, *77*, 105092 ("*Sun 2020*").

[0263] Sun, L., *et al.*, "Millisecond self-heating and quenching synthesis of Fe/carbon nanocomposite for superior reductive remediation, *Appl. Catal. B*, **2023**, *342*, 123361 ("*Sun 2023*").

[0264] Sun, X., *et al.*, "SiC nanofibers as long-life lithium-ion battery anode materials," *Front. Chem.*, **2018**, ***6***, 166 ("*Sun 2018*").

[0265] B. Trang, *et al.*, "Low-temperature mineralization of perfluorocarboxylic acids," *Science*, **2022**, *377*, 839-845 ("*Trang 2022*").

[0266] Vargette, L. D., *et al.*, "Prospects of complete mineralization of per-and polyfluoroalkyl substances by thermal destruction methods," *Curr. Opin. Chem. Eng.*, **2022**, *42*, 100954 ("*Vargette 2023*").

[0267] Vecitis, C. D., *et al.*, "Treatment technologies for aqueous perfluorooctanesulfonate (pfos) and perfluorooctanoate (pfoa)," *Front. Environ. Sci. Eng. China*, **2009**, *3*, 129-151 ("*Vecitis 2009*").

[0268] Wang, C., *et al.*, "A general method to synthesize and sinter bulk ceramics in seconds," *Science*, **2020**, *368*, 521-526 ("*Wang 2020*").

[0269] Wang, F., *et al.*, "Effectiveness and Mechanisms of Defluorination of Perfluorinated Alkyl Substances by Calcium Compounds during Waste Thermal Treatment," *Environ Sci Technol*, **2015**, *49*(9), 5672–5680 ("*Wang 2015*").

[0270] Wang, F., *et al.*, "Mineralization behavior of fluorine in perfluorooctanesulfonate (pfos) during thermal treatment of lime-conditioned sludge," *Environ. Sci. Technol.*, **2013**, *47*, 2621-

2627 ("*Wang 2013*").

[0271] Wang, F., *et al.*, "Influence of Calcium Hydroxide on the Fate of Perfluorooctanesulfonate under Thermal Conditions," *J Hazard Mater*, **2011**, *192*(3), 1067–1071 ("*Wang 2011*").

[0272] Washington, J. W., *et al.*, "Decades-Scale Degradation Of Commercial, Side-Chain, Fluorotelomer-Based Polymers In Soils And Water," *Environ. Sci. Technol.*, **2015**, *49*, 915-923 ("*Washington 2015*").

[0273] Watanabe, N., *et al.*, "Thermal Mineralization Behavior of PFOA, PFHxA, and PFOS during Reactivation of Granular Activated Carbon (GAC) in Nitrogen Atmosphere," *Environmental Science and Pollution Research*, **2018**, *25*(8), 7200–7205 ("*Watanabe 2018*").

[0274] Watanabe, N., *et al.*, "Residual Organic Fluorinated Compounds from Thermal Treatment of PFOA, PFHxA and PFOS Adsorbed onto Granular Activated Carbon (GAC)," *Journal of Material Cycles and Waste Management*, **2016**, *18*(4), 625–630 ("*Watanabe 2016*").

[0275] Weber, N. H., *et al.*, "Kinetics of Decomposition of PFOS Relevant to Thermal Desorption Remediation of Soils," *Ind Eng Chem Res*, **2021**, *60*(25), 9080–9087 ("*Weber 2021*").

[0276] Weil, R., *et al.*, *The nature and properties of soils,* 15th edition, **2017** ("*Weil 2017*").

[0277] Whitacre, D.M., *et al.*, "Aquatic toxicology of perfluorinated chemicals," *Rev. Environ. Contam. Toxicol.*, **2010**, 1-52 ("*Whitacre 2010*").

[0278] Wyss, K. M., *et al.*, "Upcycling of waste plastic into hybrid carbon nanomaterials," *Adv. Mater.*, **2023**, *35*, 2209621 ("*Wyss I 2023*").

[0279] Wyss, K. M., *et al.*, "Upcycling of waste plastic into hybrid carbon nanomaterials," *Adv. Mater.*, **2023**, *35*, 2209621 ("*Wyss II 2023*").

[0280] Wyss, K., *et al.*, "Upcycling and urban mining for nanomaterial synthesis," *Nano Today*, **2023**, *49*, 101781 ("*Wyss III 2023*").

[0281] Xiao, F., *et al.*, "Thermal Stability and Decomposition of Perfluoroalkyl Substances on Spent Granular Activated Carbon," *Environ Sci Technol Lett*, **2020**, *7*(5), 343–350 ("*Xiao 2020*").

[0282] Xiao, F., *et al.*, "PFOA and PFOS Are Generated from Zwitterionic and Cationic Precursor Compounds during Water Disinfection with Chlorine or Ozone," *Environ Sci Technol Lett*, **2018**, *5*(6), 382–388 ("*Xiao 2018*").

[0283] Xiao, F., *et al.*, "Mechanisms for Removal of Perfluorooctane Sulfonate (PFOS) and Perfluorooctanoate (PFOA) from Drinking Water by Conventional and Enhanced Coagulation," *Water Res*, **2013**, *47*(1), 49–56 ("*Xiao 2013*").

[0284] Xiao, X., *et al.*, "Sorption of Poly- and Perfluoroalkyl Substances (PFASs) Relevant to Aqueous Film-Forming Foam (AFFF)-Impacted Groundwater by Biochars and Activated Carbon," *Environ Sci Technol*, **2017**, *51*(11), 6342–6351 ("*Xiao 2017*").

[0285] Xu, T., *et al.*, "Enhanced Photocatalytic Degradation of Perfluorooctanoic Acid Using Carbon-Modified Bismuth Phosphate Composite: Effectiveness, Material Synergy and Roles of Carbon," *Chemical Engineering Journal*, **2020**, *395*, 124991 ("*Xu 2020*").

[0286] Xue, X., *et al.*, "A technology review of recycling methods for fiber-reinforced thermosets," *J. Reinf. Plast. Compos.*, **2021**, *41*, 459-480 ("*Xue 2021*").

[0287] Yakobson, B. I., *et al.*, "Flash Graphene Morphologies," *ACS Nano*, **2020**, *14*(10), 13691–13699 ("*Yakobson 2020*").

[0288] Yang, F., *et al.*, "Biomass inherent metal interfere carbothermal reduction modification of biochar for cd immobilization," *Sci. Total Environ.*, **2023**, *867*, 161425 ("*Yang 2023*").

[0289] Yang, Z., *et al.*, "Degradation of Hexafluoropropylene Oxide Tetrameric Acid (HFPO-TeA) Using Electrocatalytic Ozone Technique," *Water Cycle*, **2022**, *3*, 106–111 ("*Yang 2022*").

[0290] Yeung, L. W. Y., *et al.*, "Perfluorinated Compounds and Total and Extractable Organic

Fluorine in Human Blood Samples from China," *Environ Sci Technol*, **2008**, *42*(21), 8140–8145 ("*Yeung 2008*").

[0291] You, Y., *et al.*, "Growth of NiO nanorods, SiC nanowires and monolayer graphene via a CVD method," *Green Chem.*, **2017**, *19*, 5599-5607 ("*You 2017*").

[0292] F. Yu *et al.*, "Rapid self-heating synthesis of Fe-based nanomaterial catalyst for advanced oxidation," *Nat. Commun.*, **2023**, *14*, 4975 ("*Yu 2023*").

[0293] Yu, M., *et al.*, "Silicon carbide ("SiC) derived from agricultural waste potentially competitive with silicon anodes," *Green Chem.*, **2022**, *24*, 4061-4070 ("*Yu* 2022").

[0294] Yu, M., *et al.*, "Adjusting SiO_2 : C mole ratios in rice hull ash ("RHA) to control carbothermal reduction to nanostructured SiC, Si_3N_4 or Si_2N_2O composites," *Green Chem.*, **2021**, *23*, 7751-7762 ("*Yu 2021*").

[0295] Zhang, B., *et al.*, "Eluviation of dissolved organic carbon under wetting and drying and its influence on water infiltration in degraded soils restored with vegetation," *Eur. J. Soil Sci.*, **2004**, *55*, 725-737 ("*Zhang 2004*").

[0296] Zhang, D., *et al.*, "Sorption of Perfluoroalkylated Substances (PFASs) onto Granular Activated Carbon and Biochar," *Environ Technol.*, **2019**, *42*(12), 1798–1809 ("*Zhang 2019*").

[0297] Zhang, K., *et al.*, "Destruction of perfluorooctane sulfonate (pfos) and perfluorooctanoic acid (pfoa) by ball milling," *Environ. Sci. Technol.*, **2013**, *47*, 6471-6477 ("*Zhang 2013*").

[0298] Zhao, C., *et al.*, "Thermal desorption for remediation of contaminated soil: A review, *Chemosphere*, **2019**, *221*, 841-855 ("*Zhao 2019*").

[0299] Zuur, A. F., *et al.*, "Glm and gam for count data," *Mixed effects models extensions in ecology with R*, **2009**, 209-243 ("*Zuur 2009*").

WHAT IS CLAIMED IS:

1. A method comprising:

(a) mixing a PFAS-contaminated soil with a conductive additive to form a PFAS-contaminated soil mixture, wherein

(i) the PFAS-contaminated soil is soil that comprises a pollutant selected from the group consisting of per- and polyfluorinated alkyl substances (PFAS); and

(b) performing a rapid electrothermal mineralization (REM) process utilizing the PFAS-contaminated soil mixture to remediate the PFAS-contaminated soil.

2. The method of Claim 1, wherein the PFAS is selected from the group consisting of perfluorooctane acid (PFOA), perfluorooctane sulfonate (PFOS), perfluorohexane sulfonate (PFH_xS), perfluorobutane sulfonate (PFBS), polytetrafluoroethylene (PTFE), and combinations thereof.

3. The method of any of Claims 1-2, wherein the step of performing the REM process comprises subjecting the PFAS-contaminated soil mixture to a flash Joule heating process.

4. The method of any of Claims 1-3, the REM process remediates the PFAS-contaminated soil by removing more than 90 wt% of the PFAS from the PFAS-contaminated soil.

5. The method of Claim 4, the REM process remediates the PFAS-contaminated soil by removing more than 99 wt% of the PFAS from the PFAS-contaminated soil.

6. The method of any of Claims 1-5, wherein the method further comprises removing the PFAS-contaminated soil from the ground before the step of performing the REM process.

7. The method of any of Claims 1-6, wherein

(a) the PFAS-contaminated soil is ground soil located on the ground (PFAS-contaminated ground soil);

(b) the step of mixing the PFAS-contaminated soil with the conductive additive comprises mixing the conductive additive to the PFAS-contaminated ground soil on-site in the ground; and

(c) the step of performing the REM process comprises utilizing electrodes inserted in the ground.

8. The method of Claim 7, wherein,

(a) the step of performing the REM process comprises utilizing two or more electrode arrays, and

(b) the two or more electrode arrays comprise the electrodes inserted in the ground.

9. The method of Claim 8, wherein, during the step of performing the REM process, the two or more electrode arrays are utilized by independently discharging each of the two or more electrode arrays.

10. The method of Claim 9, wherein the independent discharging of each of the two or more electrode arrays uniformly heats the soil around the two or more electrodes.

11. The method of any of Claims 1-10, wherein the method further comprises that, after the REM process, separating at least some of the conductive carbon additive from the remediated PFAS-contaminated soil.

12. The method of Claim 11, wherein the step of separating is based upon grain size of the conductive carbon additive and particle size of the remediated PFAS-contaminated soil.

13. The method of Claim 11, wherein the step of separating is based upon difference in densities between the conductive carbon additive and the remediated PFAS-contaminated soil.

14. The method of any of Claims 1-13, wherein at least some of the PFAS are mineralized into a fluoride salt.

15. The method of any of Claims 1-14, wherein graphene is formed during the step of performing the REM process.

16. A method comprising:

(a) mixing a contaminated soil with a conductive additive to form a contaminated soil mixture, wherein

(i) the contaminated soil is soil that comprises a pollutant selected from the group consisting of halogen-containing contaminates; and

(b) performing a rapid electrothermal mineralization (REM) process utilizing the contaminated soil mixture to remediate the contaminated soil.

17. The method of Claim 16, wherein the pollutant is selected from the group consisting of tetrachloroethylene (PCE), trichloroethylene (TCE), polychlorinated biphenyls (PCB), brominated flame retardants (BFR), and halogen-containing antibiotics.

18. The method of Claim 16, wherein the pollutant comprises the halogen-containing antibiotic and the halogen-containing antibiotic is selected from the group consisting of ciprofloxacin, chloramphenicol, and iodoquinol.

19. An apparatus that performs the method of any of Claims 1-18.

20. Graphene made by the method of Claim 15.

ABSTRACT

[0300] Methods for remediating soil having persistent and bioaccumulative pollutants, and more particularly, methods for remediating soil having per- and polyfluorinated alkyl substances (PFAS) and other halogen-containing contaminates by rapid electrothermal mineralization.

METHODS FOR REMEDIATION OF CONTAMINATED SOIL BY RAPID ELECTROTHERMAL MINERALIZATION

CROSS-REFERENCED TO RELATED PATENT APPLICATIONS

[0001] The application claims priority to U.S. Patent Appl. Serial No. 63/589,489, to James Mitchell Tour, *et al.*, entitled "Methods For Remediation Of PFAS-Contaminated Soil By Rapid Electrothermal Mineralization," October 11, 2023, which patent application is commonly owned by the owner of the present invention and is incorporated herein in its entirety.

[0002] The application is related to PCT Patent Appl. Serial No. PCT/US24/033209, entitled "Methods Of Flash Joule Heating Per- And Polyfluorinated Alkyl Substances And Compositions Thereof, filed June 10, 2024, to James M. Tour, *et al* ("*Tour '209 PCT Application*"), claiming priority to U.S. Patent Appl. Serial No. 63/507,045, entitled "Methods Of Flash Joule Heating Per- And Polyfluorinated Alkyl Substances And Compositions Thereof," filed June 8, 2023, to James M. Tour, *et al*, all of which patent applications are commonly owned by the owner of the present invention. The *Tour '209 PCT Application* is incorporated herein in its entirety.

[0003] This application is also related to U.S. Patent Appl. Serial No. 18/263,831, entitled "Ultrafast Flash Joule Heating Synthesis Methods And Systems For Performing Same," filed August 1, 2023, to James M. Tour *et al.* ("*Tour '831 Application*"), which is the U.S. § 371 nationalization of PCT Patent Appl. Serial No. PCT/US22/14923, entitled "Ultrafast Flash Joule Heating Synthesis Methods And Systems For Performing Same," filed February 2, 2022, to James M. Tour *et al.*, claiming priority to U.S. Patent Appl. Serial No. 63/144,862, filed February 2, 2021, all of which patent applications are commonly owned by the owner of the present invention. The *Tour '831 Application* is incorporated herein in its entirety.

[0004] The application is also related to U.S. Patent Appl. Serial No. 18/246,460, entitled "Ultrafast Flash Joule Heating Synthesis Methods And Systems For Performing Same," filed

March 23, 2023, to James M. Tour, *et al.* ("*Tour '460 Application*"), which is the U.S. § 371 nationalization of PCT Patent Appl. Serial No. PCT/US21/52070, entitled "Ultrafast Flash Joule Heating Synthesis Methods And Systems For Performing Same," filed September 24, 2021, to James M. Tour *et al.,* claiming priority to U.S. Patent Appl. Serial No. 63/082,592, filed September 24, 2020 and U.S. Patent Appl. Seral No. 63/144,862, filed February 2, 2021. A copy of the *Tour '460 Application* is incorporated herein in its entirety.

[0005]

TECHNICAL FIELD

[0006] The present invention relates to methods for remediating soil having persistent and bioaccumulative pollutants, and, more particularly, methods for remediating soil having per- and polyfluorinated alkyl substances (PFAS) and other halogen-containing contaminates by rapid electrothermal mineralization.

GOVERNMENT INTEREST

[0007] This invention was made with government support under Grant No. FA9550-22-1-0526, awarded by the United States Air Force Office of Scientific Research, and Grant Nos. W912HZ-21-2-0050 and W912HZ-24-2-0027, awarded by the United States Engineer Research and Development Center for the United States Army Corp of Engineers. The government has certain rights in the invention.

BACKGROUND

[0008] Per- and polyfluoroalkyl substances (PFAS) are persistent and bioaccumulative pollutants that can easily accumulate in soil, posing a threat to environment and human health. PFAS include more than 10,000 man-made substances that all have tight chemical bonds between their carbon and fluorine atoms. PFAS are often referred to as "forever chemicals," in that they are recalcitrant in the environment and in biological organisms, including humans. They have entered the human food chain through freshwater fish and food grown on

contaminated fields. Current PFAS degradation processes suffer from low efficiency, high energy and water consumption, or lack of generality.

[0009] PFAS are a diverse class of anthropogenic chemicals that are extensively used in plastics, textiles, food wrapping materials, and fire-fighting foam. [*Evich 2022*; *Glüge 2020*]. PFAS can easily accumulate in soil through waste disposal and animal migration and has been proven to be bioaccumulative and toxic to humans and wildlife. [*Leeson 2021*; *Salvatore 2022*; *Schaefer 2022*; *Judy 2022*]. Due to the high bond energy of C-F (~485 kJ mol^{-1}) [*Huang 2016*] and resulting long half-lives (>100 years in soils) [*Washington 2015*], the efficient elimination of PFAS is difficult to realize by natural decomposition or microbiological treatment. [*Washington 2015*; *Maimaiti 2018*; *Duan 2020*].

[0010] Many efforts have been devoted to the remediation of PFAS-contaminated soil in the past decade, mainly including stabilization [*Hale 2017*; *Das 2013*; *Kupryianchyk 2016*], chemical oxidation [*Vecitis 2009*; *Dombrowski 2018*; *Mahinroosta 2020*] and thermal treatment [*Javaherian 2016*; *Sörengård 2020*; *Xiao 2020*]. The stabilization method involves mixing sorbents, such as activated carbon or clay, with the contaminated soil to sorb PFAS and reduces PFAS mobility and bioavailability [*Hale 2017*; *Das 2013*; *Kupryianchyk 2016*]. However, this method does not degrade PFAS in soil and sorbed PFAS could still pose long-term environmental damage. Chemical treatment uses strong oxidants to oxidize PFAS. [*Vecitis 2009*; *Dombrowski 2018*; *Mahinroosta 2020*]. The residual oxidants need to be washed out with a large amount of water to avoid its damage to the soil, where the wastewater could lead to secondary pollution to the environment. Traditional thermal treatment requires furnace heating for PFAS desorption and degradation, which often lasts for hours at 400-1100 °C. [*Javaherian 2016*; *Sörengård 2020*; *Xiao 2020*; *Vargette 2023*]. Some toxic short-chain fluorocarbon compounds, such as CF_4, C_2F_6, and C_2F_4, could be generated and emitted to the environment during this process. This is due to inadequate decomposition of C-

F bonds, which will cause secondary pollution [*Vargette 2023*; *Alinezhad 2022*] and the extended heating also degrades soil properties [*Zhao 2019*]. Therefore, developing an efficient, economical and general method for remediation of PFAS-contaminated soil is highly desirable, but remains challenging yet.

[0011] Converting PFAS into non-toxic metal fluoride with the aid of alkali or alkaline earth metal ions like calcium ions (Ca^{2+}) under thermal treatment, termed as mineralization, is promising for PFAS degradation. [*Wang 2011*; *Wang 2013*; *Wang 2015*; *Fournie 2023*]. However, traditional furnace heating often lasts hours, consuming large amounts of energy and the PFAS mineralization ratios are typically < 80%. Moreover, additional calcium compounds are always required for PFAS mineralization, leading to high material consumption. [*Wang 2011*; *Wang 2013*; *Wang 2015*; *Fournie 2023*].

[0012] Hence, developing an efficient, economical and general thermal process for remediation of PFAS-contaminated soil is highly desirable, especially if the soil can remain in place and need not be excavated or transported. Accordingly, a need remains for PFAS remediation processes that do not suffer from low efficiency, high energy and water consumption, and lack of generality.

SUMMARY OF THE INVENTION

[0013] The present invention relates to methods for remediating soil having persistent and bioaccumulative pollutants, and. more particularly, methods for remediating soil having per- and polyfluorinated alkyl substances (PFAS) and other halogen-containing contaminates by rapid electrothermal mineralization.

[0014] The present invention relates to a rapid electrothermal mineralization (REM) process to remediate PFAS-contaminated soil. With environmentally compatible biochar as the conductive additive, the soil temperature increases to >1000 °C within seconds by current pulse input, converting PFAS to calcium fluoride with inherent calcium compounds in soil This

process is applicable for remediating various PFAS contaminants in soil, with high removal efficiencies (>99%) and mineralization ratios (>90%). While retaining soil particle size, composition, water infiltration rate, and cation exchange, REM facilitates an increase of exchangeable nutrient supply and arthropod survival in soil, rendering it superior to the time-consuming calcination approach that severely degrades soil properties. REM is scaled up to remediate soil at two kilograms per batch and promising for large-scale, on-site soil remediation. Life-cycle assessment and techno-economic analysis demonstrate REM as an environmentally friendly and economic process, with a significant reduction of energy consumption, greenhouse gas emission, water consumption, and operation cost, when compared to existing soil remediation practices.

[0015] The present invention also relates to a REM process to remediate contaminated soil by mineralizing other halogen-containing contaminates, including tetrachloroethylene (PCE), trichloroethylene (TCE), polychlorinated biphenyls (PCB), tribromophenol (TBP), brominated flame retardants (BFR), and halogen-containing antibiotics, like ciprofloxacin, chloramphenicol, and iodoquinol.

[0016] In general, in one embodiment, the invention features a method that includes mixing a PFAS-contaminated soil with a conductive additive to form a PFAS-contaminated soil mixture. The PFAS-contaminated soil is soil that includes a pollutant selected from the group consisting of per- and polyfluorinated alkyl substances (PFAS). The method further includes performing a rapid electrothermal mineralization (REM) process utilizing the PFAS-contaminated soil mixture to remediate the PFAS-contaminated soil.

[0017] Implementations of the invention can include one or more of the following features:

[0018] The PFAS can be selected from the group consisting of perfluorooctane acid (PFOA), perfluorooctane sulfonate (PFOS), perfluorohexane sulfonate (PFH_xS), perfluorobutane sulfonate (PFBS), polytetrafluoroethylene (PTFE), and combinations thereof.

[0019] The PFAS can include exactly one per- and polyfluorinated alkyl substance selected from the group of the pollutant.

[0020] The PFAS can include two or more per- and polyfluorinated alkyl substances selected from the group of the pollutant.

[0021] The step of performing the REM process can include subjecting the PFAS-contaminated soil mixture to a flash Joule heating process.

[0022] The conductive additive can be selected from the group consisting of graphene, flash graphene, turbostratic graphene, anthracite coal, coconut shell-derived carbon, higher temperature-treated biochar, biochar, activated charcoal, calcined petroleum coke, metallurgical coke, coke, shungite, carbon nanomaterials, carbon nanotubes, asphaltenes, acetylene black, carbon black, ash, carbon fiber, and mixtures thereof.

[0023] The REM process can remediate the PFAS-contaminated soil by removing more than 90 wt% of the PFAS from the PFAS-contaminated soil.

[0024] The REM process can remediate the PFAS-contaminated soil by removing more than 99 wt% of the PFAS from the PFAS-contaminated soil.

[0025] The REM process can remediate the PFAS-contaminated soil by removing more than 99.9 wt% of the PFAS from the PFAS-contaminated soil.

[0026] 'The REM process can remediate the PFAS-contaminated soil by removing more than 99.99 wt% of the PFAS from the PFAS-contaminated soil.

[0027] The REM process can provide a fluorine mineralization ratio of more than 90% for the remediated PFAS-contaminated soil.

[0028] The method further can further include removing the PFAS-contaminated soil from the ground before the step of performing the REM process.

[0029] The step of removing the PFAS-contaminated soil from the ground can be performed before the step of mixing the PFAS-contaminated soil with the conductive additive.

[0030] The step of removing the PFAS-contaminated soil from the ground can be performed during the step of mixing the PFAS-contaminated soil with the conductive additive.

[0031] The step of removing the PFAS-contaminated soil from the ground can be performed after the step of mixing the PFAS-contaminated soil with the conductive additive.

[0032] The step of performing the REM process can be performed at an on-site location. The on-site location is a location at or near where the PFAS-contaminated soil was removed from the ground.

[0033] The REM process can be performed utilizing a REM reactor located at the on-site location.

[0034] The REM reactor can be a mobile REM reactor that can be transported to the on-site location.

[0035] The method can further include the step of transporting the REM reactor to the on-site location.

[0036] The step of performing the REM process can be performed at an off-site location. The off-site location is a location that is not at or near where the PFAS-contaminated soil was removed from the ground.

[0037] The method can further include transporting the PFAS-contaminated soil to the off-site location.

[0038] The REM process can be performed utilizing a REM reactor located at the off-site location.

[0039] The PFAS-contaminated soil can be ground soil located on the ground (PFAS-contaminated ground soil). The step of mixing the PFAS-contaminated soil with the conductive additive can include mixing the conductive additive to the PFAS-contaminated ground soil on-site in the ground. The step of performing the REM process can include utilizing electrodes inserted in the ground.

[0040] There can be a cover positioned over the PFAS-contaminated soil mixture when the REM process is performed.

[0041] The cover can be positioned over the PFAS-contaminated soil mixture after the step of mixing the PFAS-contaminated soil with the conductive additive.

[0042] The cover can form a seal about the PFAS-contaminated soil mixture.

[0043] The pressure about the PFAS-contaminated soil mixture can be at a low vacuum pressure during the REM process.

[0044] The method can further include inserting one or more evacuation tubes into the ground soil. The evacuation tubes can be utilized to assist in capturing one or more volatile components formed during the REM process.

[0045] The step of performing the REM process can include utilizing two or more electrode arrays. The two or more electrode arrays can include the electrodes inserted in the ground.

[0046] During the step of performing the REM process, the two or more electrode arrays can be utilized by independently discharging each of the two or more electrode arrays.

[0047] The independent discharging of each of the two or more electrode arrays can uniformly heat the soil around the two or more electrodes.

[0048] The two or more electrode arrays can be independently discharged in a predetermined pattern.

[0049] The conductive additive can be injected between the electrodes inserted in the ground.

[0050] The conductive additive can be injected in a predetermined pattern between the electrodes inserted in the ground.

[0051] The conductive additive can be injected as granules or as a slurry.

[0052] The conductive additive can be biochar.

[0053] The REM process can be performed under a vacuum.

[0054] The method can further include that, after the REM process, separating at least some of

the conductive carbon additive from the remediated PFAS-contaminated soil.

[0055] The step of separating can be based upon grain size of the conductive carbon additive and particle size of the remediated PFAS-contaminated soil.

[0056] The step of separating can include sieving to separate the at least some of the conductive carbon additive from the remediated PFAS-contaminated soil.

[0057] The step of separating can be based upon difference in densities between the conductive carbon additive and the remediated PFAS-contaminated soil.

[0058] The step of separating can include utilizing water to separating the at least some of the conductive carbon additive from the remediated PFAS-contaminated soil.

[0059] The at least some of the conductive carbon additive can float at or near the top surface of the water utilized for separating.

[0060] The step of separating can include decanting and/or skimming the at least some of the conductive carbon additive from the remediated PFAS-contaminated soil.

[0061] At least some of the PFAS can be mineralized into a fluoride salt.

[0062] The fluoride salt can be selected from the group consisting of calcium fluoride (CaF_2), magnesium fluoride (MgF_2), sodium fluoride (NaF), and potassium fluoride (KF).

[0063] Graphene can be formed during the step of performing the REM process.

[0064] The method can further include separating the graphene from the remediated PFAS-contaminated soil.

[0065] The method can further include collecting the graphene after the step of separating.

[0066] In general, in another embodiment, the invention features a method that includes mixing a contaminated soil with a conductive additive to form a contaminated soil mixture. The contaminated soil is soil that includes a pollutant selected from the group consisting of halogen-containing contaminates. The method further includes performing a rapid electrothermal mineralization (REM) process utilizing the contaminated soil mixture to remediate the

contaminated soil.

[0067] Implementations of the invention can include one or more of the following features:

[0068] The pollutant can be selected from the group consisting of tetrachloroethylene (PCE), trichloroethylene (TCE), polychlorinated biphenyls (PCB), brominated flame retardants (BFR), and halogen-containing antibiotics.

[0069] The pollutant can include halogen-containing antibiotics. The halogen-containing antibiotics can be selected from the group consisting of ciprofloxacin, chloramphenicol, and iodoquinol.

[0070] The pollutant can be tribromophenol (TBP).

[0071] In general, in another embodiment, the invention features an apparatus that performs any of the above-described methods.

[0072] Implementations of the invention can include one or more of the following features:

[0073] The apparatus can include a REM reactor.

[0074] In general, in another embodiment, the invention features graphene made any of the above-described methods.

BRIEF DESCRIPTION OF THE DRAWINGS

[0075] **FIGS. 1A-1G** show schematics rapid electrothermal mineralization (REM) process for the remediation of PFOA-contaminated soil. **FIG. 1A** is a conceptional schematic of REM process for soil remediation. **FIG. 1B** are pictures of the sample before (top) and during (bottom) the REM reaction. A spring coiled around the quartz tube is used to increase the mechanical integrity of the tube. **FIG. 1C** is a current curve with an input voltage of 100 V and a duration time of 1 s. **FIG. 1D** is a real-time temperature curve at an electric input of 100 V for 1 s recorded by an infrared thermometer. The temperature detection range of the thermometer is 200 to 1500 °C. **FIG. 1E** shows concentrations of organic fluorine and mineralized fluorine ion in PFOA-contaminated soil varied with input voltages. **FIG. 1F** shows

residual PFOA concentrations in soil after repetitive electric pulses, with voltage of 100 V and duration of 1 s each time. The error bars in **FIGS. 1E-1F** denote standard deviations, where $N = 3$. **FIG. 1G** is ^{19}F NMR spectra of the PFOA-contaminated soil extractant before (top) and after (bottom) REM. Inset of **FIG. 1G** shows the molecular structure of PFOA.

[0076] FIGS. 2A-2H show generality of REM process for various PFAS. **FIGS. 2A-2C** show concentrations of organic fluorine and mineralized fluorine ion varied with input voltages for, respectively, (a) PFOS-contaminated soil, (b) PFH_xS-contaminated soil and (c) PFBS-contaminated soil. **FIGS. 2D-2F** show ^{19}F NMR spectra of, respectively, the (d) PFOS, (e) PFH_xS and (f) PFBS -contaminated soil extractant before (top) and after (bottom) REM process. Inset in **FIGS. 2D-2F** are the molecular structure of PFOS, PFH_xS and PFBS, respectively. (The dots denote the F peaks and corresponding F-attached C atoms. **FIG. 2G** shows removal efficiencies of different kinds of PFASs. **FIG. 2H** shows mineralization ratios of different kinds of PFASs. The error bars in **FIGS 2A-2C** and **2G-2H** denote standard deviations, where $N = 3$.

[0077] FIGS. 3A-3H show mechanism of PFAS mineralization during the REM process. **FIG. 3A** shows XRD patterns of PFOA/biochar before (red) and after (blue) REM. **FIG. 3B** shows C 1*s* XPS fine spectra of PFOA/biochar before (top) and after (bottom) REM. **FIG. 3C** shows F 1*s* XPS fine spectra of PFOA/biochar before (top) and after (bottom) REM. **FIG. 3D** shows IR spectra of PFOA/biochar before (red) and after (blue) REM. **FIG. 3E** shows the Gibbs free energy change (ΔG) of each PFOA degradation step with (solid line) and without (dash line) Ca^{2+} varied with temperature. The dash line denotes $\Delta G = 0$ kJ mol^{-1}. **FIG. 3F** shows simulated variation of C-F bond ratio during REM process with calcium and without calcium. **FIG. 3G** shows optimized structure snapshots after simulated heating treatment with calcium (left, F105Ca96) or without calcium (right). **FIG. 3H** shows the relationship between C-F bond ratio after REM and the input atomic ratio of calcium and fluorine. Insets are the original

structure of PFOA (top right) and mineralized CaF_2 (bottom left).

[0078] FIGS. 4A-4H show soil properties after REM treatment. **FIG. 4A** is a picture of raw soil (left), REM soil (middle), and calcined soil (right). **FIG. 4B** shows particle size distribution of raw soil, REM soil, and calcined soil. The shadows denote standard deviations, where $N = 5$. **FIG. 4C** shows XRD patterns of raw soil, REM soil, and calcined soil. The powder diffraction file (PDF) reference card for quartz, 01-086-1629 (triangle). **FIG. 4D** shows XRF of raw soil, REM soil and calcined soil. **FIG. 4E** shows water penetration liquid level varied with time for raw soil, REM soil and calcined soil. **FIG. 4F** shows exchangeable soil nutrient content change after REM and calcination processes. c_0 and c are the concentrations of nutrients in raw soil and REM-treated soil, respectively. The error bars in **FIGS. 4E-4F** denote standard deviations, where $N = 3$. **FIG. 4G** shows survival ratio of springtail cultured in different soil samples. **FIG. 4H** shows survival ratio of isopod cultured in different soil samples. The error bars in **FIG. 4G-4H** denote standard deviations, which are calculated from model-predicted values from the generalized linear models with $N = 7$ and $N = 8$, respectively.

[0079] FIGS. 5A-5H show scalability, LCA and TEA for the remediation of PFAS-contaminated soil. **FIG. 5A** is a picture of the kilogram-scale REM process. **FIG. 5B** shows simulated distribution of current density on the soil surface with external voltage input. **FIG. 5C** shows the 3D mapping of PFOA removal efficiency. The mapping was sampled from 52 positions of 4 plane depths with an interval of 2 cm. **FIG. 5D** shows a materials flow analysis of REM. The dash rectangle denotes the system boundary. **FIG. 5E** shows comparison of cumulative energy demand. **FIG. 5F** shows comparison of cumulative GHG emission, **FIG. 5G** shows comparison of operating cost. **FIG. 5H** shows comprehensive comparison of different soil-remediation methods.

[0080] FIGS. 6A-6C show flow chart representation and boundary conditions for different LCA scenarios of (**FIG. 6A**) thermal treatment, (**FIG. 6B**) ball milling, and (**FIG. 6C**)

chemical oxidation. The dash rectangles denote the system boundaries.

[0081] FIGS. 7A-7E show TGA results for five different contaminates: (**FIG. 7A**) trichloroethylene (TCE); (**FIG. 7B**) tetrachloroethylene (PCE), (**FIG. 7C**) 2,4,6-tribromophenol (TBP), (**FIG. 7D**) 3-chlorobiphenyl (PCB 2), and (**FIG. 7A**) decachlorobiphenyl (PCB 209).

[0082] FIGS. 8A-8B show concentration of residue PCE in flash soil under different parameters. **FIG. 8A** shows PCE concentrations versus input voltage. **FIG. 8B** shows PCE concentrations versus flash times with different flash times. The error bars indicate the standard deviations, where $N = 3$.

[0083] FIG. 9 shows total Cl and Cl^- concentration in PCE-contaminated soil versus input voltage. The error bars indicate the standard deviations, where $N = 3$.

[0084] FIG. 10 shows total Cl and Cl^- concentration in TCE-contaminated soil versus input voltage. The error bars indicate the standard deviations, where $N = 3$.

[0085] FIG. 11 shows total Br and Br^- concentration in TBP-contaminated soil versus input voltage. The error bars indicate the standard deviations, where $N = 3$.

DETAILED DESCRIPTION

[0086] The present invention relates to methods for remediating soil having persistent and bioaccumulative pollutants, and more particularly, methods for remediating soil having per- and polyfluorinated alkyl substances (PFAS) and other halogen-containing contaminates by rapid electrothermal mineralization.

[0087] The emerging electric heating techniques, possessing the merits of rapid heating and cooling rates, short treatment duration and thus ultralow energy consumption, energy-efficient thermal treatment in material synthesis

[0088] The emerging direct electric heating techniques, possessing the merits of rapid heating and cooling rates, short treatment duration and thus ultralow energy consumption, can provide

a promising opportunity for PFAS mineralization. [*Jiang 2021*; *Luong 2020*; *Deng 2022*; *Deng I 2023*; *Deng II 2023*; Wyss *I 2023*; *Jia 2022*; *Dong 2023*; *Cheng 2021*; *Yu 2023*; *Sun 2023*].

[0089] The present invention relates to a rapid electrothermal mineralization (REM) method for the effective remediation of PFAS-contaminated soil. Using environmentally compatible biochar [*Yang 2023*; *Luo 2021*; *Lin 2022*] as the conductive additive, the temperature of contaminated soil rapidly escalates to >1000 °C within seconds through a direct current pulse input, with an ultrafast heating (~10^4 °C s^{-1}) and cooling rate (~10^3 °C s^{-1}). During REM, by virtue of the high Ca content inherent in soil and biochar, PFAS can be mineralized into calcium fluoride (CaF_2), a naturally occurring and non-toxic mineral.

[0090] In embodiments, this REM process conducted in a sealed system produces negligible harmful fluorocarbon gas emissions. High removal efficiencies (>99%) and fluorine mineralization ratios (>90%) for various PFAS were simultaneously realized, demonstrating the broad applicability of the REM process. REM facilitates an increased exchangeable nutrient supply of the treated soil, while maintaining soil particle size, composition, and water infiltration rate, rendering it superior to the time-extended calcination approach that severely degrades soil properties.

[0091] When further used for arthropod culture, REM soil exhibits a comparable arthropod survival ratio with the clean raw soil, while the arthropods die rapidly in the PFAS-contaminated soil. Remediation of soil on kilogram scale per batch has been accomplished here, suggesting the potential applicability of REM for large-scale deployment. Furthermore, life-cycle assessment shows that REM exhibits low energy consumption (~420 kWh ton^{-1}), no-water consumption, and, minimal greenhouse gas emission, making it an environmentally attractive alternative over existing remediation techniques.

REM For The Remediation Of PFOA-Contaminated Soil

[0092] In an embodiment of the REM process of the present invention, a design of on-site

REM is shown in **FIG. 1A**, which leverages mature agricultural techniques and soil remediation practices. In the first step (biochar mixing **101**), contaminated soil **104** is premixed with conductive additives, such as biochar **103** (from biochar tank **109**), to ensure appropriate electrical conductivity. As shown in **FIG. 1A**, the biochar mixing **101** can be performed using auger **110**). In the second step (REM treatment **102**), the electrodes **107** fixed in an insulating cap **106** are inserted into the soil. Using power source **105**, a high-voltage pulse input within seconds controllably brings the soil to a typical temperature of >1000°C, facilitating the rapid mineralization of toxic PFAS, with existing Ca compounds in soil and biochar into the nontoxic natural mineral, CaF_2, resulting in remediated soil **108**.

[0093] The REM process was performed on a bench scale. **FIG. 1B**. Raw soil was collected from the Rice University campus, which contained undetectable content of PFAS (<1 ppb) by liquid chromatography-mass spectrometry (LC-MS). The raw soil was separately spiked with different kinds of PFAS with the content of ~100 ppm. *See* **TABLE I**.

TABLE I
Physical Properties Of Different Kinds Of PFAS Utilized

Precursors	Formula	Molecular weight ($g\ mol^{-1}$)	F mass ratio (%)	Mixed concentration in the soil (ppm)
PFOA	$C_8HF_{15}O_2$	414.1	68.8	146.5
PFOS	$C_{24}H_{36}F_{17}NO_3S$	741.6	43.6	223.2
PFH_xS	$C_6HF_{13}O_3SK$	438.2	56.4	155.0
PFBS	$C_4F_9O_3SK$	338.2	50.6	119.2
PTFE	$-CF_2CF_2-$	/	76.0	105.2

[0094] PFAS-contaminated soil was mixed with appropriate amounts of biochar, and then loaded into a quartz tube reactor. No additional Ca-containing compound was added, considering there are sufficient Ca species inherent in the soil for PFAS mineralization. The sample resistance was regulated by compressing the graphite electrodes inserted at the end of the quartz tube, which were connected to a capacitor bank.

[0095] In a typical experiment, with an input voltage of 100 V, discharging time of 1 s, and sample resistance of 3.5 Ω (**TABLE II**), the peak current reached ~140 A (**FIG. 1C**) and the

peak temperature was ~1370 °C (**FIG. 1D**). The heating and cooling rates during REM were calculated to be ~10^4 °C s^{-1} and ~10^3 °C s^{-1}, respectively, using an infrared thermometer.

TABLE II
Parameters For REM Of Soil

Precursors	Mass Ratio	Mass (mg) **	Res (Ω)	Voltage (V)	Time (s)	Mass after REM (mg) ***
c-Soil(PFOA):biochar	2:1	300	3.5	40	1	271
c-Soil(PFOA):biochar	2:1	300	3.5	60	1	253
c-Soil(PFOA):biochar	2:1	300	3.5	80	1	245
c-Soil(PFOA):biochar	2:1	300	3.5	100	1	238
c-Soil(PFOA):biochar	2:1	300	3.5	120	1	227
c-Soil(PFOA):biochar	2:1	300	3.5	150	1	223
c-Soil(PFOA):biochar	1:1	300	2.5	100	1	221
c-Soil(PFOA):biochar	3:1	300	10.5	100	1	249
c-Soil(PFOA):biochar	4:1	300	18.5	100	1	282
c-Soil(wet, PFOA): biochar	2:1	300	4.5	100	1	192
c-Soil(PFOA): biochar (4 mm inner diameter tube)	2:1	108	2.1	60	1	76
c-Soil(PFOA):recycled biochar	2:1	300	3.5	100	1	247
c-Soil(PFOA):carbon black	2:1	300	1.0	100	1	241
c-Soil(PFOA):metcoke	2:1	302	1.5	100	1	236
c-Soil(PFOA):recycled metcoke	2:1	305	1.0	100	1	243
c-Soil(PFOA):metcoke	1:1	300	1.0	100	1	219
c-Soil(PFOA):metcoke	3:1	300	1.5	100	1	238
c-Soil(PFOA):metcoke	4:1	300	1.5	100	1	247
SiO_2(PFOA):metcoke	2:1	300	1.5	100	1	265
c-Soil(PFOA):flash graphene	2:1	305	1.0	100	1	249
c-Soil(PFOS):biochar	2:1	300	3.5	120	1	242
c-Soil(PFH_xS):biochar	2:1	300	3.5	120	1	248
c-Soil(PFBS):biochar	2:1	300	3.5	120	1	241
c-Soil(PTFE):biochar	2:1	300	3.5	80	1	252
c-Soil(PTFE):biochar	2:1	300	3.5	100	1	229
c-Soil(PTFE):biochar	2:1	300	3.5	120	1	212
c-Soil(PTFE):biochar	2:1	300	3.5	150	1	206

*c-Soil is abbreviation of contaminated soil. **The total mass includes c-Soil and carbon additives; ***The total mass includes residual carbon additives.

[0096] By tailoring the input voltage from 40 to 150 V, the REM temperature was tunable ranging from 300 to 2500°C, which meets the required temperature of PFAS degradation, as determined by thermogravimetric analysis (TGA). After REM, the residual PFAS content was quantified by high-performance liquid chromatography with a diode array detector (HPLC-

DAD) and QQQ LC-MS. The detecting limits of each PFAS characterization methods are listed in **TABLE III**. The mineralized fluorine ion (F^-) content was tested by ion chromatography (IC).

TABLE III
Detecting Limits of Different PFAS Characterization Methods

Characterization methods	Detecting limit
FT-IR	1 wt% [*Gorrochategui 2016*]
XRD	0.5 wt% [*Hillier 1999*]
^{19}F-NMR	50 ppb [*Camdzic 2023*]
HPLC-DAD	500 ppb
QQQ LC-MS	0.1 ppb

[0097] The degradation process of perfluorooctanoic acid (PFOA), a representative type of PFAS was first tested. REM was initially conducted in an open system without O-rings to seal the quartz tube. With the increase of input voltage, the PFOA content decreased, benefitting from a higher reaction temperature. However, the total fluorine content significantly decreased with the increase of input voltage, with only half of the organic fluorine mineralized into fluorine ions, which can be ascribed to the emission of PFOA-degraded short-chain species.

[0098] To avoid the emission of short-chain fluorocarbon species, a sealed reactor was constructed with two O-rings on each electrode to seal the reacting tube during REM (**FIG. 1B**). With the increase of input voltage, the PFOA content progressively decreased, benefiting from a higher reacting temperature. Consequently, the F^- content increased with an increase of input voltage from 0 to 100 V and an optimal mineralization ratio of 94% was obtained (**FIG. 1E** with plots **141-143** for organic F, F ion, and sum, respectively). By virtue of the sealing design, REM soil showed a much higher mineralization ratio (94%) compared with the furnace-calcined soil (0.34%), while keeping a high and comparable PFOA removal efficiency of >99%. The gaseous byproduct was collected and tested by gas chromatography mass spectrometry (GC-MS).

[0099] Compared to the clean raw soil as the control, no additional peaks corresponding to known PFOA degradation products were observed. On the contrary, some PFOA-degraded

fluorinated compounds, such as CF_4, CH_3F, C_2F_6, C_2F_4, and C_6H_5F, were observed when replacing soil with SiO_2. This indicated that REM in the presence of Ca effectively mineralizes F from soil contaminated with PFAS and avoids the emission of PFAS-degraded short-chain fluorocarbon species. Thus, the total fluorine mass was calculated by adding the organic fluorine in residual PFOA and the mineralized F^-. **FIG. 1E**. The slight decrease of mineralization ratio and quantifiable total fluorine mass when the REM voltage increases from 100 V to 150 V (**FIG. 1E**), may be attributed to the increased amount of insoluble F-containing compounds deposited on the quartz tube with the increase of REM temperature.

[0100] The PFOA content in the soil can be reduced to below the residential soil remediation standards (130 ppb, the New Jersey Department of Environmental Protection, "Residential soil remediation standards for the ingestion-dermal exposure"), after 2 electric pulses and further to an ultralow value of ~1.1 ppb after 4 electric pulses. **FIG. 1F**. ^{19}F NMR spectra were conducted using deuteroxide to extract PFOA and F^- in the soil before and after REM. **FIG. 1G**. The ^{19}F NMR spectrum of contaminated soil has several peaks, all of which fit well with PFOA standard. [*Camdzic 2021*; *Trang 2022*]. On the contrary, the REM-treated soil had a single peak at -128 ppm, corresponding to hydrated fluoride ions [*Camdzic 2021*], further proving the PFOA can be effectively converted into fluorine ions in the soil by the REM process.

REM For Soil Remediation

[0101] For generality of REM for PFAS degradation, other than PFOA, the mineralization behaviors were investigated of various PFAS, including heptadecafluorooctanesulfonic acid tetraethylammonium salt (PFOS), tridecafluorohexane-1-sulfonic acid potassium salt (PFH_xS), and nonafluorobutane-1-sulfonic acid potassium salt (PFBS). The trends of PFAS mineralization versus input voltage are similar to that of PFOA, where higher input voltages often facilitate higher degradation ratios of C-F bonds. **FIGS. 2A-2C** (plots **201-203** in **FIG.**

2A for organic F, F ion, and sum, respectively; plots **211-213** in **FIG. 2B** for organic F, F ion, and sum, respectively; and plots **221-223** in **FIG. 2C** for organic F, F ion, and sum, respectively).

[0102] In the ^{19}F NMR spectra, only the -128 ppm peak that assigned to hydrated F^- [*Camdzic 2021*] was observed for all REM treated soil samples (**FIGS. 2D-2F**), indicating the effective removal of PFAS by REM. The removal efficiencies of all the tested PFAS were calculated to be higher than 99% (**FIG. 2G**) and >90% mineralized fluorine ratios were quantified with a single electric pulse (**FIG. 2H**). In addition to short-chain PFAS, REM is also applicable to mineralize F-containing polymers, such as polytetrafluoroethylene (PTFE) with a high mineralization ratio of ~95%. Trace amounts of PTFE degradation compounds, including tetrafluoroethylene and trifluoromethanol, were detected in the gaseous phase during REM, while none of the fluorinated compounds were detected in the REM soil.

[0103] In addition to biochar, other carbon materials with sufficient conductivity, including carbon black, metallurgical coke (metcoke) and flash graphene [*Luong 2020*], were also used as the conductive additives for the REM process. Taking PFOA as an example, all tested carbon conductive additives can achieve a high mineralization ratio of >90%, proving the broad applicability of carbon additives. The used carbon additive can be optionally separated from the soil mixture and then reused for next-batch soil remediation. For example, biochar was separated from soil by dispersion and centrifugation with a recycling ratio of ~85 wt%, and reused in a second REM process with a comparable PFAS mineralization performance.

[0104] Similarly, when metcoke was used as the conductive additives, ~91 wt% can be recycled after REM by simply sieving and then reused with similar performance. This significantly reduces materials consumption of the REM process while requiring greater processing. The optimal ratio between soil and different carbon additives was also investigated, where sufficient carbon additive content (>33 wt%) was required to ensure REM temperature

for PFAS mineralization. For deployed applications, the choice of carbon additives depended on the specific scenarios and requirements.

Mechanism of PFAS Mineralization

[0105] Ca^{2+} is suggested to be a critical counterion for PFAS mineralization under thermal treatment. [*Wang 2013*; *Wang 2015*]. To confirm the influence of Ca on PFAS mineralization, mineralization performance of Ca^{2+} was compared with other alkali and alkaline earth metal ions, such as Mg^{2+} and Na^{+}, where calcium carbonate ($CaCO_3$, a representative calcium species in soil [*Pilbeam 2016*]), magnesium carbonate ($MgCO_3$) and sodium carbonate (Na_2CO_3), were separately mixed with PFOA and the metal counterion content is 1.2 mole equivalent compared with F. *See* **TABLE IV**.

TABLE IV
Parameters For REM By Mixing Metal Salt With PFOA*

Metal salts	Mass (mg)**	PFAS type	Mass (mg)	Mass of metcoke (mg)	Resistance (Ω)	Mass after REM (mg)***
$CaCO_3$	137	PFOA	63	100	2.5	212
$CaCO_3$	116	PFOS	84	99	2.5	216
$CaCO_3$	128	PFH_xS	72	100	2.5	208
$CaCO_3$	123	PFBS	77	102	2.5	205
$CaCO_3$	140	PTFE	59	101	3.0	220
$MgCO_3$	131	PFOA	70	100	2.6	197
Na_2CO_3	139	PFOA	61	100	2.2	221

* The input voltage was set as 100 V, REM time was set as 1 s and total mass for each REM is ~300 mg. **Metal counterion content was 1.2 mole equivalents compared with the F mole content in PFAS. ***The total mass included residual carbon additives.

[0106] After REM treatment, X-ray diffraction (XRD) patterns showed the loss of PFOA peaks and the appearance of metal fluoride peaks, indicating that all these alkaline and alkaline earth metal ions can be used for PFAS mineralization. However, Ca achieved a highest PFOA removal efficiency (~99.7%) over Mg (~94.2%) and Na (~98.5%, proving that Ca has the best mineralization performance for PFAS, greater than Mg and Na. Meanwhile, Ca-F bond has the highest bond energy among different metal-fluorine bonds. *See* **TABLE V**.

TABLE V
Metal-Fluorine Bond Energy

M-F type	Bond energy (kJ mol^{-1})
Na-F	477
Mg-F	463
K-F	489
Ca-F	529

[0107] Theoretical calculation revealed that once other metal fluorides (like MgF_2 or NaF) were formed, these fluoride compounds were thermodynamically favorable to convert to CaF_2 during REM under the temperature higher than 400 °C. The above analysis evinces that Ca dominates the PFAS mineralization process. Then, $CaCO_3$ was mixed with other kinds of PFAS and the same mineralization phenomena was observed, explicitly demonstrating the critical role of Ca^{2+} in PFAS mineralization.

[0108] When biochar was used as the conductive additive, a slightly higher mineralization ratio of ~94% was observed, compared to that of other carbon additives (90 - 91%). The composition of these carbon additives was examined by XPS, and it was found that Ca content is highest in biochar (~4 at%), while undetectable by XPS in the other carbon additives.

[0109] To verify that the Ca^{2+} in biochar can benefit PFAS mineralization, PFOA (5 wt%) and biochar (95 wt%) were mixed and REM was conducted. After the treatment, the peaks of PFOA diminished while CaF_2 peak appeared in the XRD patterns. **FIG. 3A**. The same phenomenon pertains to other PFAS. *See* **TABLE I**. The X-ray photoelectron spectroscopy (XPS) spectra show that the C 1*s* peak at ~292 eV (assigned to C-F) and the F 1*s* peak at ~689 eV (assigned to F-C) of PFOA disappeared after the REM process, while the new F 1*s* at ~684 eV (assigned to F-Ca) appeared. **FIGS. 3B-3C** (circles **311a-311b** in **FIG. 3B** for C 1*s*; areas **312a-312b**, **313a-313b**, and **314a** in **FIG. 3B** for C-C, C-O, and C-F, respectively; circles **321a-321b** in **FIG. 3C** for F 1*s*; areas **322** and **323** in **FIG. 3C** for F-C and F-Ca, respectively). In the infrared (IR) spectrum of initial PFOA, the peaks in the range of 1100-1200 cm^{-1} and 650-750 cm^{-1} correspond to stretching and rocking vibrations of C-F bonds [*Huang 2018*], respectively (**FIG.**

3D, with plots **331-332** for biochar+PFOA and after REM, respectively), disappeared after REM. The IR spectra for other PFAS exhibited the same behaviors, demonstrating that Ca in biochar facilitates effective mineralization of PFOA.

[0110] Theoretical analysis was further conducted to clarify the PFAS mineralization mechanism assisted by Ca^{2+}. Thermodynamically, the Gibbs free energy change (ΔG) was calculated for each degradation step of C_7F_{16}, which is the first-step degradation product of PFOA after decarboxylation. [*Trang 2022*]. Without Ca^{2+}, the thermal pyrolysis of the perfluorinated species required a high temperature >1500 °C (**FIG. 3E**, dashed lines **341**). In contrast, ΔG turns negative (favorable) with the existence of Ca^{2+} under broad temperature range (**FIG. 3E**, solid lines **342**), indicating that the PFOA mineralization reaction is spontaneous.

[0111] Molecular dynamic (MD) simulations were further performed to reveal the kinetics of PFOA mineralization. Since the cleavage of C-F bonds occurs for PFOA mineralization, the C-F bond ratio is used as an indicator to evaluate the mineralization efficiency. With Ca, F is more favorable to ionically bond with the Ca atom than forming a covalent bond with the C atom. The reaction barrier of C-F bond cleavage was calculated to be 0.67 eV and the total energy was lowered by 1.24 eV in the presence of Ca, indicating that the mineralization process is an energy-favorable reaction step. On the contrary, without Ca, the F atom spontaneously returned to its original position in the PFOA and reformed a covalent bond with the C atom.

[0112] Without Ca^{2+}, ~80% of C-F bonds in PFOA were maintained after thermal treatment in the temperature range of 1500 to 2500 K, and PFOA tends to degrade into short-chain perfluorinated species. **FIGS. 3F-3G** (with plots **351-352** in **FIG. 3F** for with Ca^{2+} and without Ca^{2+}, respectively. In contrast, with the presence of Ca^{2+}, >90% of C-F bonds in PFOA cleaved and the F were affiliated to Ca. **FIGS. 3F-3G**. With the increase of atomic ratio of Ca and F, more C-F bonds tended to cleave (**FIG. 3H**), demonstrating that more Ca^{2-} can facilitate a

higher mineralization ratio of PFAS. The Ca^{2+} content in both soil and biochar, as tested by X-ray fluorescence (XRF) and XPS, was in the range of 4 to 5 at%, which is hundreds of times excess relative to the reaction stoichiometry. PFAS can thus be effectively mineralized using the inherent Ca^{2+} in soil and biochar, without additional Ca^{2+} consumption, further reducing the materials expense of the REM process.

Soil Properties After REM

[0113] The soil properties after REM were investigated, which are significant for the soil reuse in the ecosystem. The soil after REM treatment and carbon additive removal (denoted as REM soil) was compared with raw soil and calcined soil as a control, since calcination has been reported to be an effective method to remove PFAS from the contaminated soil. [*Javaherian 2016*; *Sörengård 2020*].

[0114] The soil physical properties were first examined. The REM soil **402** exhibited a darker contrast than raw soil **401**, due to the trace residual biochar. **FIG. 4A**. The calcined soil **403** showed a brick-red contrast, indicating possible composition or structure change during the calcination process. **FIG. 4A**. The REM soil exhibited a similar fine powder feature with that of raw soil, while the calcined soil particle was severely aggregated. Laser particle size analysis results also revealed comparable size distributions between raw soil and REM soil, but a significant increase of particle sizes with much lower clay and silt ratio [*Faé 2019*; *Barman 2020*] after calcination. **FIG. 4B** (plots **411-413** for raw soil, REM soil, and calcined soil, respectively). Consequently, the calcined soil showed a drastically decreased surface area compared with raw soil and REM soil. The main crystalline composition was quartz for all tested soil samples (**FIG. 4C**), and XRF results showed that no obvious change for various oxides in the soil after treatment (**FIG. 4D** with bars **431-433** for raw soil, REM soil, and calcined soil, respectively).

[0115] Additionally, the soil water infiltration rates were assessed. **FIG. 4E** with plots **441-**

443 for raw soil, REM soil, and calcined soil, respectively. REM soil showed a slightly higher infiltration rate (~34 cm h^{-1}) than raw soil (~28 cm h^{-1}). Considering a larger porosity of biochar to soil, the small amounts of residual biochar in REM soil could contribute to the higher water infiltration rate. In contrast, the infiltration rate of calcined soil (~455 cm h^{-1}) was >10 times higher, probably due to its severely enlarged particle size (**FIG. 4B**), as water flows faster through the enlarged pores between soil particles. [*Weil 2017*]. The excessively high infiltration rate would lead to degradation of soil fertility by eluviation. [*Zhang 2004*].

[0116] Moreover, soil pH, cation exchange capacity (CEC), soil carbon and nutrients contents were analyzed. REM soil exhibited a pH of 7.58, which was slightly higher than that of raw soil (pH = 7.19). CEC of REM soil was 15.45 cmol kg^{-1}, which is comparable to that of raw soil (15.25 cmol kg^{-1}, **TABLE VI**). On the contrary, the pH of calcined soil increased to 10.63 and its CEC decreases to 4.08 cmol kg^{-1} (**TABLE VI**), indicating the inapplicability for its reuse.

TABLE VI
pH And Cation Exchange Capacity (CEC) Of Different Soil Samples

Soil types	pH	CEC (cmol kg^{-1})
Raw soil	7.19 ± 0.02	15.25 ± 0.81
REM soil	7.58 ± 0.03	15.45 ± 1.04
Calcined soil	10.63 ± 0.08	4.08 ± 0.37

[0117] Soil carbon content measurement showed that REM soil had a slightly higher carbon content (4.3 wt%) than raw soil (3.7 wt%,), possibly due to the existence of small amount of residual biochar. On the contrary, the calcined soil had a carbon content of <0.1 wt%. The contents of extractable organic compounds, including humic acid and fulvic acid, were quantified by the Walkley–Black method [*Baglieri 2007*], where <1 wt% of these compounds remained in the REM soil, indicating the decomposition of these compounds during REM process. The exchangeable nutrient content, including P, Ca, K, Mg, Mn, Fe, and N, is a critical parameter to evaluate soil fertility and directly related to soil biodiversity. [*Sicilaiano 2014*; *Inkotte 2023*]. The contents of most exchangeable nutrients in REM soil increased by 10% to

102%, except a ~5% decrease of Fe content. **FIG. 4F** (bars **451-452** for REM soil and calcined soil, respectively).

[0118] The influence of different carbon additives on soil nutrient contents was also evaluated and it was found that nutrient-rich biochar can facilitate higher exchangeable nutrient contents of REM soil, comparing with those of the REM soil using metcoke as carbon additive. Therefore, the increase of nutrient contents in REM soil can be attributed to the ion-exchange from biochar (**TABLE VII**) to the soil, and/or the mineralization of soil organic matter during REM. [*Bahureksa 2022*; *Chungu 2020*]. However, most of these nutrient contents dramatically decreased for the calcined soil.

TABLE VII
Soil Nutrient Concentrations

Nutrients	Raw soil (ppm)	Calcinated soil (ppm)	REM soil (ppm) **	Biochar (ppm)
P	68 ± 1	50 ± 2	137 ± 14	328 ± 69
Mg	255 ± 20	139 ± 9	406 ± 9	1189 ± 92
K	280 ± 11	71 ± 3	423 ± 7	3232 ± 195
Ca	2605 ± 109	1281 ± 569	3230 ± 275	3942 ± 168
Mn	133 ± 3	265 ± 40	156 ± 17	265 ± 40
N*	16 ± 3	0.74 ± 0.08	17 ± 2	0.23 ± 0.05
Fe	311 ± 12	432 ± 138	294 ± 64	307 ± 64

*The nutrient N refers to nitrate nitrogen; **REM soil tested here is the soil after removing the biochar inside.

[0119] Further, the arthropod culture was conducted to evaluate the applicability of REM soil in ecosystems. Springtail and isopod were used as two representative arthropods. The survival ratios were compared of four kinds of soil samples, including PFOA-contaminated soil (denoted as PFOA soil), raw soil, REM soil, and calcined soil. Because of the toxicity of PFOA [*Whitacre 2010*; *Labine 2022*], both springtails and isopods underwent rapid mortality in PFOA soil within the initial 1 to 2 weeks. **FIGS. 4G-4H** (plots **461-464** in **FIG. 4G** for PFOA soil, raw soil, REM soil, and calcined soil, respectively; plots **471-474** in **FIG. 4H** for PFOA soil, raw soil, REM soil, and calcined soil, respectively); **TABLES VIII-IX**.

TABLE VIII
Results From The Generalized Linear Models Testing For The Main And Interactive Effects Of Soil Types And Culture Time On Springtail Survival

	Survival ratio	
Predictors	*CI*	*p*
(Intercept)	0.18 – 1.44	0.203
Soil Type [Raw soil]	0.29 – 4.83	0.819
Soil Type [REM soil]	0.46 – 6.26	0.430
Soil Type [PFOA soil]	0.00 – Inf.	0.997
Week [Week_2]	0.00 – Inf.	0.997
Week [Week_3]	0.00 – Inf.	0.997
Soil Type [Raw soil] × Week [Week_2]	0.00 – Inf.	0.997
Soil Type [REM soil] × Week [Week_2]	0.00 – Inf.	0.997
Soil Type [PFOA soil] × Week [Week_2]	0.00 – Inf.	0.998
Soil Type [Raw soil] × Week [Week_3]	0.00 – Inf.	1.000
Soil Type [REM soil] × Week [Week_3]	0.00 – Inf.	0.998
Soil Type [PFOA soil] × Week [Week_3]	0.00 – Inf.	0.998
Observations	84	

TABLE IX
Results From The Generalized Linear Models Testing For The Main And Interactive Effects Of Soil Types And Culture Time On Isopod Survival

	Survival ratio		
Predictors	*Odds Ratios*	*CI*	*p*
(Intercept)	7.00	1.25 – 130.85	0.069
Soil Type [Raw soil]	1.00	0.03 – 28.82	1.000
Soil Type [REM soil]	1.00	0.03 – 28.82	1.000
Soil Type [PFOA soil]	0.05	0.00 – 0.49	0.024
Week [Week_2]	0.43	0.02 – 5.61	0.529
Week [Week_3]	0.14	0.01 – 1.39	0.129
Soil Type [Raw soil] × Week [Week_2]	1.44	0.03 – 84.59	0.850
Soil Type [REM soil] × Week [Week_2]	1.44	0.03 – 84.59	0.850
Soil Type [PFOA soil] × Week [Week_2]	1.00	0.02 – 52.84	1.000
Soil Type [Raw soil] × Week [Week_3]	1.00	0.02 – 45.26	1.000
Soil Type [REM soil] × Week [Week_3]	1.00	0.02 – 45.26	1.000
Soil Type [PFOA soil] × Week [Week_3]	0.00	0.00 – Inf.	0.995
Observations	96		

[0120] In contrast, REM soil exhibited a comparable arthropod survival ratio with raw soil (**FIGS. 4G-4H**), demonstrating the effective elimination of toxic substances and the restoration of soil properties. The calcined soil displayed a lessening in arthropods survival ratio compared with raw soil (**FIGS. 4G-4H**), which could originate from the nutrient loss and soil structure change. These results reveal that apart from the PFAS mineralization, REM maintains soil

morphology, particle size, crystal components and water infiltration rate, while promoting soil nutrients and biodiversity. This is in striking contrast to the calcination process, which leads to soil degradation. This difference can be attributed to the short duration of the REM process that lasts only seconds with rapid heating and cooling rates.

Scaling-Up REM Process

[0121] To outline the practical applicability of REM for PFAS-contaminated soil remediation, an initial scale-up study was first conducted. The PFAS mineralization efficiency depends mainly on the peak temperature and reaction duration during REM. Therefore, maintaining a constant temperature can be critical for the scale-up, which can be realized by increasing the input voltage or capacitance of the REM system.

[0122] For the REM process, the PFAS mineralization in the soil mostly depends on the treating temperature and the time. *See* **FIG. 1D**; **FIGS 2A-2C**. Hence, the REM temperature across the soil sample has import when scaling up the process. For REM process, the input heat (Q) can be calculated by Eq. (1),

$$Q = I^2Rt \qquad (1),$$

where I is the current passing through the sample, R is the sample resistance, and t is the discharging time.

[0123] The heat amount per volume (Q_v) is calculated by Eq. (2),

$$Q_v = j^2\rho_e t \qquad (2),$$

where j is the current density, and ρ_e is the electrical resistivity. For a specific sample, the electrical resistivity (ρ_e) is constant.

[0124] The temperature difference (ΔT) is proportional to the heat amount by Eq. (3),

$$Q = C_p m\Delta T \quad (3),$$

where C_p is heat capacity and m is the mass of the sample.

[0125] Eq. (3) could be reformulated per volume to Eq. (4),

$$Q_v = C_p \rho_m \Delta T \qquad (4),$$

where ρ_m is the density of the sample. For a specific sample, the C_p and ρ_m were constant; hence, maintaining a constant Q_v is proportional to ΔT.

[0126] The charge amount (q) in the capacitor bank could be calculated by Eq. (5),

$$q = CV \qquad (5),$$

where C is the capacitance of the capacitor bank, and V is the voltage of the capacitor bank.

[0127] Assuming that all the charges in the capacitor bank are discharged within the time of t, the current density (j) could be calculated by Eq. (6),

$$j = \frac{I}{S} = \frac{CV}{St} \qquad (6),$$

where S is the cross-sectional area of the sample.

[0128] Since the cylinder-shaped sample is typically used, the mass (m) could be calculated by Eq. (7),

$$m = \rho_m SL \qquad (7),$$

where ρ_m is the density of the sample, S is the cross-sectional area of the sample, and L is the length of the sample.

[0129] For a specific type of sample, such as soil and biochar, the density (ρ_m) is the same.

[0130] To summarize, Eq. (8) was obtained that determines the current density,

$$j = \frac{CV\rho_m L}{mt} \qquad (8).$$

[0131] Hence, ΔT can be calculated following the Eq. (9).

$$\Delta T = \frac{C^2 V^2 L^2 \rho_m \rho_e}{m^2 t C_p} \qquad (9).$$

[0132] As aforementioned, to scale up the REM process, increasing the mass (m) of the sample is required, while a constant temperature difference (ΔT) should be maintained. Two routes can be adopted: (1) increasing the input voltage (V), and/or (2) increasing the capacitance (C) of the REM system.

[0133] In a first-generation REM setup, a capacitor bank composed of 10 aluminum electrolytic capacitors (450 V, 6 mF, Mouser #80-PEH200YX460BQU2) was used with a total capacitance of C_0 = 0.06 F. In a small-scale experiment, the input voltage (V_0) of 100 V and capacitance (C_0) of 0.06 F were used for the sample mass of m_0 = 0.30 g. The scaling up of the REM process was demonstrated to a mass of m_1 = 10 g based on a second-generation setup with larger capacitance of C_1 = 0.624 F. Thus, the below formula of Eq. (10) was obtained,

$$\frac{m_1}{m_0} = \frac{C_1 V_1}{C_0 V_0} \qquad (10).$$

[0134] For the mass of m_1 = 11 g and C_1 = 0.624 F, a REM voltage of $V_1 \approx$ 300 V was used, which basically fits with Eq. (10). The peak temperature during this REM process was ~1600 °C, similar to small-batch temperature (**FIG. 1C**), proving the efficiency of the scale-up.

[0135] Utilizing the REM system (developed with a larger capacitance of C = 0.624 F), with an input voltage of 300 V, the sample temperature can ramp to 1700 °C, and ~7 g of contaminated soil per batch can be remediated within 6 s.

[0136] Furthermore, an alternating current (AC) source with better scalability was integrated into a subsequent REM system, which directly converted commercial AC into DC output instead of using capacitors. 2 kg of PFOA-contaminated soil was mixed with 500 g of metcoke in a 10-inch-diameter clay pot **501** with a plastic cap **502**, where four graphite rods **503** were applied as the electrodes. **FIG. 5A**. During REM, bright light emission was observed through cap **502** (**FIG. 5A**), with a steady current of ~18 A and the temperature of ~1000 °C. Afterwards, the soil samples from different positions in the pot were collected for the PFOA quantification. The average PFOA removal efficiency of the kilogram-scale REM reached ~97% with high uniformity both radically and axially (**FIG. 5B**), comparable to that of small-scale samples. Numeric simulation of the current density across the soil under external voltage input were further conducted.

[0137] Electric field simulation. The simulation was conducted based on the finite element method using the COMSOL Multiphysics 5.5 software. The Electric Currents interface under the AC/DC module was used as the model. The geometric configuration and materials parameters are shown in **TABLE X**.

TABLE X
Parameters Of Electric Field Simulation

Parameters	Soil	Graphite electrode
Shape	Cyclinder	Cyclinder
Size	15 cm (diameter), 6 cm (height)	6.36 mm (diameter), 8 cm (height)
Electrical conductivity	0.83 S m^{-1}	2×10^5 S m^{-1}
Relative permittivity	4	18
Boundary condition	200 V input	

[0138] The electrical conductivity of the mixed soil/carbon additive was calculated by measuring the resistance. Other material parameters were from the physical constant table. A simulated electric potential map showed the linear decrease of electric potential from the electrical potential electrodes to the ground electrodes. The simulated in-plane current density map is shown in **FIG 5C**. The maps were uniform, proving the homogeneous heating capability of the REM process. (The current density was uniform both in-plane (**FIG. 5C**) and in-depth, substantiating the homogeneous heating capability of the REM process for soil remediation).

[0139] Current density can have import for the Joule heating. According to $Q = I^2Rt$, since soil conductivity is the same, similar current density leads to a similar heating effect. In the kilogram-scale sample with 200 V input, the current density was ~1000 A m^{-2}.

[0140] To assess the practical applicability of the REM process, the simulation was further extended to a 1 m × 1 m × 1 m scale. The material properties and boundary conditions were the same as in the aforementioned small-scale sample. In this case, the voltage input with 1000 V was applied. The current density in the central position was calculated to be ~800 A m^{-2}, similar to that in the small-scale clay pot. According to the theoretical analysis as discussed

above, the current density determined the accessible temperature of the sample during the REM process. This indicated that a comparable temperature of ~1000 °C can be achieved under such a voltage input for the large-scale 1 m^3 sample.

[0141] To reveal the relationship of electrode surface area on the heating efficacy, a simulation was conducted on a 1 m × 1 m × 1 m volume sample with different electrode surface area. With the increase of each electrode surface area from 0.25 to 0.75 m^2, the current density at the center position increases from 730 to 870 A m^2, which indicated a higher REM temperature since the current density determines the temperature according to the analysis discussed above. Therefore, during REM, a higher electrode surface area can facilitate a higher REM temperature and thus a higher PFOA removal efficiency.

[0142] Again, the current density is uniform both in-plane (**FIG. 5C**) and in-depth, substantiating the homogeneous heating capability of the REM process for soil remediation. The field-scale application potential of REM was evaluated by simulation at a 1 m × 1 m × 1 m scale. Under the voltage input at 1000 V, the current density of the 1 m^3 scale soil sample was similar to that in the small-scale clay pot (**FIG. 5B**). Since, as discussed above, the current density mainly determines the accessible temperature, it is projected that a similar heating pattern can be achieved for the large-scale sample.

[0143] In addition, the current density of the large-scale soil sample uniformly distributes both in-plane and in-depth, confirming the homogenous heating capability of REM for on-site soil remediation. Meanwhile, based on the simulation results, the increase of electrode surface areas facilitates an increase of current density with a certain voltage input, leading to a higher REM temperature for PFAS mineralization. For the practical application, considering the moisture contained in field soil, it is assessed that REM is applicable for PFAS mineralization in wet soil. After REM, the wet soil with a moisture content of ~30 wt% achieved a PFOA mineralization ratio comparable to pre-dried soil, further suggesting the feasibility of REM for

practical deployment.

[0144] In certain embodiments, scalability in the field include a process by which the conductive additive (such as biochar) can be introduced, with or without an auger, at various (and strategic) locations relative to one or more electrode arrays. In such manner, this can reduce the conductive additive content to a lower weight percentage (such as 1 wt%) relative to the contaminated soil (as opposed to a higher wt% such 20 wt%). The electrode array can be inserted at strategic locations, and a desired depth. The electrodes can then be used to strategically flash the soil, such as by firing across several pairs, to heat the ground.

[0145] By way of example, such approach can be biochar added to the soil by solid or slurry injection at strategic locations between the inserted electrodes (or the biochar can be injected at strategic locations between where the electrodes will be inserted). The biochar can be injected before or after the insertion of the electrode array the soil, or even during the time when the electrodes are being inserted. The biochar can be injected at as little at 0.1 wt% relative to the soil weight to be flashed, and up to 25 wt%. Generally, this would be in amount of biochar at ~1 wt% of the contaminated soil to be treated. There can generally be between two electrodes and 120 electrodes inserted per electrode array insertion. Strategically firing can be performed across multiple electrode pairs over a timed sequence to heat the soil. The electrode arrays and biochar can be inserted to desired locations (such as within a 1 square meter area) based upon the contaminant concentration at a particular depth (such as 3 meters).

Life Cycle Assessment

[0146] The environmental impact of the REM process was thereafter assessed. The energy consumption of the REM process is calculated to be ~420 kWh ton^{-1}. This low energy consumption benefits from the short duration, ultrafast heating/cooling rates, and in-place soil treatment.

[0147] Furthermore, a comparative cradle-to-gate life cycle assessment (LCA) was conducted

to compare the environmental impact and cumulative energy demand of REM with existing remediation approaches. Four scenarios were considered in this study, including thermal treatment (**FIG. 6A**), ball milling (**FIG. 6B**) chemical oxidation (**FIG. 6C**), and REM (**FIG. 5D**). *See* **TABLS XI-XVI**.

TABLE XI
Materials Flow For Various Scenarios

Scenarios	Thermal treatment (tonne)	Chemical oxidation (tonne)	Ball milling (tonne)	REM by biochar (tonne)	REM by metcoke (tonne)
PFAS-contaminated soil	1	1	1	1	1
Biochar	0	0	0	0.075	0
Biochar pretreatment	0	0	0	0.075	0
Metcoke	0	0	0	0	0.035
Potassium permanganate	0	0.01	0	0	0
Water	0	10	0	0	0
Potassium hydroxide	0	0	0.0095	0	0
Excavation and transportation	1	1	1	0	0
Mixing	0	1.01	1.0095	1.5	1.5
Furnace heating	1	0	0	0	0
Water bath heating	0	11.01	0	0	0
Filtration	0	11.01	0	0	0
Ball milling	0	0	1.0095	0	0
Transportation and refilling	1	1	1	0	0
REM	0	0	0	1.5	1.5
Cyclone separation	0	0	0	1.5	0
Sieving	0	0	0	0	1.5

The material mass flows are normalized to treat 1 tonne of PFAS-contaminated soil. **PFAS concentration in the contaminated soil is set as 100 ppm. ***REM, rapid electrothermal mineralization.

TABLE XII
Life Cycle Inventory

Impact Category	Energy consumption (MJ)	GHG emission (kg)	Water consumption (kg)
Biochar	20025	5.04	4.7
Metcoke	28030	362.6	416.9
Potassium permanganate	19480	1891	8682
Potassium hydroxide	28000	1980	17221
Biochar pretreatment	360	46.8	241.2
Excavation and transportation	451.5	33.8	302.5
Mixing	9.43	1.23	6.3
Furnace heating	3874	504	2595.6
Water bath heating	1866	243	1260.2
Filtration	2.2	0.29	1.5
Ball milling	3456	449	2315.5
Transportation and refilling	466.6	35.7	312.6
REM	1000	130	670
Cyclone separation	6.75	19	4.5
Sieving	4.2	0.55	2.8

*The material mass flows are normalized to treat 1 tonne of PFAS-contaminated soil. **PFAS concentration in the contaminated soil is set as 100 ppm. ***REM, rapid electrothermal mineralization. ****GHG, greenhouse gas.

TABLE XIII
Energy Consumption For Various Scenarios

Scenarios	Thermal treatment (MJ)	Chemical oxidation (MJ)	Ball milling (MJ)	REM by biochar (MJ)	REM by metcoke (kg)
Biochar	0	0	0	1501.9	0
Metcoke	0	0	0	0	981.05
Potassium permanganate	0	194.8	0	0	0
Potassium hydroxide	0	0	266	0	0
SUM of Materials	0	194.8	266	1501.9	981.05
Excavation and transportation	451.5	451.5	451.5	0	0
Biochar pretreatment	0	0	0	27	0
Mixing	0	9.43	9.44	14.15	14.15
Furnace heating	3874	0	0	0	0
Water bath heating	0	1866	0	0	0
Filtration	0	24.2	0	0	0

Ball milling	0	0	3460	0	0
Transportation and refilling	466.6	466.6	466.6	0	0
REM	0	0	0	1500	1500
Cyclone separation	0	0	0	10.13	0
Sieving	0	0	0	0	6.30
SUM of Process	4792.1	2817.7	4387.5	1551.3	1520.45
SUM	**4792**	**3013**	**4654**	**3053**	**2502**

*The material mass flows are normalized to treat 1 tonne of PFAS-contaminated soil. **PFAS concentration in the contaminated soil is set as 100 ppm. ***REM, rapid electrothermal mineralization.

TABLE XIV
GHG Emissions For Various Scenarios

Scenarios	Thermal treatment (kg)	Chemical oxidation (kg)	Ball milling (kg)	REM by biochar (kg)	REM by metcoke (kg)
Biochar	0	0	0	0.38	0
Metcoke	0	0	0	0	12.69
Potassium permanganate	0	18.9	0	0	0
Potassium hydroxide	0	0	18.81	0	0
SUM of Materials	0	18.9	18.8	0.4	12.69
Excavation and transportation	33.79	33.79	33.79	0	0
Biochar pretreatment	0	0	0	3.51	0
Mixing	0	1.23	1.24	1.84	1.84
Furnace heating	504	0	0	0	0
Water bath heating	0	243	0	0	0
Filtration	0	3.19	0	0	0
Ball milling	0	0	453	0	0
Transportation and refilling	35.75	35.75	35.75	0	0
REM	0	0	0	195	195
Cyclone separation	0	0	0	1.32	0
Sieving	0	0	0	0	0.83
SUM of Process	573.5	317.0	523.8	201.7	197.7
SUM	**574**	**336**	**543**	**202**	**210**

*The material mass flows are normalized to treat 1 tonne of PFAS-contaminated soil. **PFAS concentration in the contaminated soil is set as 100 ppm. ***REM, rapid electrothermal mineralization. ****GHG, greenhouse gas.

TABLE XV
Water Consumption For Various Scenarios

Scenarios	Thermal treatment (kg)	Chemical oxidation (kg)	Ball milling (kg)	REM by biochar (kg)	REM by biochar (kg)
Biochar	0	0	0	0.35	0
Metcoke	0	0	0	0	145.9
Potassium permanganate	0	86.82	0	0	0
Potassium hydroxide	0	0	163.6	0	0
SUM of Materials	0	86.8	163.6	0.35	145.9
Excavation and transportation	302.5	302.5	302.5	0	0
Biochar pretreatment	0	0	0	27	0
Mixing	0	6.36	6.36	9.45	9.45
Furnace heating	2595.6	0	0	0	0
Water bath heating	0	1272.8	0	0	0
Filtration	0	16.52	0	0	0
Ball milling	0	0	2337.5	0	0
Transportation and refilling	312.6	312.6	312.6	0	0
REM	0	0	0	1005	1005
Cyclone separation	0	0	0	6.75	0
Sieving	0	0	0	0	4.22
SUM of Process	3210.7	1910.8	2959	1048.2	1018.67
SUM	**3211**	**1998**	**3123**	**1049**	**1165**

*The material mass flows are normalized to treat 1 tonne of PFAS-contaminated soil. **PFAS concentration in the contaminated soil is set as 100 ppm. ***REM, rapid electrothermal mineralization.

TABLE XVI
Materials And Energy Cost Inventory

Scenarios	Materials cost ($)	Energy cost ($)
Biochar	1400	0
Metcoke	150	0
Potassium permanganate	37700	0
Potassium hydroxide	31600	0
Water	1.085	0
Excavation and transportation	0	26.50
Biochar pretreatment	0	5.87
Mixing	0	0.15
Furnace heating	0	63.17
Water bath heating	0	30.43
Filtration	0	0.036

Ball milling	0	56.36
Transportation and refilling	0	27.39
REM	0	16.31
Cyclone separation	0	0.17
Sieving	0	0.068

Note: *The material mass flows are normalized to treat 1 tonne of PFAS-contaminated soil. **PFAS concentration in the contaminated soil is set as 100 ppm. ***REM, rapid electrothermal mineralization. ****The consumed energy is assumed to be from electricity, and the industrial price of electrical energy in Texas, USA is \$0.0587 kWh^{1}.

[0148] REM demonstrated a low cumulative energy demand (CED) of 3053 MJ $tonne^{-1}$. This value is comparable with that of the chemical oxidation process (3013 MJ $tonne^{-1}$), but 31% to 33% lower than traditional thermal treatment and ball milling methods. **FIG. 5E** (bars **541-542** for materials and process, respectively). REM also exhibited 40% to 65% reduction in greenhouse gas emission (GHG) (**FIG. 5F**, with bars **551-552** for materials and process, respectively), and 47% to 67% reduction in water consumption compared to other methods. REM also has no chemical waste generation because of no consumption of chemicals. Additionally, REM can realize >99% PFAS removal within seconds, achieving the best performance in overcoming the trade-off between removal efficiency and processing time among reported methods. [*Javaherian 2016*; *Sörengård 2020*].

Techno-Economic Assessment

[0149] Additionally, a techno-economic analysis (TEA) was conducted, since economic incentives play a vital role in utilization. It was shown that REM had an operating expense of \$130 $tonne^{-1}$ of soil treated, which is comparable to thermal treatment (\$117 $tonne^{-1}$), but much lower than ball milling (\$411 $tonne^{-1}$) and chemical oxidation (\$473 $tonne^{-1}$). **FIG. 5G** (bars **561-562** for materials and process, respectively); **TABLE XVII**. With the merits of low cost, high PFAS removal and degradation efficiency, rapid treating process, zero water use, and the preservation of soil properties (**FIG. 5H**, with areas **571-574** for thermal, ball milling, chemical oxidation, and REM, respectively), REM shows potential superiorities over existing thermal treatment and chemical oxidation methods toward practical applications.

TABLE XVII
Cost Evaluation Of Various Scenarios

Scenarios	Thermal treatment ($)	Chemical oxidation ($)	Ball milling ($)	REM by biochar ($)	REM by metcoke ($)
Biochar	0	0	0	105	0
Metcoke	0	0	0	0	5.25
Potassium permanganate	0	377	0	0	0
Potassium hydroxide	0	0	300.2	0	0
Water	0	10.85	0	0	0
SUM of Materials	0	388	300	105	5.25
Transportation and refilling	26.50	26.50	26.50	0	0
Biochar pretreatment	0	0	0	0.44	0.23
Mixing	0	0.15	0.15	0.23	0
Furnace heating	63.17	0	0	0	0
Water bath heating	0	30.43	0	0	0
Filtration	0	0.39	0	0	0
Ball milling	0	0	56.42	0	0
Transportation and refilling	27.39	27.39	27.39	0	0
REM	0	0	0	24.46	24.46
Cyclone separation	0	0	0	0.17	0
Sieving	0	0	0	0	0.10
SUM of Process	117	85	110	25	24.89
SUM	**117**	**473**	**411**	**130**	**30**

*REM, rapid electrothermal mineralization. **PFOA, perfluorooctanoic acid; PFOS, perfluorooctane sulfonates. ***Material price: industrial water ($1.085 per tonne), $KMnO_4$ ($37.7 per kg), KOH ($31.6 per kg) biochar ($1400 per tonne) and metcoke ($150 per tonne). ****The consumed amount of biochar during REM process is calculated by subscribing the recycled mass from the input mass.

Remediating Soil Contaminated With Other Halogen-Containing Contaminates

[0150] In addition to PFAS mineralization, REM can also be extended to remediation soil by mineralizing other halogen-containing contaminates, including tetrachloroethylene (PCE), trichloroethylene (TCE), polychlorinated biphenyls (PCB), tribromophenol (TBP), brominated flame retardants (BFR), and halogen-containing antibiotics, like ciprofloxacin, chloramphenicol, iodoquinol.

[0151] TGA results revealed that all these contaminates degrades under a temperature lower than 600 °C. *See* **FIGS. 1A-1E** for TCE, PCE, TBP, PCB 2m and PCB 209, respectively. (The TGA was conducted under 100 mL min-1 N2 gas with a heating rate of 10 °C min-1.) These

TGA indicate that all these contaminates can be easily degraded under flash temperature.

[0152] For the PCE-contaminated soil, the REM process was performed by flashing it under different input voltages in an O-ring sealed system, then extracted the residue PCE from the flash soil using 5× hexane, and then tested the residual PCE contents by GC-MS. GC results showed that with the increasing input voltage and flash times, the lower PCE residue contents in the soil. **FIGS. 8A-8B**. With an input voltage of 80 V, the residue PCE contents were lower than the safety limits for the residential soil (~5.5 ppm).

[0153] IC and combustion IC (CIC) were used to quantify the mineralized Cl^- and total Cl contents in the soil before and after flash, which can realize an 85% mineralization of organic Cl into Cl^-. *See* **FIG. 9** (plots **901-902** for total Cl and Cl^-, respectively). Considering initial raw soil has a high content of Cl^- with a distinct variation (30-70 ppm), the mineralization of Cl has a relatively large error bar.

[0154] Similar evaluations were performed for TCE-contaminated soil. The corresponding IC and CIC data also shows a >80% mineralization ratios of TCE after flash. *See* **FIG. 10** (plots **1001-1002** for total Cl and Cl^-, respectively).

[0155] Using the similar processes, the degradation process of 2,4,6-tribromophenol (TBP) (which is a typical BFR compound) in the contaminated soil was evaluated, using IC and CIC. **FIG. 11** ((plots **1001-1002** for total Br and Br^-, respectively). When conducted in the sealed system, ~93% Br can be effectively mineralized into Br^-, which proves the efficiency of REM process to mineralize any kind of halogen-contained contaminants.

Applications

[0156] A facile and versatile REM methods can be used for the effective remediation of PFAS-contaminated soil. Through a rapid reaction with inherent Ca^{2+} in soil as well as biochar additives, harmful PFAS can be converted into its naturally mineralized form, CaF_2, in seconds. REM demonstrates high removal efficiencies (>99.9%) and fluorine mineralization ratios

(>90%) for various kinds of PFAS. Distinguished from some existing PFAS removal processes that could degrade soil and are PFAS-type-specific, REM can destroy a host of PFAS types and it preserves most of the soil properties, which is crucial to maintain the overall health and function of the soil ecosystem. With low time- and energy-consumption, high efficiency, and potential scalability, REM provides a promising method to remediate soil from PFAS contamination.

[0157] In addition to soil, these REM methods can be utilized to remedy other PFAS-contaminated solid waste.

[0158] The REM method can also be utilized for the for the effective remediation of soil that has other halogen-containing contaminates, including tetrachloroethylene (PCE), trichloroethylene (TCE), polychlorinated biphenyls (PCB), tribromophenol (TBP), brominated flame retardants (BFR), and halogen-containing antibiotics, like ciprofloxacin, chloramphenicol, iodoquinol.

[0159] While embodiments of the invention have been shown and described, modifications thereof can be made by one skilled in the art without departing from the spirit and teachings of the invention. The embodiments described and the examples provided herein are exemplary only, and are not intended to be limiting. Many variations and modifications of the invention disclosed herein are possible and are within the scope of the invention. The scope of protection is not limited by the description set out above, but is only limited by the claims which follow, that scope including all equivalents of the subject matter of the claims.

[0160] The disclosures of all patents, patent applications, and publications cited herein are hereby incorporated herein by reference in their entirety, to the extent that they provide exemplary, procedural, or other details supplementary to those set forth herein.

[0161] Amounts and other numerical data may be presented herein in a range format. It is to be understood that such range format is used merely for convenience and brevity and should

be interpreted flexibly to include not only the numerical values explicitly recited as the limits of the range, but also to include all the individual numerical values or sub-ranges encompassed within that range as if each numerical value and sub-range is explicitly recited. For example, a numerical range of approximately 1 to approximately 4.5 should be interpreted to include not only the explicitly recited limits of 1 to approximately 4.5, but also to include individual numerals such as 2, 3, 4, and sub-ranges such as 1 to 3, 2 to 4, *etc*. The same principle applies to ranges reciting only one numerical value, such as "less than approximately 4.5," which should be interpreted to include all of the above-recited values and ranges. Further, such an interpretation should apply regardless of the breadth of the range or the characteristic being described.

[0162] Unless defined otherwise, all technical and scientific terms used herein have the same meaning as commonly understood to one of ordinary skill in the art to which the presently disclosed subject matter belongs. Although any methods, devices, and materials similar or equivalent to those described herein can be used in the practice or testing of the presently disclosed subject matter, representative methods, devices, and materials are now described.

[0163] Following long-standing patent law convention, the terms "a" and "an" mean "one or more" when used in this application, including the claims.

[0164] Unless otherwise indicated, all numbers expressing quantities of ingredients, reaction conditions, and so forth used in the specification and claims are to be understood as being modified in all instances by the term "about." Accordingly, unless indicated to the contrary, the numerical parameters set forth in this specification and attached claims are approximations that can vary depending upon the desired properties sought to be obtained by the presently disclosed subject matter.

[0165] As used herein, the term "about" and "substantially" when referring to a value or to an amount of mass, weight, time, volume, concentration or percentage is meant to encompass

variations of in some embodiments ±20%, in some embodiments ±10%, in some embodiments ±5%, in some embodiments ±1%, in some embodiments ±0.5%, and in some embodiments ±0.1% from the specified amount, as such variations are appropriate to perform the disclosed method.

[0166] As used herein, the term "substantially perpendicular" and "substantially parallel" is meant to encompass variations of in some embodiments within ±10° of the perpendicular and parallel directions, respectively, in some embodiments within ±5° of the perpendicular and parallel directions, respectively, in some embodiments within ±1° of the perpendicular and parallel directions, respectively, and in some embodiments within ±0.5° of the perpendicular and parallel directions, respectively.

[0167] As used herein, the term "and/or" when used in the context of a listing of entities, refers to the entities being present singly or in combination. Thus, for example, the phrase "A, B, C, and/or D" includes A, B, C, and D individually, but also includes any and all combinations and subcombinations of A, B, C, and D.

REFERENCES

[0168] Al Amin, M., *et al.*, "Recent Advances in the Analysis of Per- and Polyfluoroalkyl Substances (PFAS)—A Review," *Environ Technol Innov*, **2020**, *19*, 100879 ("*Al Amin 2020*").

[0169] Algozeeb, W. A., *et al.*, "Flash Graphene from Plastic Waste," *ACS Nano*, **2020**, *14*(11), 15595–15604 ("*Algoeeb 2020*").

[0170] Alinezhad, A., *et al.*, "An investigation of thermal air degradation and pyrolysis of per- and polyfluoroalkyl substances and aqueous film-forming foams in soil," *ACS EST Engg.*, **2022**, *2*, 198-209 ("*Alinezhad 2022*").

[0171] Aro, R., *et al.*, "Organofluorine Mass Balance Analysis of Whole Blood Samples in Relation to Gender and Age," *Environ Sci Technol*, **2021**, *55*(19), 13142–13151 ("*Aro 2021*").

[0172] Baglieri, A., *et al.*, "A method for isolating soil organic matter after the extraction of

humic and fulvic acids," *Org. Geochem.*, **2007**, *38*, 140-150 ("*Baglieri 2007*").

[0173] Bahureksa, W., *et al.*, "Nitrogen enrichment during soil organic matter burning and molecular evidence of maillard reactions," *Environ. Sci. Technol.*, **2022**, *56*, 4597-4609 ("*Bahureksa 2022*").

[0174] Barman, U., *et al.*, "Soil texture classification using multi class support vector machine," *Inf. Process. Agric.*, **2020**, *7*, 318-332 ("*Barman 2020*").

[0175] Blöchl, P. E., "Projector augmented-wave method," *Phys. Rev. B*, **1994**, *50*, 17953 ("*Blöchl 1994*").

[0176] Bolan, N., *et al.*, "Remediation of poly-and perfluoroalkyl substances (pfas) contaminated soils–to mobilize or to immobilize or to degrade?" *J. Hazard. Mater.*, **2021**, *401*, 123892 ("*Bolan 2021*").

[0177] Booker, I. D., *et al.*, "Chloride-based SiC growth on a-axis 4H–SiC substrates," *Physica B Condens. Matter*, **2016**, *480*, 23-25 ("*Booker 2016*").

[0178] Brusseau, M. L., *et al.*, "PFAS Concentrations in Soils: Background Levels versus Contaminated Sites," *Sci Total Environ*, **2020**, *740* ("*Brusseau 2020*").

[0179] Buck, R. C., *et al.*, "Perfluoroalkyl and Polyfluoroalkyl Substances in the Environment: Terminology, Classification, and Origins," *Integr Environ Assess Manag*, **2011**, *7*(4), 513–541 ("*Buck 2011*").

[0180] Camdzic, D., *et al.*, "Quantitation of total pfas including trifluoroacetic acid with fluorine nuclear magnetic resonance spectroscopy," *Anal. Chem.*, **2023**, *95*, 5484-5488 ("*Camdzic 2023*").

[0181] Camdzic, D., *et al.*, "Total and class-specific analysis of per-and polyfluoroalkyl substances in environmental samples using nuclear magnetic resonance spectroscopy," *J. Hazard. Mater. Lett.*, **2021**, *2*, 100023 ("*Camdzic 2021*").

[0182] Carter, M. R., *et al.*, *Soil sampling and methods of analysis*, CRC press, **2007** ("*Carter*

2007").

[0183] Chen, W., *et al.*, "Flash Recycling of Graphite Anodes," *Advanced Materials*, **2023**, *35*(8), 2207303 ("*Chen 2023*").

[0184] Chen, W., *et al.*, "Heteroatom-Doped Flash Graphene," *ACS Nano*, **2022**, *16*(4), 6646–6656 ("*Chen 2022*").

[0185] Chen, Y., *et al.*, "Ultra-fast self-assembly and stabilization of reactive nanoparticles in reduced graphene oxide films," *Nat. Commun.*, **2016**, *7*, 12332 ("*Chen 2016*").

[0186] Cheng, Y., *et al.*, "Electric current aligning component units during graphene fiber Joule heating," *Adv. Funct. Mater.*, **2021**, *32*, 2103493 ("*Cheng 2021*").

[0187] Chow, S. J., *et al.*, "Comparative Investigation of PFAS Adsorption onto Activated Carbon and Anion Exchange Resins during Long-Term Operation of a Pilot Treatment Plant," *Water Res*, **2022**, *226*, 119198 ("*Chow 2022*").

[0188] Chungu, D., *et al.*, "Fire alters the availability of soil nutrients and accelerates growth of eucalyptus grandis in Zambia," *J. Forest. Res.*, **2020**, *31*, 1637-1645 ("*Chungu 2020*").

[0189] Clavaguera-Mora, M. T., *et al.*, "Growth of SiC films obtained by LPCVD," *Diam. Relat. Mater.*, **1997**, *6*, 1306-1310 ("*Clavaguera-Mora 1997*").

[0190] Crosby, N. T., "Equilibria of Fluorosilicate Solutions with Special Reference to the Fluoridation of Public Water Supplies," *Journal of Applied Chemistry*, **1969**, *19*(4), 100–102 ("*Crosby 1969*").

[0191] Cui, B., *et al.*, "Waste to wealth: Defect-rich ni-incorporated spent lifepo4 for efficient oxygen evolution reaction," *Sci. China Mater.*, **2021**, *64*, 2710-2718 ("*Cui 2021*").

[0192] Das, P., *et al.*, "Remediation of perfluorooctane sulfonate in contaminated soils by modified clay adsorbent—a risk-based approach," *Water Air Soil Pollut.*, **2013**, *224*, 1-14 ("*Das 2013*").

[0193] Dastgheib, S. A., *et al.*, "Thermogravimetric Studies for the Incineration of an Anion

Exchange Resin Laden with Short- or Long-Chain PFAS Compounds Containing Carboxylic or Sulfonic Acid Functionalities in the Presence or Absence of Calcium Oxide," *Ind Eng Chem Res*, **2021**, *60*(47), 16961–16968 ("*Dastgheib 2021*").

[0194] Deng, B., *et al.*, "Heavy metal removal from coal fly ash for low carbon footprint cement," *Commun. Eng.*, **2023**, *2*, 13 ("*Deng I 2023*").

[0195] Deng, B., *et al.*, "High-temperature electrothermal remediation of multi-pollutants in soil," *Nat. Commun.*, **2023**, *14*, 6371 ("*Deng II 2023*").

[0196] Deng, B., *et al.*, "Rare earth elements from waste," *Sci. Adv.*, **2022**, *8*, eabm3132 ("*Deng 2022*").

[0197] Deng, B., *et al.*, "Urban mining by flash Joule heating," *Nat. Commun.*, **2021**, *12*, 5794 ("*Deng 2021*").

[0198] Dombrowski, P. M., *et al.*, "Technology review and evaluation of different chemical oxidation conditions on treatability of pfas.," *Remediation*, **2018**, *28*, 135-150 ("*Dombrowski 2018*").

[0199] Dong, P. A. V., *et al.*, "Economic and environmental assessment of recovery and disposal pathways for CFRP waste management," *Resour. Conserv. Recycl.*, **2018**, *133*, 63-75 ("*Dong 2018*").

[0200] Dong, Q., *et al.*, "Depolymerization of plastics by means of electrified spatiotemporal heating," *Nature*, **2023**, *616*, 488-494 ("*Dong 2023*").

[0201] Dong, Q., *et al.*, "Programmable heating and quenching for efficient thermochemical synthesis, *Nature*, **2022**, *605*, 470-476 ("*Dong 2022*").

[0202] Duan, L., *et al.*, "Efficient photocatalytic pfoa degradation over boron nitride," *Environ. Sci. Technol. Lett.*, **2020**, *7*, 613-619 ("*Duan 2020*").

[0203] Duchesne, A. L., *et al.*, "Remediation of PFAS-Contaminated Soil and Granular Activated Carbon by Smoldering Combustion," *Environ Sci Technol*, **2020**, *54*(19), 12631–

12640 ("*Duchesne 2020*").

[0204] Dudarev, S. L., *et al.*, "Electron-energy-loss spectra and the structural stability of nickel oxide: An LSDA+ U study," *Phys. Rev. B*, **1988**, *57*, 1505 ("*Dudarev 1998*").

[0205] Ellis, D. A., *et al.*, "Thermolysis of Fluoropolymers as a Potential Source of Halogenated Organic Acids in the Environment," *Nature*, **2001**, *412*(6844), 321–324 ("*Ellis 2001*").

[0206] Evich, M. G., *et al.*, "Per-and Polyfluoroalkyl Substances in the Environment," *Science*, **2022**, *375*, eabg9065 ("*Evich 2022*").

[0207] Faé, G. S., *et al.*, "Making soil particle size analysis by laser diffraction compatible with standard soil texture determination methods," *Soil Sci. Soc. Am. J.*, **2019**, *83*, 1244-1252 ("*Faé 2019*").

[0208] Feng, G., *et al.*, "Highly selective photoelectroreduction of carbon dioxide to ethanol over graphene/silicon carbide composites," *Angew. Chem. Int. Ed.*, **2023**, *135*, e202218664 ("*Feng 2023*").

[0209] Flores, C., *et al.*, "Occurrence of Perfluorooctane Sulfonate (PFOS) and Perfluorooctanoate (PFOA) in N.E. Spanish Surface Waters and Their Removal in a Drinking Water Treatment Plant That Combines Conventional and Advanced Treatments in Parallel Lines," *Sci Total Environ*, **2013**, *461 462*, 618–626 ("*Flores 2013*").

[0210] Fournie, T., *et al.*, "Smouldering to treat PFAS in sewage sludge," *Waste Management*, **2023**, *164*, 219-227 ("*Fournie 2023*").

[0211] Glüge, J., *et al.*, "An Overview of the Uses of Per-and Polyfluoroalkyl Substances (PFAS)," *Environ. Sci. Process. Impacts*, **2020**, *22*, 2345-2373 ("*Glüge 2020*").

[0212] Gorrochategui, E., *et al.*, "Perfluoroalkylated substance effects in Xenopus laevis A6 kidney epithelial cells determined by ATR-FTIR spectroscopy and chemometric analysis," *Chem. Res. Toxicol.*, **2016**, *29*, 924-932 ("*Gorrochategui 2016*").

[0213] Guin, J. P., *et al.*, "Challenges Facing Sustainable Visible Light Induced Degradation of Poly- and Perfluoroalkyls (PFA) in Water: A Critical Review," *ACS Engineering Au*, **2022**, *2*(3), 134–150 ("*Guin 2022*").

[0214] Guo, X., *et al.*, "Nonlinear optical properties of 6H-SiC and 4H-SiC in an extensive spectral range," *Opt. Mater. Express*, **2021**, *11*, 1080-1092 ("*Guo 2021*").

[0215] Guo, X., *et al.*, "Preparation of SiC powders by carbothermal reduction with bamboo charcoal as renewable carbon source," *J. Adv. Ceram.*, **2013**, *2*, 128-134 ("*Guo 2013*").

[0216] Hale, S. E., *et al.*, "Sorbent amendment as a remediation strategy to reduce pfas mobility and leaching in a contaminated sandy soil from a norwegian firefighting training facility," *Chemosphere*, **2017**, *171*, 9-18 ("*Hale 2017*").

[0217] Han, X., *et al.* "Epitaxial cubic silicon carbide photocathodes for visible-light-driven water splitting," *Chem. Eur. J.*, **2020**, *26*, 3586-3590 ("*Han 2020*").

[0218] Helalia, A. M., "The relation between soil infiltration and effective porosity in different soils," *Agr. Water Manage.*, **1993**, *24*, 39-47 ("*Helalia 1993*").

[0219] Henkelman, G., *et al.*, "A climbing image nudged elastic band method for finding saddle points and minimum energy paths," *J. Chem. Phys.*, **2000**, *113*, 9901-9904 ("*Henkelman 2000*").

[0220] Hillier, S., "Quantitative analysis of clay and other minerals in sandstones by X-ray powder diffraction (XRPD), *Clay mineral cements in sandstones*, **1999**, 213-251 ("*Hillier 1999*").

[0221] Huang, D., *et al.*, "Photoinduced hydrodefluorination mechanisms of perfluorooctanoic acid by the sic/graphene catalyst," *Environ. Sci. Technol.*, **2016**, *50*, 5857-5863 ("*Huang 2016*").

[0222] Huang, P.-J. *et al.*, "Reusable functionalized hydrogel sorbents for removing long-and short-chain perfluoroalkyl acids (PFAAs) and GenX from aqueous solution," *ACS omega*,

2018, *3*, 17447-17455 ("*Huang 2018*").

[0223] Hunter Anderson, R., *et al.*, "Partitioning of Poly- and Perfluoroalkyl Substances from Soil to Groundwater within Aqueous Film-Forming Foam Source Zones," *J Contam Hydrol*, **2019**, *220*, 59–65 ("*Hunter Anderson 2019*").

[0224] Inkotte, J., *et al.*, "Litter removal impacts on soil biodiversity and eucalypt plantation development in the seasonal tropics," *J. Forest. Res.*, **2023**, *34*, 735-748 ("*Inkotte 2023*").

[0225] Javaherian, M., *et. al.*, "Bench-scale veg research & development study: Implementation memorandum for ex-situ thermal desorption of perfluoroalkyl compounds (pfcs) in soils," Endpoint Consulting Technical Memorandum, **2016** ("*Javaherian 2016*").

[0226] Jha, H. S., *et al.*, "Highly crystalline silicon carbide thin films grown at low substrate temperature by HWCVD technique," *J. Mater. Sci: Mater. Electron.*, **2015**, *26*, 1381-1388 ("*Jha 2015*").

[0227] Jia, C., *et al.*, "Graphene environmental footprint greatly reduced when derived from biomass waste via flash Joule heating," *One Earth*, **2022**, *5*, 1394-1403 ("*Jia 2022*").

[0228] Jia, X., *et al.*, "Emerging and Legacy Per- and Polyfluoroalkyl Substances in an Elderly Population in Jinan, China: The Exposure Level, Short-Term Variation, and Intake Assessment," *Environ Sci Technol*, **2022**, *56*(12), 7905–7916 ("*Jia 2022*").

[0229] Jiang, R., *et al.*, "Ultrafast synthesis for functional nanomaterials," *Cell Rep. Phys. Sci.*, **2021**, *2* ("*Jiang 2021*").

[0230] Judy, J. D., *et al.*, "Trophic Transfer Of Pfas From Tomato (Solanum Lycopersicum) To Tobacco Hornworm (Manduca Sexta) Caterpillars," *Environ. Pollut.*, **2022**, *310*, 119814 ("*Judy 2022*").

[0231] Kresse, G., *et al.*, "Efficient iterative schemes for ab initio total-energy calculations using a plane-wave basis set," *Phys. Rev. B*, **1996**, *54*, 11169-11186 ("*Kresse 1996*").

[0232] Kupryianchyk, D., *et al.*, "Treatment of sites contaminated with perfluorinated

compounds using biochar amendment," *Chemosphere*, **2016**, *142*, 35-40 ("*Kupryianchyk 2016*").

[0233] Labine, L. M, *et al.*, "Comparison of sub-lethal metabolic perturbations of select legacy and novel perfluorinated alkyl substances (PFAS) in Daphnia magna," *Environ. Res.*, **2022**, *212*, 113582 ("*Labine 2022*").

[0234] Lee, M. C., *et al.*, "Efficient Destruction of CF_4 through in Situ Generation of Alkali Metals from Heated Alkali Halide Reducing Mixtures," *Environ Sci Technol*, **2002**, *36*(6), 1367–1371 ("*Lee 2002*").

[0235] Leeson, A., *et al.*, "Identifying and Managing Aqueous Film-Forming Foam-Derived Per- and Polyfluoroalkyl Substances in the Environment," *Environ. Toxicol. Chem.*, **2021**, *40*, 24-36 ("*Leeson 2021*").

[0236] Lin, L., *et al.*, "Copyrolysis of recycled plastics and biomass reduces biochar bioavailable silicon production and cadmium phytotoxicity," *ACS EST Engg.*, **2022**, *2*, 1356-1364 ("*Lin 2022*").

[0237] Liu, C. S., *et al.*, "Oxidative decomposition of perfluorooctanesulfonate in water by permanganate," *Sep. Purif. Technol.*, **2012**, *87*, 95-100 ("*Liu 2012*").

[0238] Liu, S., *et al.*, "Extreme environmental thermal shock induced dislocation-rich Pt nanoparticles boosting hydrogen evolution reaction," *Adv. Mater.*, **2022**, *34*, 2106973-2106979 ("*Liu 2022*").

[0239] Liu, Y. L., *et al.*, "Ion Exchange Removal and Resin Regeneration to Treat Per- and Polyfluoroalkyl Ether Acids and Other Emerging PFAS in Drinking Water," *Water Res*, **2021**, *207*, 117781 ("*Liu 2021*").

[0240] Liu, Y., *et al.*, "Method of recovering the fibrous fraction of glass/epoxy composites," *J. Reinf. Plast. Compos.*, **2006**, *25*, 1525-1533 ("*Liu 2006*").

[0241] Luo, J., *et al.*, "Waste plastics complement biochar: Innovative approach in curbing

toxicants (kcn/nacn) in n-containing biochar," *ACS Sustainable Chem. Eng.*, **2021**, *9*, 4617-4624 ("*Luo 2021*").

[0242] Luong, D. X., *et al.*, "Gram-Scale Bottom-up Flash Graphene Synthesis," *Nature*, **2020**, *577*, 647 ("*Luong 2020*").

[0243] Mahinroosta, R., *et al.*, "A review of the emerging treatment technologies for pfas contaminated soils," *J. Environ. Manage.*, **2020**, *255*, 109896 ("*Mahinroosta 2020*").

[0244] Maimaiti, A., *et al.*, "Competitive adsorption of perfluoroalkyl substances on anion exchange resins in simulated afff-impacted groundwater," *Chem. Eng. J.*, **2018**, *348*, 494-502 ("*Maimaiti 2018*").

[0245] Makuła, P., *et al.*, "How to correctly determine the band gap energy of modified semiconductor photocatalysts based on UV–Vis spectra," *J. Phys. Chem. Lett*, **2018**, *9*, 6814-6817 ("*Makula 2018*").

[0246] McCleaf, P., *et al.*, "Removal Efficiency of Multiple Poly- and Perfluoroalkyl Substances (PFASs) in Drinking Water Using Granular Activated Carbon (GAC) and Anion Exchange (AE) Column Tests," *Water Res*, **2017**, *120*, 77–87 ("*McCleaf 2017*").

[0247] Mehlich, A., "Mehlich 3 soil test extractant: A modification of mehlich 2 extractant," *Commun. Soil Sci. Plant Anal.*, **1984**, *15*, 1409-1416 ("*Mehlich 1984*").

[0248] Min, T. B., *et al.*, "Experimental Study on the Development of Compressive Strength of Early Concrete Age Using Calcium-Based Hardening Accelerator and High Early Strength Cement," *Constr Build Mater*, **2014**, *64*, 208–214 ("*Min 2014*").

[0249] Monkhorst, H. J., *et al.*, "Special points for Brillouin-zone integrations," *Phys. Rev. B*, **1976**, *13*, 5188 ("*Monkhorst 1976*").

[0250] Nath, P., *et al.*, "Use of OPC to Improve Setting and Early Strength Properties of Low Calcium Fly Ash Geopolymer Concrete Cured at Room Temperature," *Cem Concr Compos*, **2015**, *55*, 205–214 ("*Nath 2015*").

[0251] Perdew, J. P., *et al.*, "Generalized gradient approximation made simple," *Phys. Rev. Lett.*, **1996**, *77*, 3865-3868 ("*Perdew 1996*").

[0252] Pilbeam, D. J., *et al.*, *Handbook of plant nutrition*, CRC Press, **2016** ("*Pilbeam 2016*").

[0253] Salvatore, D., *et al.*, "Presumptive Contamination: A New Approach to PFAS Contamination Based on Likely Sources," *Environ. Sci. Technol. Lett.*, **2022**, *9*, 983-990 ("*Salvatore 2022*").

[0254] Schaefer, C. E., *et al.*, "Release Of Poly- And Perfluoroalkyl Substances From Finished Biosolids In Soil Mesocosms," *Water Res.*, **2022**, *217*, 118405 ("*Schaefer 2022*").

[0255] Scher, D. P., *et al.*, "Occurrence of Perfluoroalkyl Substances (PFAS) in Garden Produce at Homes with a History of PFAS-Contaminated Drinking Water," *Chemosphere*, **2018**, *196*, 548–555 ("*Scher 2018*").

[0256] Shin, Y., *et al.*, "Synthesis of SiC ceramics by the carbothermal reduction of mineralized wood with silica," *Adv. Mater.*, **2005**, *17*, 73-77 ("*Shin 2005*").

[0257] Siciliano, S. D., *et al.*, "Soil fertility is associated with fungal and bacterial richness, whereas pH is associated with community composition in polar soil microbial communities," *Soil Biol. Biochem.*, **2014**, *78*, 10-20 ("*Siciliano 2014*").

[0258] Sonmez Baghirzade, B., *et al.*, "Thermal Regeneration of Spent Granular Activated Carbon Presents an Opportunity to Break the Forever PFAS Cycle," *Environ Sci Technol*, **2021**, *55*(9), 5608–5619 ("*Sonmez Baghirzade 2021*").

[0259] Sörengård, M., Lindh, *et al.*, "Thermal desorption as a high removal remediation technique for soils contaminated with per-and polyfluoroalkyl substances (pfass)," *PloS one*, **2020**, *15*, e0234476 ("*Sörengård 2020*").

[0260] Stanford, M. G., *et al.*, "Flash graphene morphologies," *ACS Nano*, **2020**, *14*, 13691-13699 ("*Stanford 2020*").

[0261] Stoiber, T., *et al.*, "Disposal of Products and Materials Containing Per- and

Polyfluoroalkyl Substances (PFAS): A Cyclical Problem," *Chemosphere*, **2020**, *260*, 127659 ("*Stoiber 2020*").

[0262] Sun, C., *et al.*, "Interfacial coupled design of epitaxial graphene@SiC schottky junction with built-in electric field for high-performance anodes of lithium ion batteries," *Nano Energy*, **2020**, *77*, 105092 ("*Sun 2020*").

[0263] Sun, L., *et al.*, "Millisecond self-heating and quenching synthesis of Fe/carbon nanocomposite for superior reductive remediation, *Appl. Catal. B*, **2023**, *342*, 123361 ("*Sun 2023*").

[0264] Sun, X., *et al.*, "SiC nanofibers as long-life lithium-ion battery anode materials," *Front. Chem.*, **2018**, ***6***, 166 ("*Sun 2018*").

[0265] B. Trang, *et al.*, "Low-temperature mineralization of perfluorocarboxylic acids," *Science*, **2022**, *377*, 839-845 ("*Trang 2022*").

[0266] Vargette, L. D., *et al.*, "Prospects of complete mineralization of per-and polyfluoroalkyl substances by thermal destruction methods," *Curr. Opin. Chem. Eng.*, **2022**, *42*, 100954 ("*Vargette 2023*").

[0267] Vecitis, C. D., *et al.*, "Treatment technologies for aqueous perfluorooctanesulfonate (pfos) and perfluorooctanoate (pfoa)," *Front. Environ. Sci. Eng. China*, **2009**, *3*, 129-151 ("*Vecitis 2009*").

[0268] Wang, C., *et al.*, "A general method to synthesize and sinter bulk ceramics in seconds," *Science*, **2020**, *368*, 521-526 ("*Wang 2020*").

[0269] Wang, F., *et al.*, "Effectiveness and Mechanisms of Defluorination of Perfluorinated Alkyl Substances by Calcium Compounds during Waste Thermal Treatment," *Environ Sci Technol*, **2015**, *49*(9), 5672–5680 ("*Wang 2015*").

[0270] Wang, F., *et al.*, "Mineralization behavior of fluorine in perfluorooctanesulfonate (pfos) during thermal treatment of lime-conditioned sludge," *Environ. Sci. Technol.*, **2013**, *47*, 2621-

2627 ("*Wang 2013*").

[0271] Wang, F., *et al.*, "Influence of Calcium Hydroxide on the Fate of Perfluorooctanesulfonate under Thermal Conditions," *J Hazard Mater*, **2011**, *192*(3), 1067–1071 ("*Wang 2011*").

[0272] Washington, J. W., *et al.*, "Decades-Scale Degradation Of Commercial, Side-Chain, Fluorotelomer-Based Polymers In Soils And Water," *Environ. Sci. Technol.*, **2015**, *49*, 915-923 ("*Washington 2015*").

[0273] Watanabe, N., *et al.*, "Thermal Mineralization Behavior of PFOA, PFHxA, and PFOS during Reactivation of Granular Activated Carbon (GAC) in Nitrogen Atmosphere," *Environmental Science and Pollution Research*, **2018**, *25*(8), 7200–7205 ("*Watanabe 2018*").

[0274] Watanabe, N., *et al.*, "Residual Organic Fluorinated Compounds from Thermal Treatment of PFOA, PFHxA and PFOS Adsorbed onto Granular Activated Carbon (GAC)," *Journal of Material Cycles and Waste Management*, **2016**, *18*(4), 625–630 ("*Watanabe 2016*").

[0275] Weber, N. H., *et al.*, "Kinetics of Decomposition of PFOS Relevant to Thermal Desorption Remediation of Soils," *Ind Eng Chem Res*, **2021**, *60*(25), 9080–9087 ("*Weber 2021*").

[0276] Weil, R., *et al.*, *The nature and properties of soils,* 15th edition, **2017** ("*Weil 2017*").

[0277] Whitacre, D.M., *et al.*, "Aquatic toxicology of perfluorinated chemicals," *Rev. Environ. Contam. Toxicol.*, **2010**, 1-52 ("*Whitacre 2010*").

[0278] Wyss, K. M., *et al.*, "Upcycling of waste plastic into hybrid carbon nanomaterials," *Adv. Mater.*, **2023**, *35*, 2209621 ("*Wyss I 2023*").

[0279] Wyss, K. M., *et al.*, "Upcycling of waste plastic into hybrid carbon nanomaterials," *Adv. Mater.*, **2023**, *35*, 2209621 ("*Wyss II 2023*").

[0280] Wyss, K., *et al.*, "Upcycling and urban mining for nanomaterial synthesis," *Nano Today*, **2023**, *49*, 101781 ("*Wyss III 2023*").

[0281] Xiao, F., *et al.*, "Thermal Stability and Decomposition of Perfluoroalkyl Substances on Spent Granular Activated Carbon," *Environ Sci Technol Lett*, **2020**, *7*(5), 343–350 ("*Xiao 2020*").

[0282] Xiao, F., *et al.*, "PFOA and PFOS Are Generated from Zwitterionic and Cationic Precursor Compounds during Water Disinfection with Chlorine or Ozone," *Environ Sci Technol Lett*, **2018**, *5*(6), 382–388 ("*Xiao 2018*").

[0283] Xiao, F., *et al.*, "Mechanisms for Removal of Perfluorooctane Sulfonate (PFOS) and Perfluorooctanoate (PFOA) from Drinking Water by Conventional and Enhanced Coagulation," *Water Res*, **2013**, *47*(1), 49–56 ("*Xiao 2013*").

[0284] Xiao, X., *et al.*, "Sorption of Poly- and Perfluoroalkyl Substances (PFASs) Relevant to Aqueous Film-Forming Foam (AFFF)-Impacted Groundwater by Biochars and Activated Carbon," *Environ Sci Technol*, **2017**, *51*(11), 6342–6351 ("*Xiao 2017*").

[0285] Xu, T., *et al.*, "Enhanced Photocatalytic Degradation of Perfluorooctanoic Acid Using Carbon-Modified Bismuth Phosphate Composite: Effectiveness, Material Synergy and Roles of Carbon," *Chemical Engineering Journal*, **2020**, *395*, 124991 ("*Xu 2020*").

[0286] Xue, X., *et al.*, "A technology review of recycling methods for fiber-reinforced thermosets," *J. Reinf. Plast. Compos.*, **2021**, *41*, 459-480 ("*Xue 2021*").

[0287] Yakobson, B. I., *et al.*, "Flash Graphene Morphologies," *ACS Nano*, **2020**, *14*(10), 13691–13699 ("*Yakobson 2020*").

[0288] Yang, F., *et al.*, "Biomass inherent metal interfere carbothermal reduction modification of biochar for cd immobilization," *Sci. Total Environ.*, **2023**, *867*, 161425 ("*Yang 2023*").

[0289] Yang, Z., *et al.*, "Degradation of Hexafluoropropylene Oxide Tetrameric Acid (HFPO-TeA) Using Electrocatalytic Ozone Technique," *Water Cycle*, **2022**, *3*, 106–111 ("*Yang 2022*").

[0290] Yeung, L. W. Y., *et al.*, "Perfluorinated Compounds and Total and Extractable Organic

Fluorine in Human Blood Samples from China," *Environ Sci Technol*, **2008**, *42*(21), 8140–8145 ("*Yeung 2008*").

[0291] You, Y., *et al.*, "Growth of NiO nanorods, SiC nanowires and monolayer graphene via a CVD method," *Green Chem.*, **2017**, *19*, 5599-5607 ("*You 2017*").

[0292] F. Yu *et al.*, "Rapid self-heating synthesis of Fe-based nanomaterial catalyst for advanced oxidation," *Nat. Commun.*, **2023**, *14*, 4975 ("*Yu 2023*").

[0293] Yu, M., *et al.*, "Silicon carbide ("SiC) derived from agricultural waste potentially competitive with silicon anodes," *Green Chem.*, **2022**, *24*, 4061-4070 ("*Yu* 2022").

[0294] Yu, M., *et al.*, "Adjusting SiO_2 : C mole ratios in rice hull ash ("RHA) to control carbothermal reduction to nanostructured SiC, Si_3N_4 or Si_2N_2O composites," *Green Chem.*, **2021**, *23*, 7751-7762 ("*Yu 2021*").

[0295] Zhang, B., *et al.*, "Eluviation of dissolved organic carbon under wetting and drying and its influence on water infiltration in degraded soils restored with vegetation," *Eur. J. Soil Sci.*, **2004**, *55*, 725-737 ("*Zhang 2004*").

[0296] Zhang, D., *et al.*, "Sorption of Perfluoroalkylated Substances (PFASs) onto Granular Activated Carbon and Biochar," *Environ Technol.*, **2019**, *42*(12), 1798–1809 ("*Zhang 2019*").

[0297] Zhang, K., *et al.*, "Destruction of perfluorooctane sulfonate (pfos) and perfluorooctanoic acid (pfoa) by ball milling," *Environ. Sci. Technol.*, **2013**, *47*, 6471-6477 ("*Zhang 2013*").

[0298] Zhao, C., *et al.*, "Thermal desorption for remediation of contaminated soil: A review, *Chemosphere*, **2019**, *221*, 841-855 ("*Zhao 2019*").

[0299] Zuur, A. F., *et al.*, "Glm and gam for count data," *Mixed effects models extensions in ecology with R*, **2009**, 209-243 ("*Zuur 2009*").

WHAT IS CLAIMED IS:

1. A method comprising:

(a) mixing a PFAS-contaminated soil with a conductive additive to form a PFAS-contaminated soil mixture, wherein

(i) the PFAS-contaminated soil is soil that comprises a pollutant selected from the group consisting of per- and polyfluorinated alkyl substances (PFAS); and

(b) performing a rapid electrothermal mineralization (REM) process utilizing the PFAS-contaminated soil mixture to remediate the PFAS-contaminated soil.

2. The method of Claim 1, wherein the PFAS is selected from the group consisting of perfluorooctane acid (PFOA), perfluorooctane sulfonate (PFOS), perfluorohexane sulfonate (PFH_xS), perfluorobutane sulfonate (PFBS), polytetrafluoroethylene (PTFE), and combinations thereof.

3. The method of any of Claims 1-2, wherein the step of performing the REM process comprises subjecting the PFAS-contaminated soil mixture to a flash Joule heating process.

4. The method of any of Claims 1-3, the REM process remediates the PFAS-contaminated soil by removing more than 90 wt% of the PFAS from the PFAS-contaminated soil.

5. The method of Claim 4, the REM process remediates the PFAS-contaminated soil by removing more than 99 wt% of the PFAS from the PFAS-contaminated soil.

6. The method of any of Claims 1-5, wherein the method further comprises removing the PFAS-contaminated soil from the ground before the step of performing the REM process.

7. The method of any of Claims 1-6, wherein

(a) the PFAS-contaminated soil is ground soil located on the ground (PFAS-contaminated ground soil);

(b) the step of mixing the PFAS-contaminated soil with the conductive additive comprises mixing the conductive additive to the PFAS-contaminated ground soil on-site in the ground; and

(c) the step of performing the REM process comprises utilizing electrodes inserted in the ground.

8. The method of Claim 7, wherein,

(a) the step of performing the REM process comprises utilizing two or more electrode arrays, and

(b) the two or more electrode arrays comprise the electrodes inserted in the ground.

9. The method of Claim 8, wherein, during the step of performing the REM process, the two or more electrode arrays are utilized by independently discharging each of the two or more electrode arrays.

10. The method of Claim 9, wherein the independent discharging of each of the two or more electrode arrays uniformly heats the soil around the two or more electrodes.

11. The method of any of Claims 1-10, wherein the method further comprises that, after the REM process, separating at least some of the conductive carbon additive from the remediated PFAS-contaminated soil.

12. The method of Claim 11, wherein the step of separating is based upon grain size of the conductive carbon additive and particle size of the remediated PFAS-contaminated soil.

13. The method of Claim 11, wherein the step of separating is based upon difference in densities between the conductive carbon additive and the remediated PFAS-contaminated soil.

14. The method of any of Claims 1-13, wherein at least some of the PFAS are mineralized into a fluoride salt.

15. The method of any of Claims 1-14, wherein graphene is formed during the step of performing the REM process.

16. A method comprising:

(a) mixing a contaminated soil with a conductive additive to form a contaminated soil mixture, wherein

(i) the contaminated soil is soil that comprises a pollutant selected from the group consisting of halogen-containing contaminates; and

(b) performing a rapid electrothermal mineralization (REM) process utilizing the contaminated soil mixture to remediate the contaminated soil.

17. The method of Claim 16, wherein the pollutant is selected from the group consisting of tetrachloroethylene (PCE), trichloroethylene (TCE), polychlorinated biphenyls (PCB), brominated flame retardants (BFR), and halogen-containing antibiotics.

18. The method of Claim 16, wherein the pollutant comprises the halogen-containing antibiotic and the halogen-containing antibiotic is selected from the group consisting of ciprofloxacin, chloramphenicol, and iodoquinol.

19. An apparatus that performs the method of any of Claims 1-18.

20. Graphene made by the method of Claim 15.

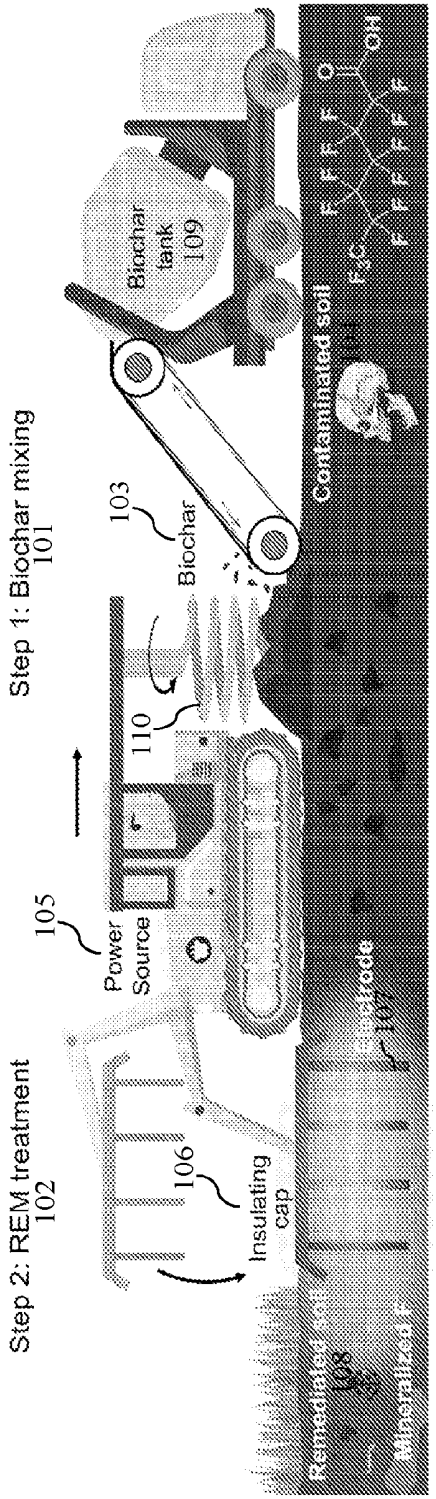
Step 1: Biochar mixing
101
Step 2: REM treatment
102
Biochar
103
Biochar tank
109
Power Source
105
Insulating cap
106
Electrode
107
110
Contaminated soil
Remediated soil
108
Mineralized f
OH

FIG. 1A

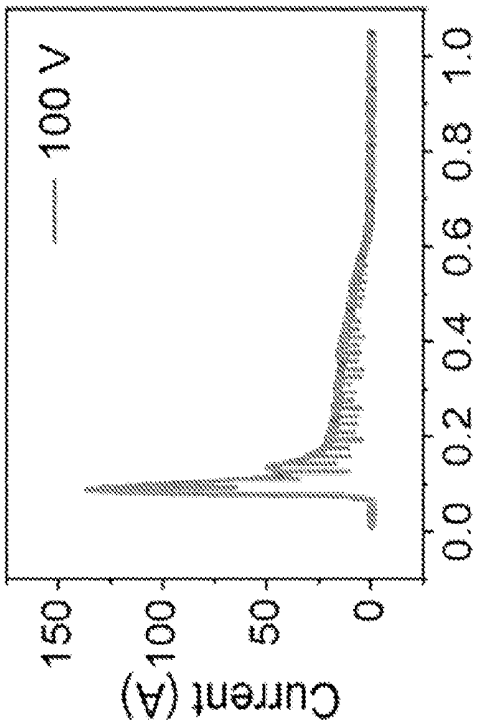
100 V
Current (A)
150
100
50
0
0.0
0.2
0.4
0.6
0.8
1.0
Time (s)

FIG. 1C

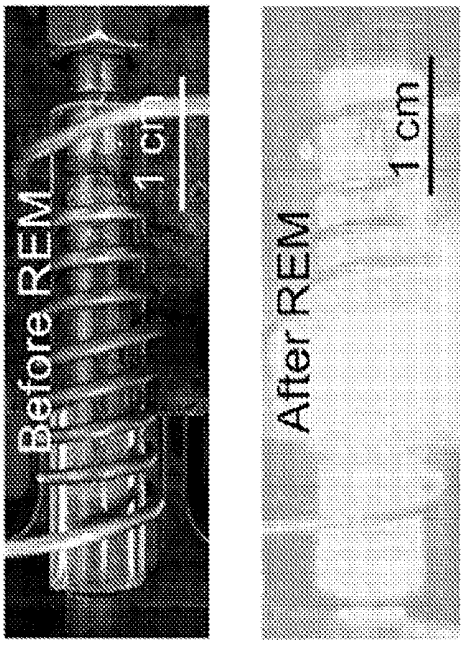
Before REM
1 cm
After REM
1 cm

FIG. 1B

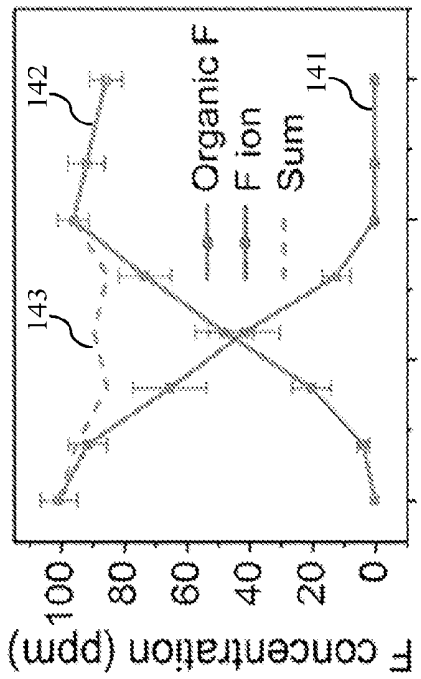
F concentration (ppm)
0
20
40
60
80
100
0
50
100
150
Input voltage (V)
Organic F
F ion
Sum
141
142
143

FIG. 1E

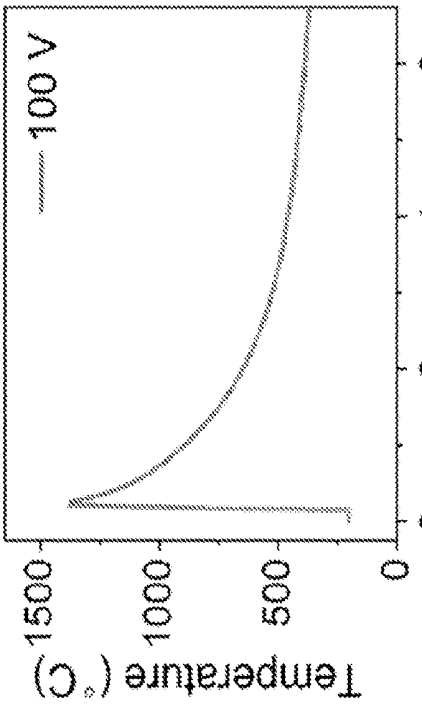
Temperature (°C)
0
500
1000
1500
0
2
4
6
Time (s)
100 V

FIG. 1D

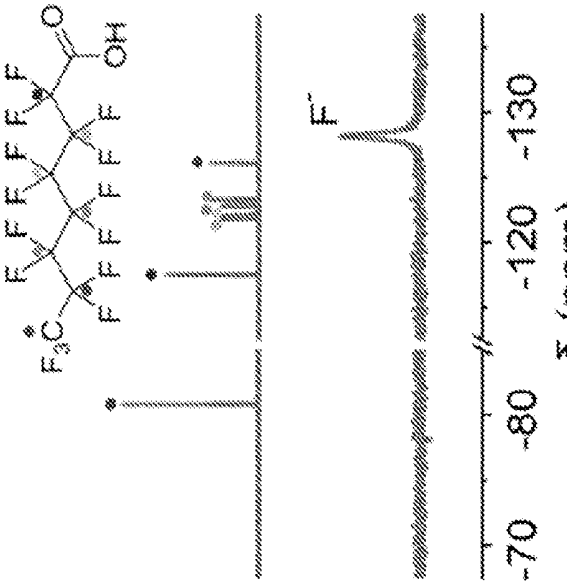
F
F
F
F
F
F
F
F
F
F
F
F
F
F
O
OH
F3C
F⁻
-70
-80
-120
-130
δ (ppm)

FIG. 1G

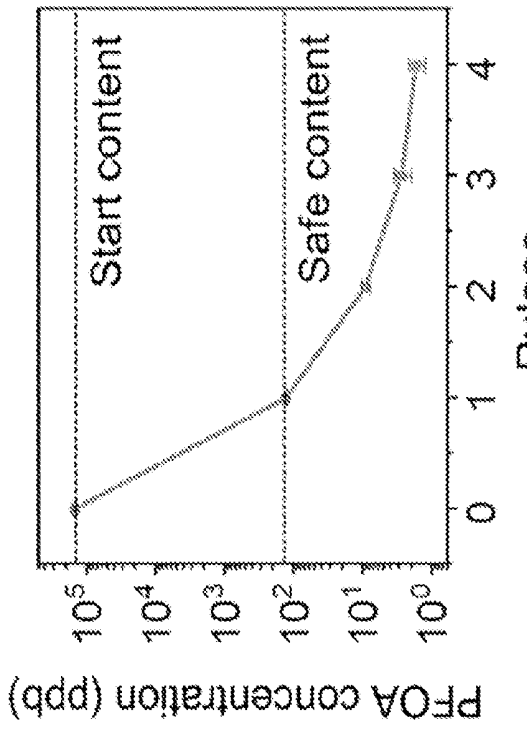
Start content
Safe content
10^5
10^4
10^3
10^2
10^1
10^0
0
1
2
3
4
Pulses
PFOA concentration (ppb)

FIG. 1F

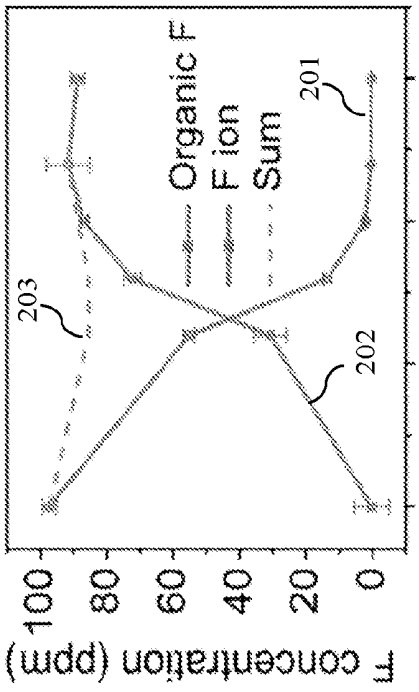

FIG. 2A

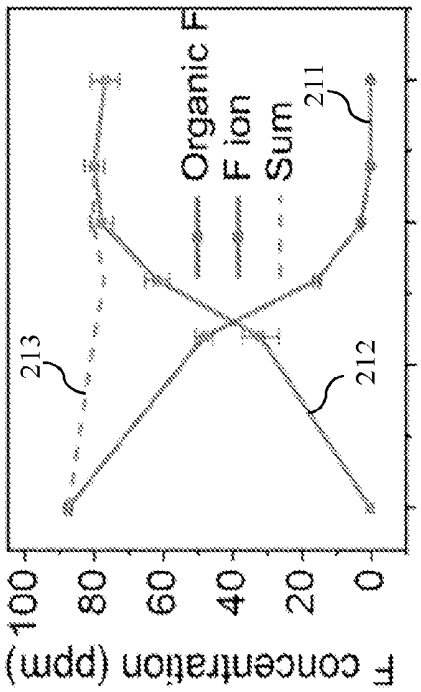

FIG. 2B

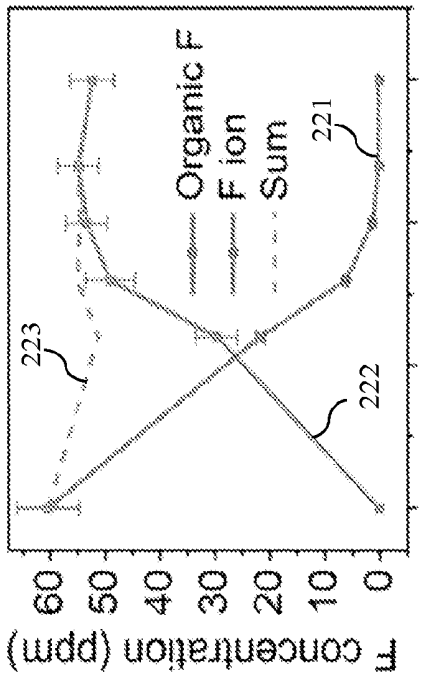

FIG. 2C

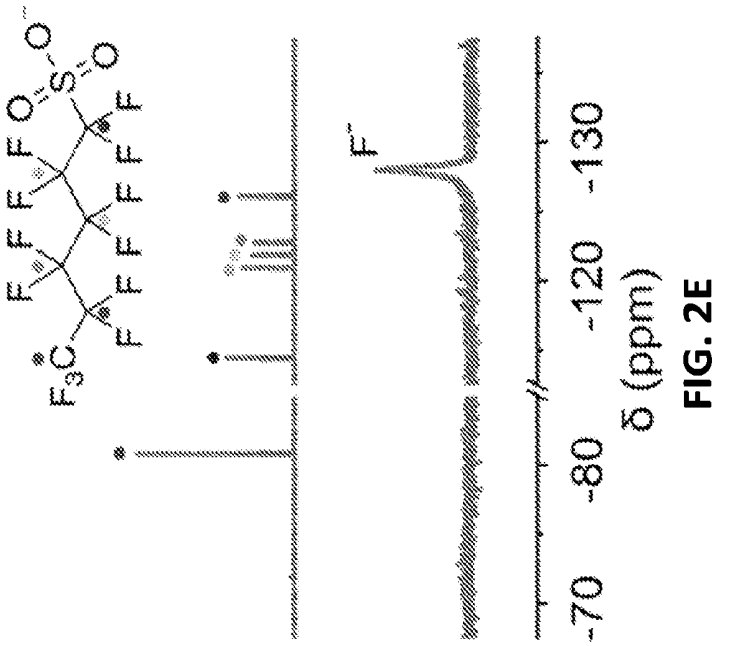
F3C
F
F
F
F
F
F
F
F
F
F
F
F
O
S
O
O
O
F
-70
-80
-120
-130
δ (ppm)

FIG. 2E

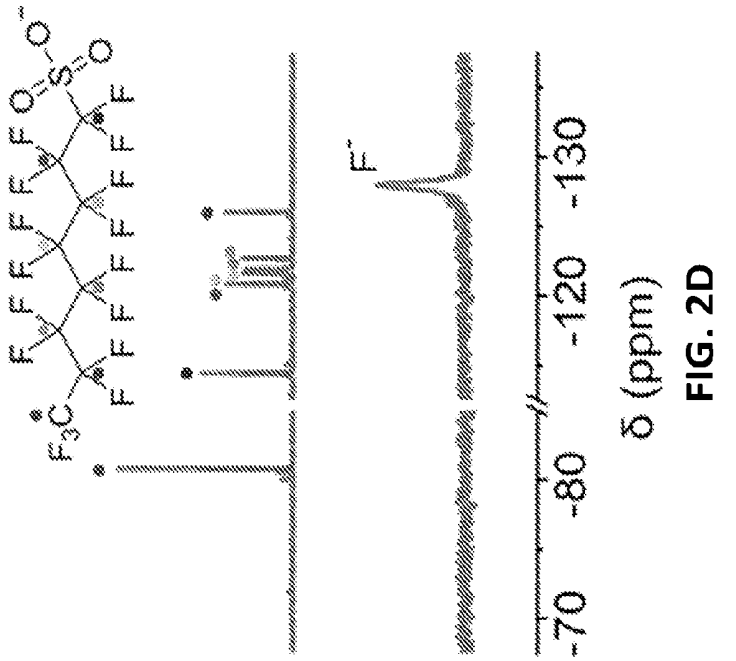
F3C
F
F
F
F
F
F
F
F
F
F
F
F
O
S
O
O
O
F
-70
-80
-120
-130
δ (ppm)

FIG. 2D

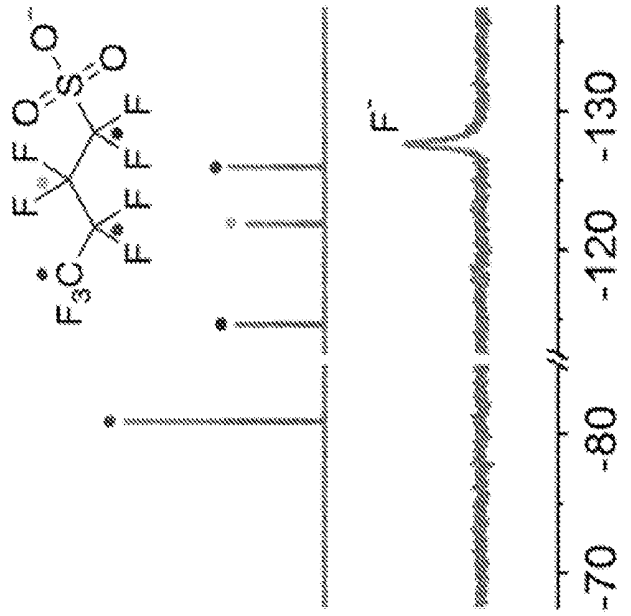

FIG. 2F

FIG. 2G

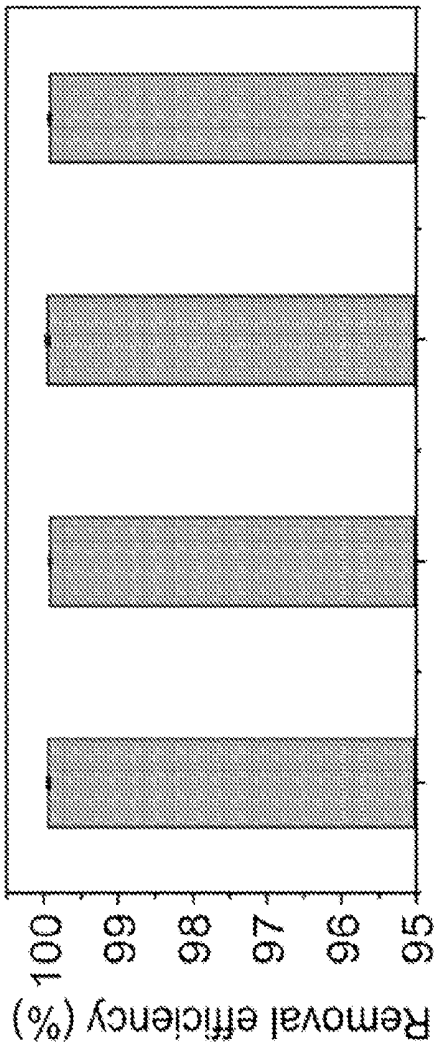
Removal efficiency (%)
100
99
98
97
96
95
PFOA
PFOS
PFH$_x$S
PFBS

FIG. 2H

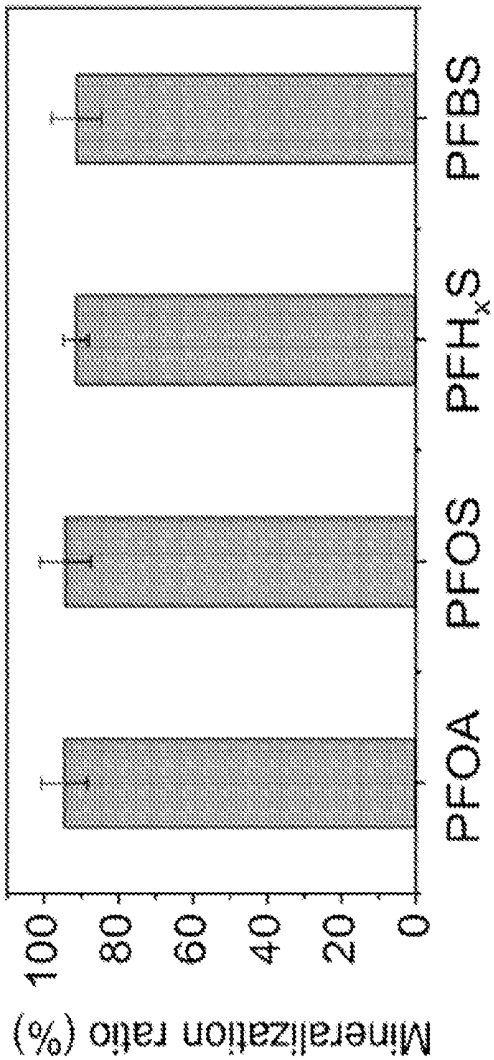
Mineralization ratio (%)
100
80
60
40
20
0
PFOA
PFOS
PFH$_x$S
PFBS

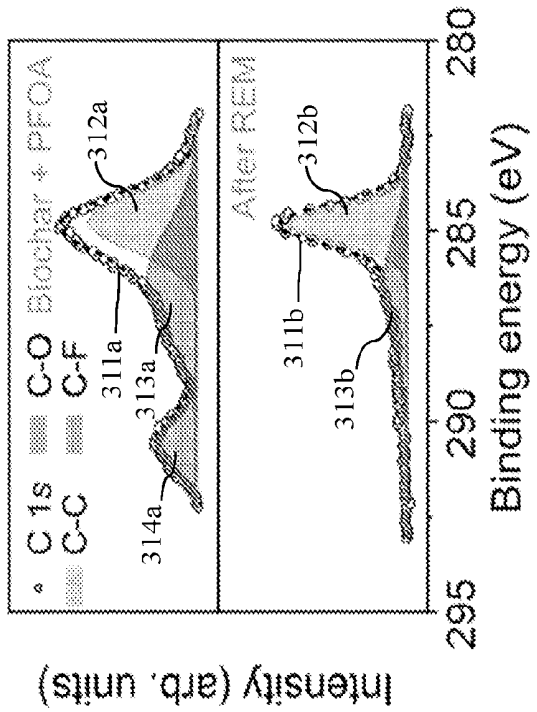
C 1s
C-C
C-O
C-F
Biochar + PFOA
After REM
311a
312a
313a
314a
311b
312b
313b
295
290
285
280
Binding energy (eV)
Intensity (arb. units)

FIG. 3B

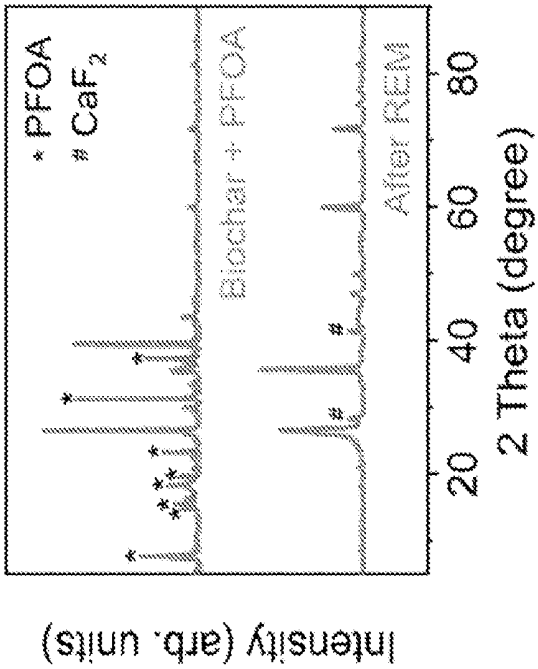
* PFOA
# CaF_2
Biochar + PFOA
After REM
20
40
60
80
2 Theta (degree)
Intensity (arb. units)

FIG. 3A

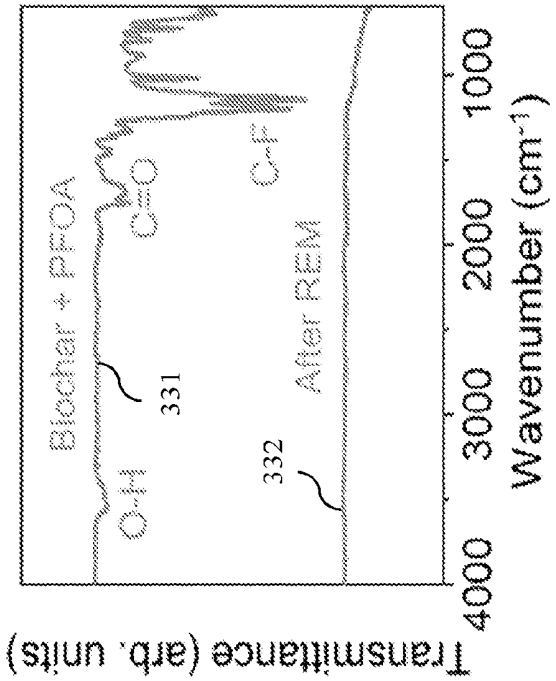
Transmittance (arb. units)
4000
3000
2000
1000
Wavenumber (cm-1)
Biochar + PFOA
O-H
331
C=O
C-F
332
After REM

FIG. 3D

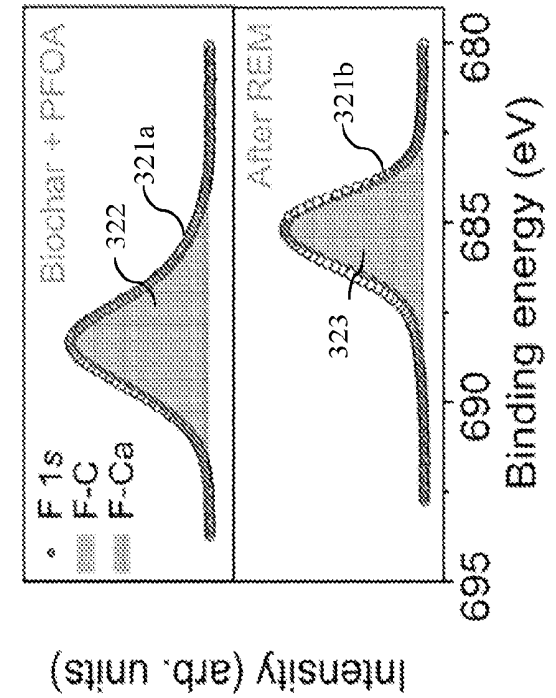
Intensity (arb. units)
695
690
685
680
Binding energy (eV)
F 1s
F-C
F-Ca
Biochar + PFOA
322
321a
After REM
321b
323

FIG. 3C

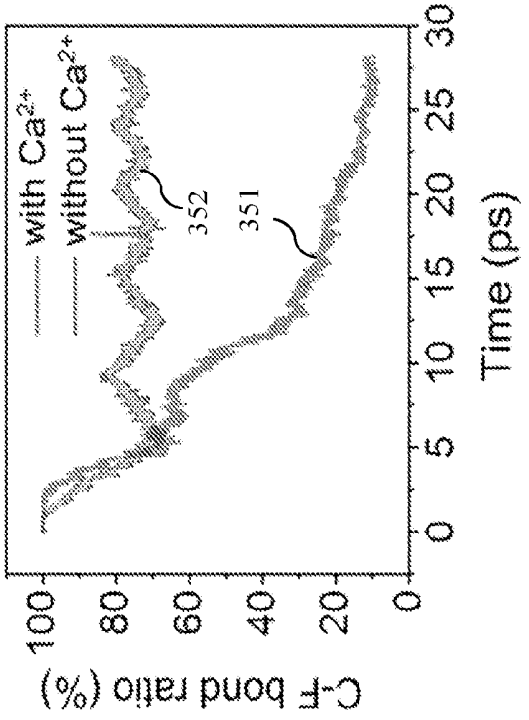
C-F bond ratio (%)
100
80
60
40
20
0
0
5
10
15
20
25
30
Time (ps)
with Ca2+
without Ca2+
352
351

FIG. 3F

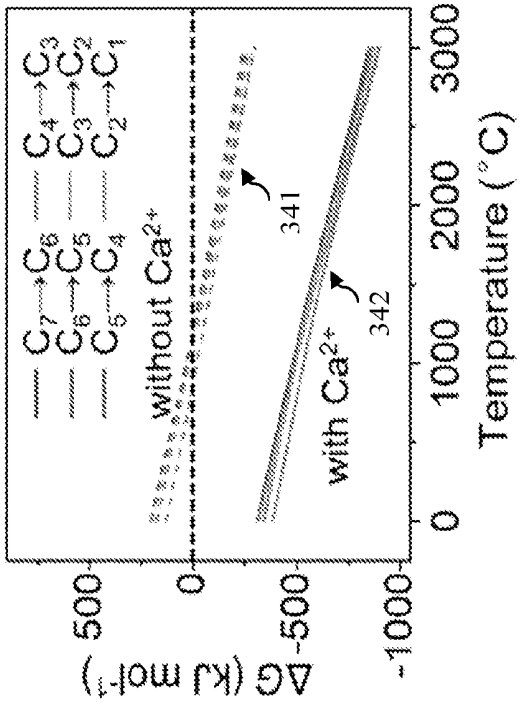
ΔG (kJ mol-1)
500
0
-500
-1000
0
1000
2000
3000
Temperature (°C)
C7→C6
C6→C5
C5→C4
C4→C3
C3→C2
C2→C1
without Ca2+
with Ca2+
341
342

FIG. 3E

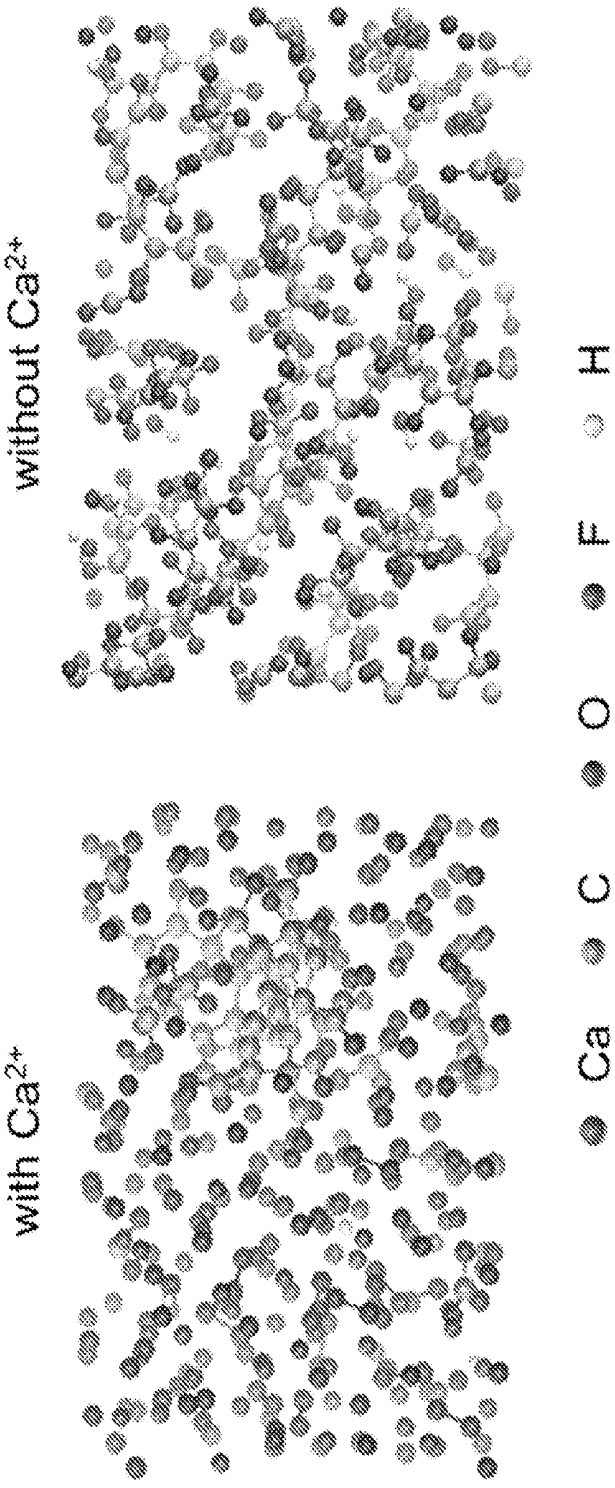

FIG. 3G

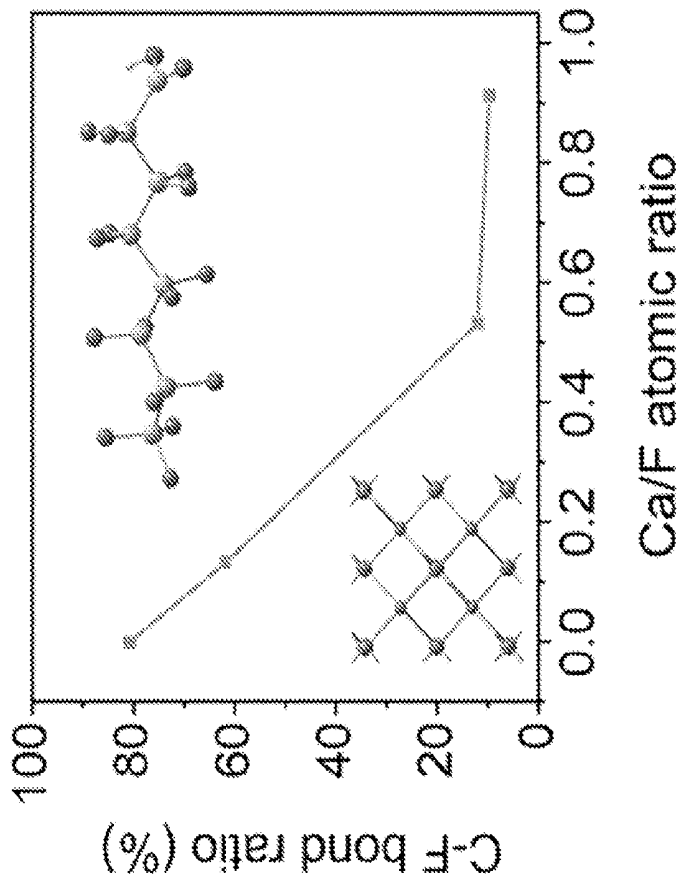

FIG. 3H

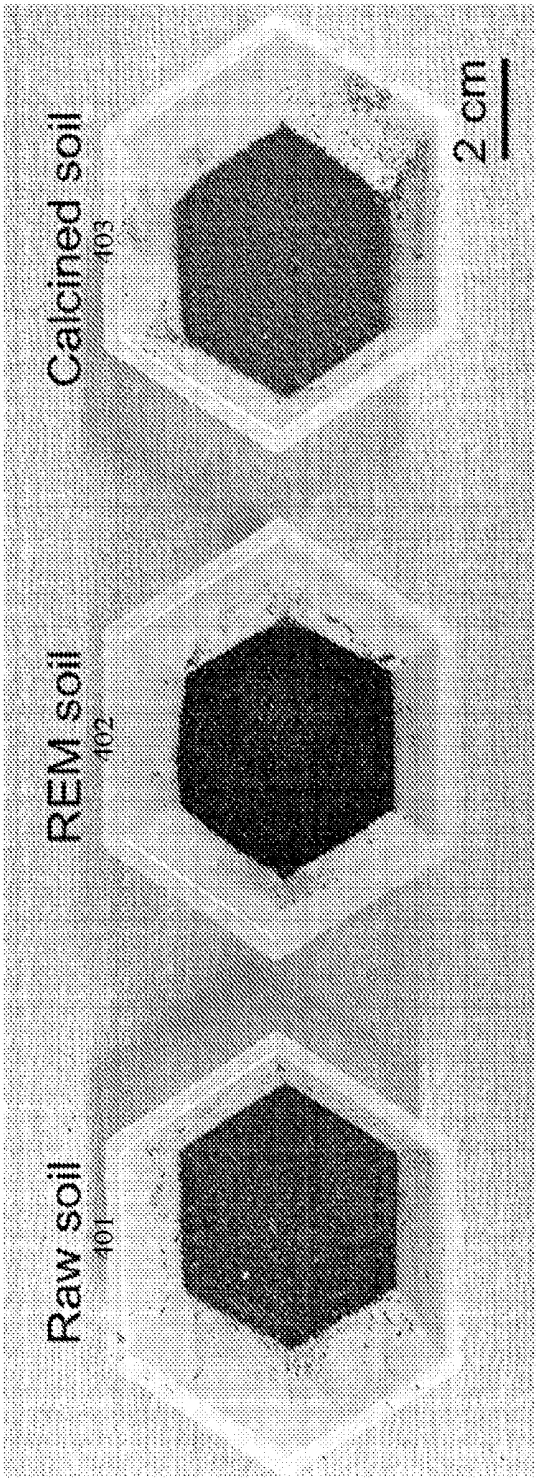

FIG. 4A

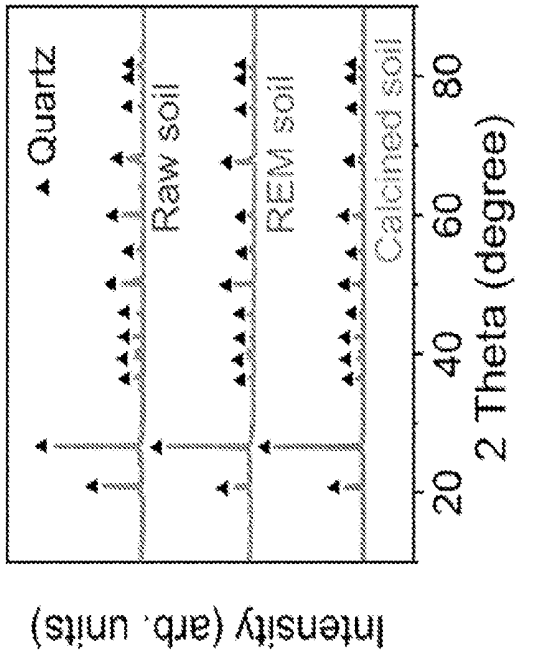
Quartz
Raw soil
REM soil
Calcined soil
20
40
60
80
2 Theta (degree)
Intensity (arb. units)

FIG. 4C

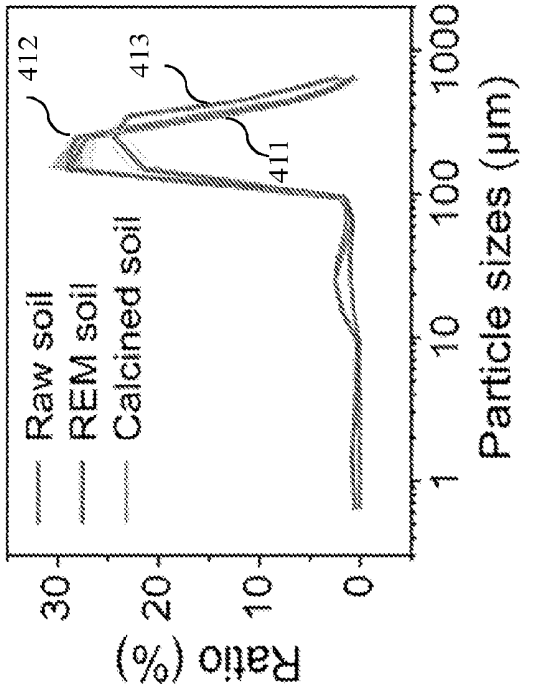
Raw soil
REM soil
Calcined soil
412
413
411
30
20
10
0
Ratio (%)
1
10
100
1000
Particle sizes (μm)

FIG. 4B

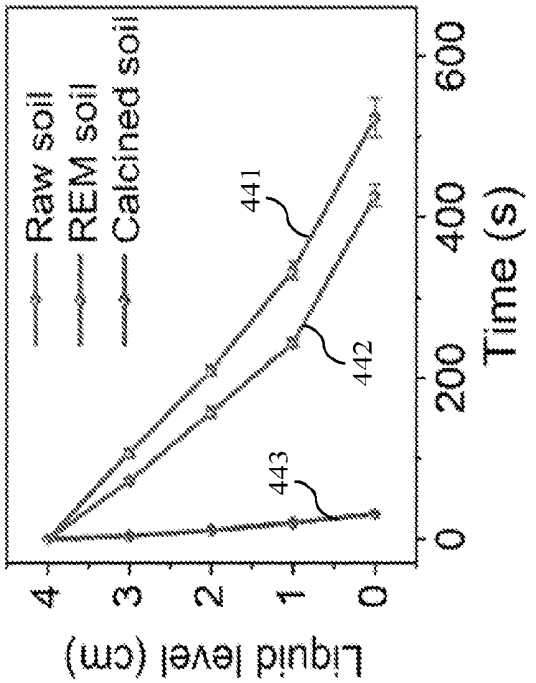
Raw soil
REM soil
Calcined soil
441
442
443
Liquid level (cm)
Time (s)
0
1
2
3
4
0
200
400
600

FIG. 4E

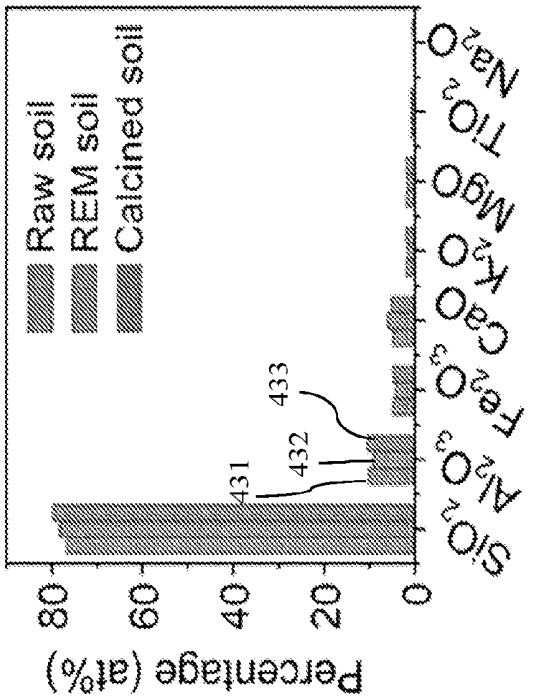
Raw soil
REM soil
Calcined soil
431
432
433
Percentage (at%)
0
20
40
60
80
SiO2
Al2O3
Fe2O3
CaO
K2O
MgO
TiO2
Na2O

FIG. 4D

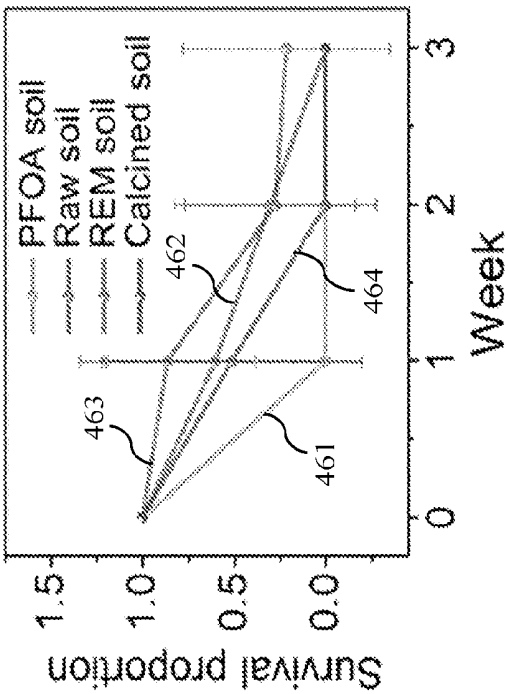
PFOA soil
Raw soil
REM soil
Calcined soil
462
464
463
461
Survival proportion
1.5
1.0
0.5
0.0
0
1
2
3
Week

FIG. 4G

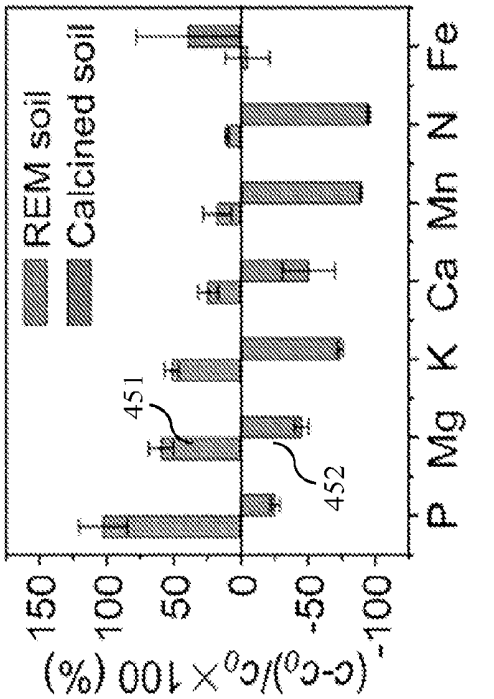
REM soil
Calcined soil
451
452
$(c-c_0)/c_0 \times 100$ (%)
150
100
50
0
-50
-100
P
Mg
K
Ca
Mn
N
Fe

FIG. 4F

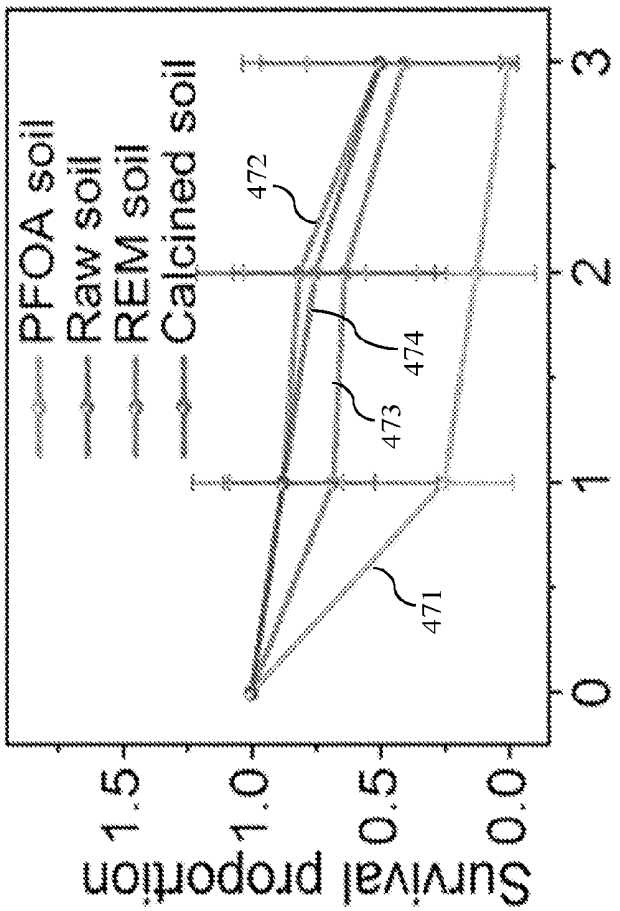
PFOA soil
Raw soil
REM soil
Calcined soil
472
473
474
471
Survival proportion
0.0
0.5
1.0
1.5
0
1
2
3
Week

FIG. 4H

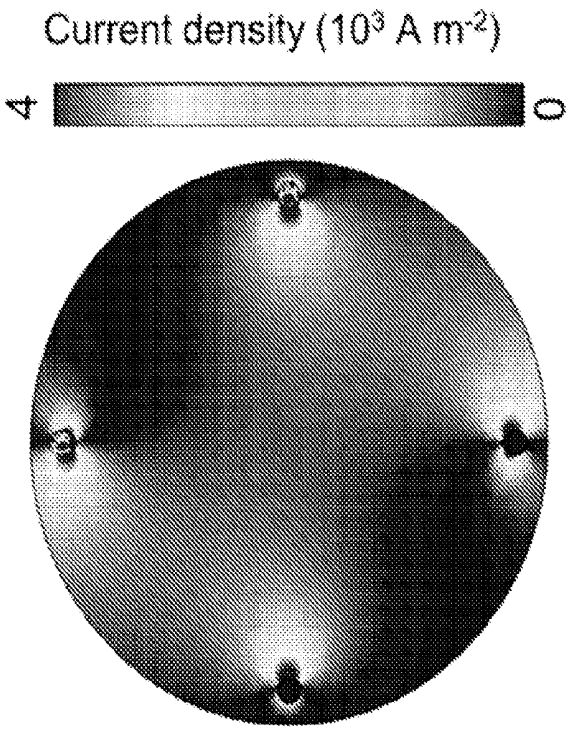
Current density (10^3 A m^{-2})
4
0

FIG. 5B

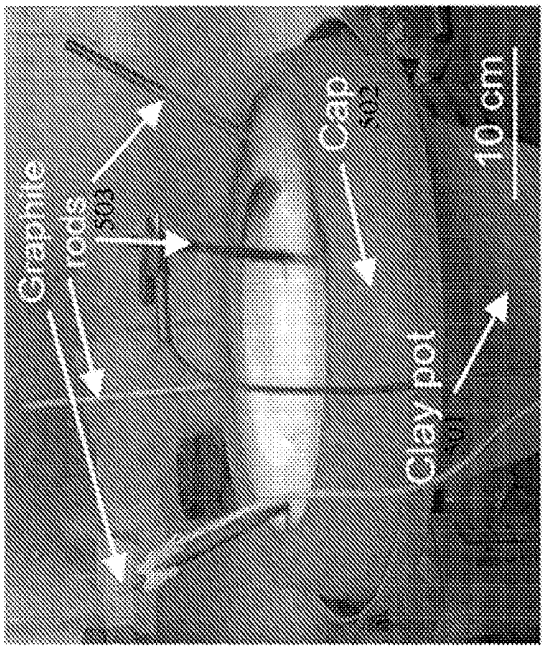
Crappie
roads
Cap
pot
Clay pot
10 cm

FIG. 5A

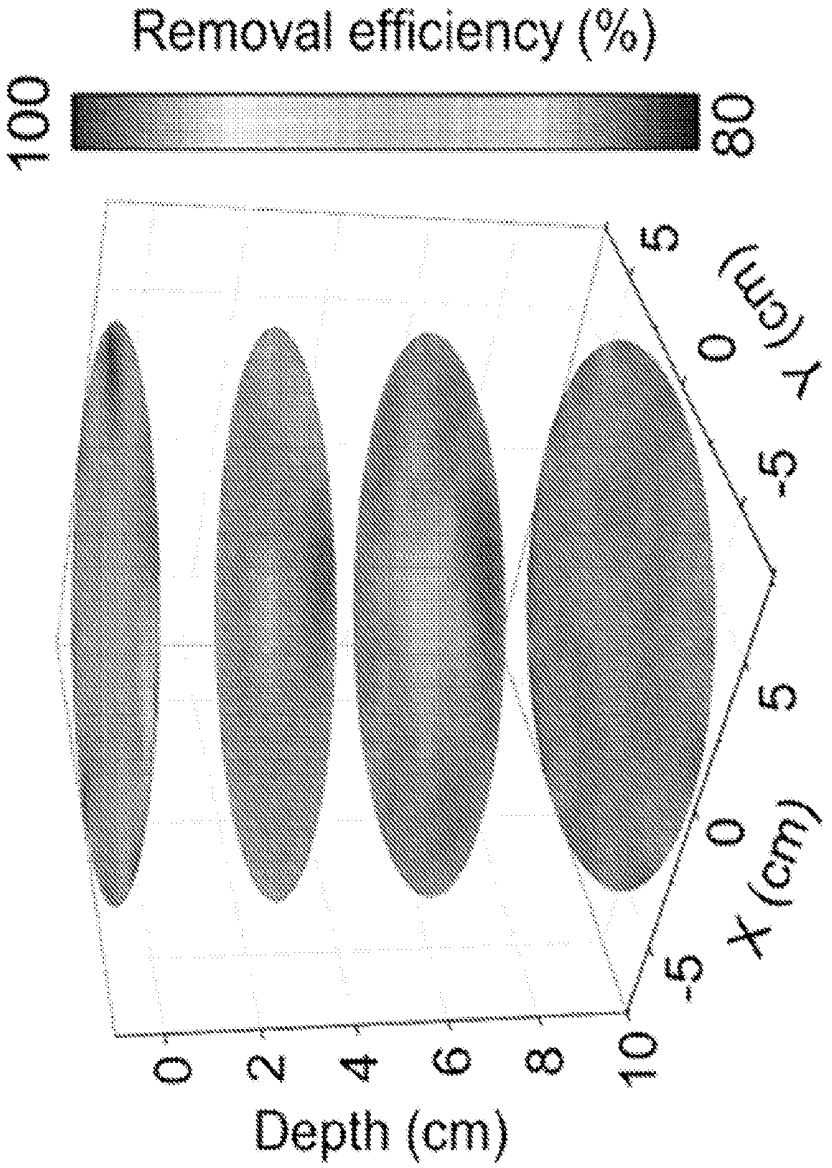

FIG. 5C

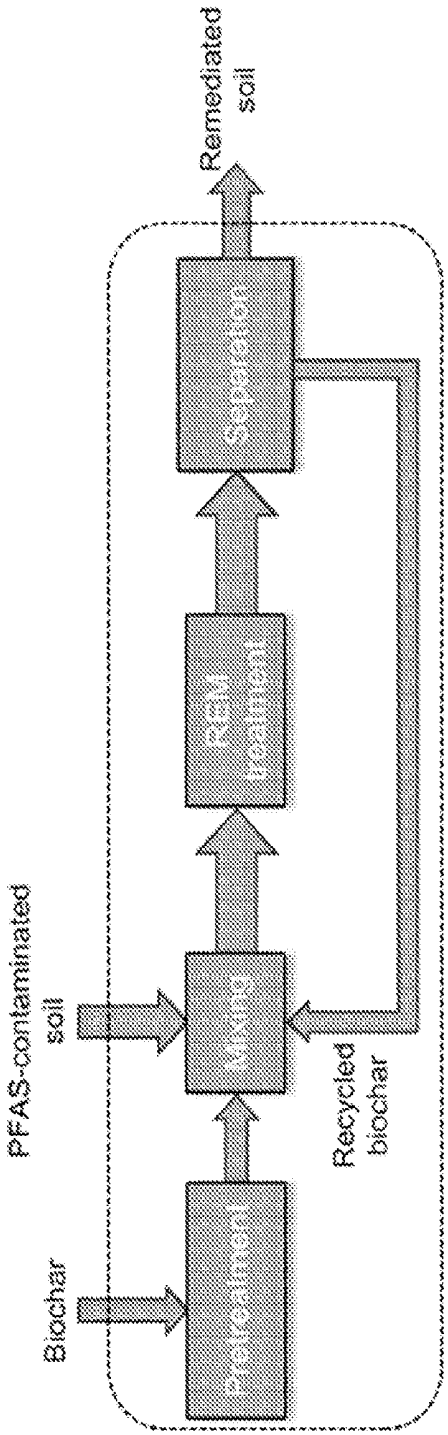
Remediated soil
Separation
REM treatment
Mixing
PFAS-contaminated soil
Recycled biochar
Pretreatment
Biochar

FIG. 5D

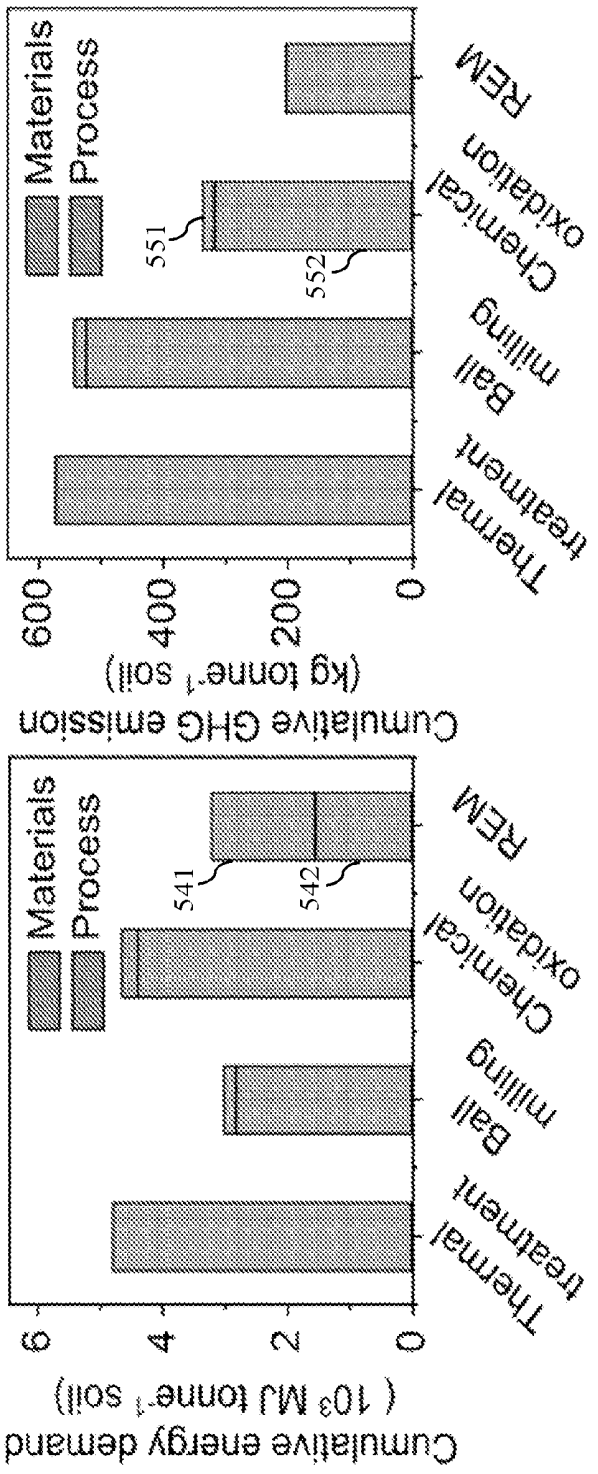
Cumulative energy demand
(10³ MJ tonne⁻¹ soil)
0
2
4
6
Thermal treatment
Ball milling
Chemical oxidation
REM
Materials
Process
541
542
Cumulative GHG emission
(kg tonne⁻¹ soil)
0
200
400
600
Thermal treatment
Ball milling
Chemical oxidation
REM
Materials
Process
551
552

FIG. 5E

FIG. 5F

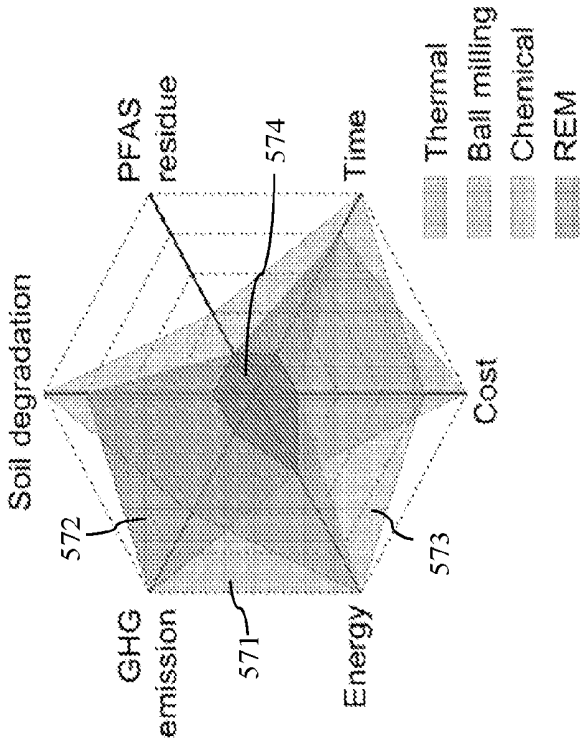
Thermal
Ball milling
Chemical
REM
PFAS residue
Time
Cost
Energy
GHG emission
Soil degradation
572
571
573
574

FIG. 5H

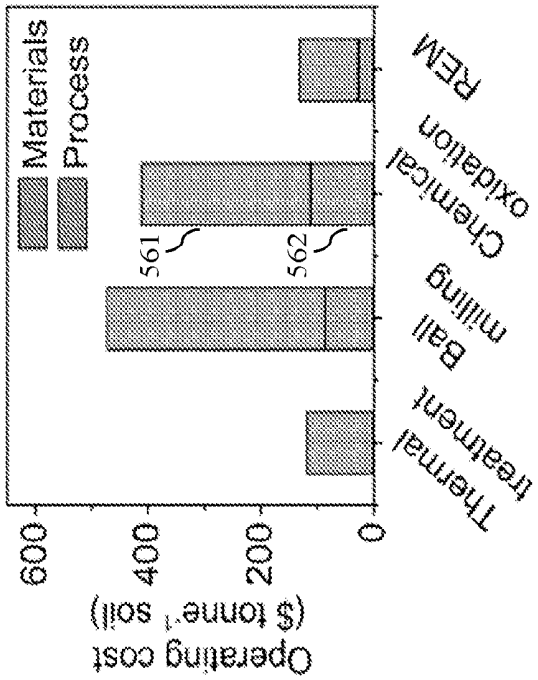
Operating cost ($ tonne⁻¹ soil)
0
200
400
600
Materials
Process
561
562
Thermal treatment
Ball milling
Chemical oxidation
REM

FIG. 5G

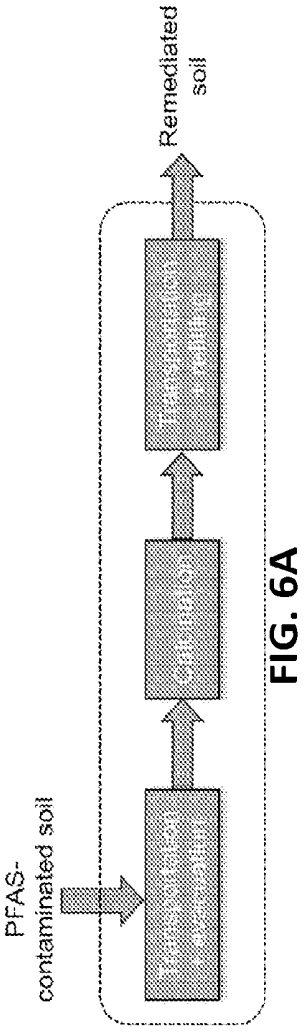

FIG. 6A

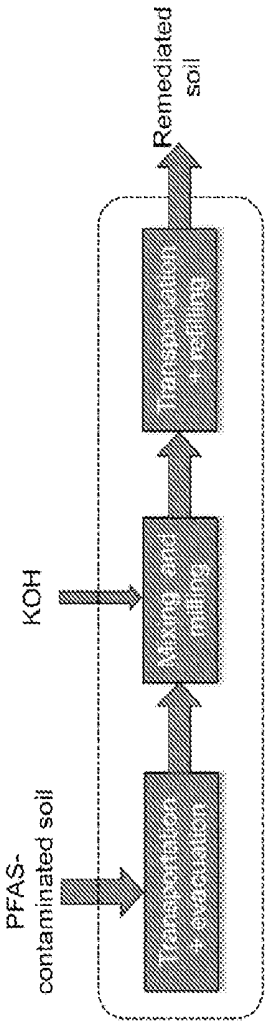

FIG. 6B

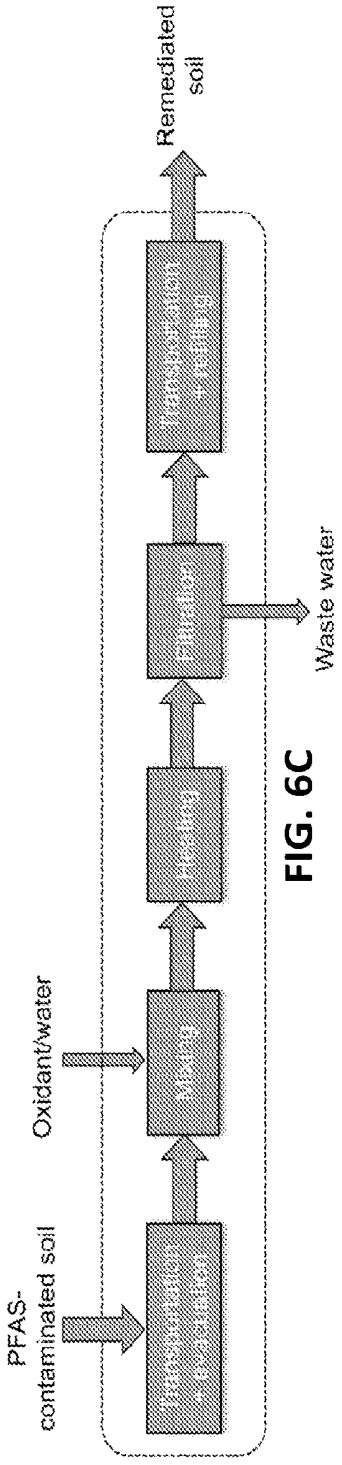

FIG. 6C

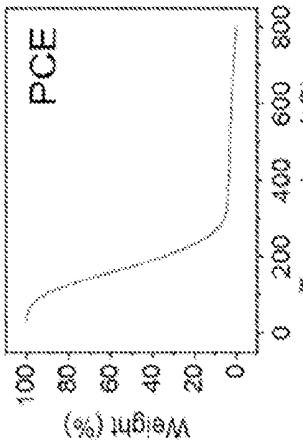

FIG. 7B

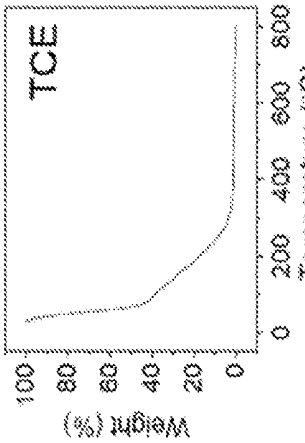

FIG. 7A

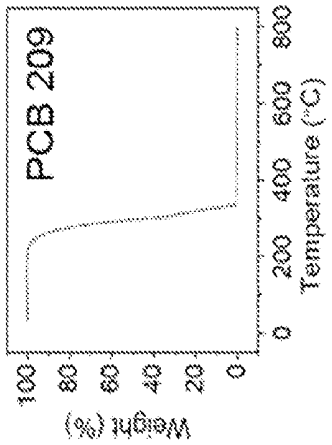

FIG. 7E

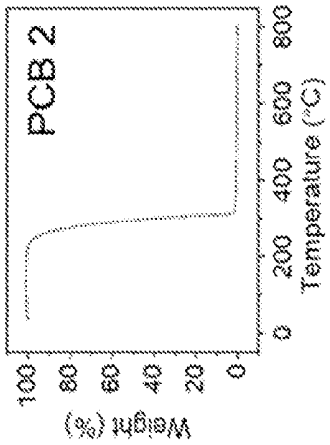

FIG. 7D

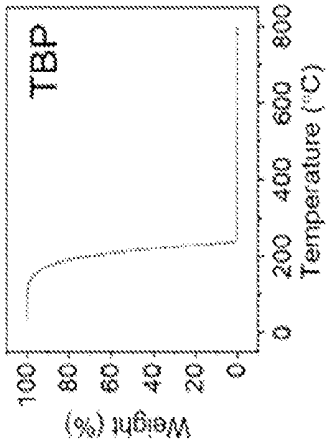

FIG. 7C

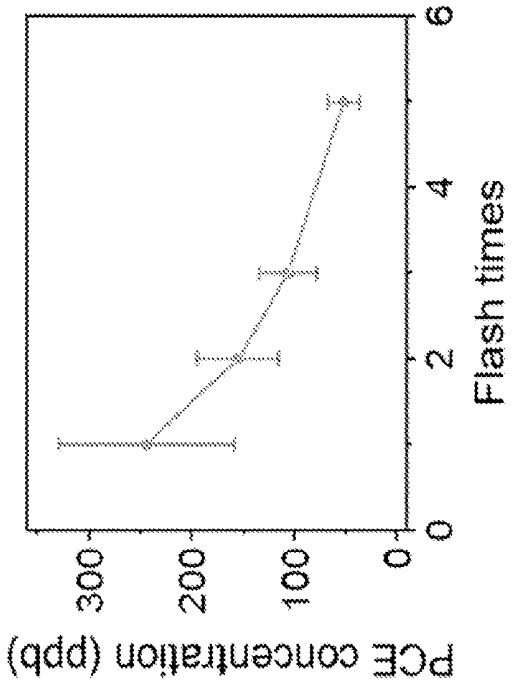
PCE concentration (ppb)
300
200
100
0
0
2
4
6
Flash times

FIG. 8B

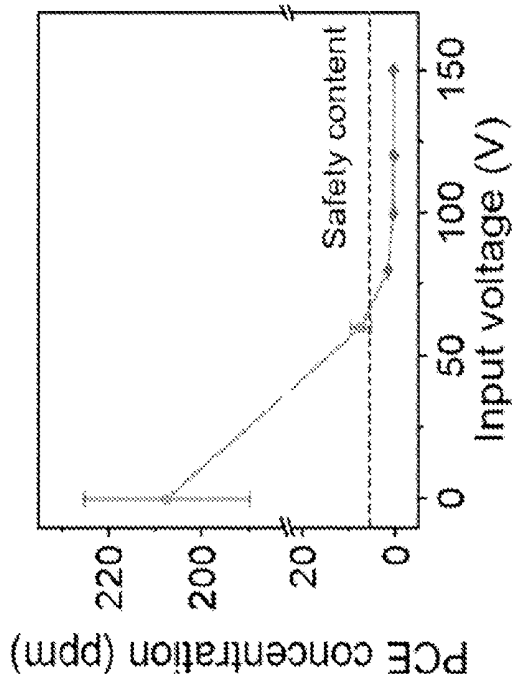
PCE concentration (ppm)
220
200
20
0
Safety content
0
50
100
150
Input voltage (V)

FIG. 8A

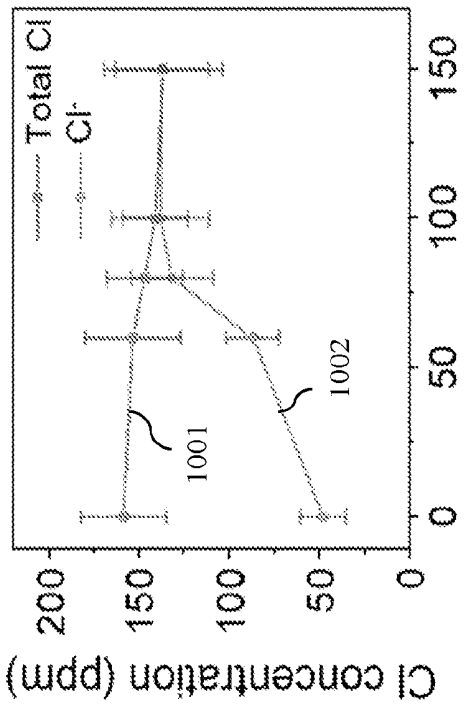
Total Cl
Cl-
1001
1002
Cl concentration (ppm)
Input voltage (V)
0
50
100
150
200

FIG. 10

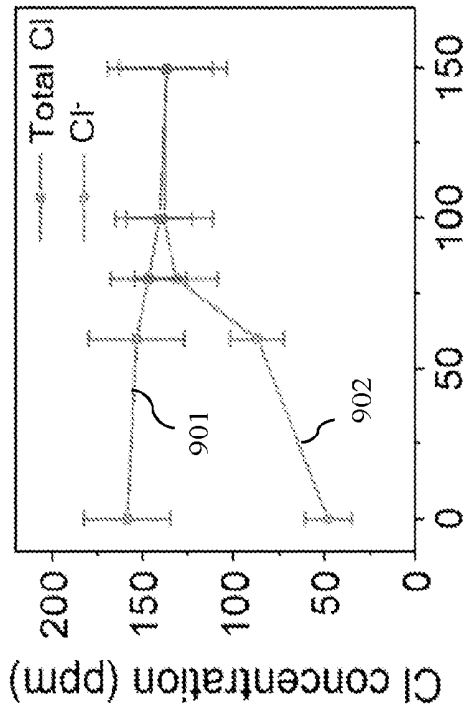
Total Cl
Cl-
901
902
Cl concentration (ppm)
Input voltage (V)
0
50
100
150
200

FIG. 9

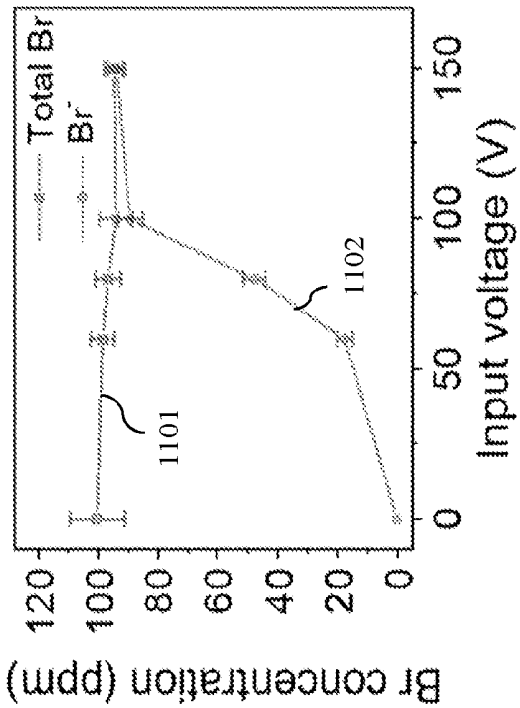
Total Br
Br
1101
1102
Br concentration (ppm)
0
20
40
60
80
100
120
0
50
100
150
Input voltage (V)

FIG. 11

INTERNATIONAL SEARCH REPORT

International application No
PCT/US2024/050478

A. CLASSIFICATION OF SUBJECT MATTER
INV. B09C1/06 B09C1/08
ADD.

According to International Patent Classification (IPC) or to both national classification and IPC

B. FIELDS SEARCHED

Minimum documentation searched (classification system followed by classification symbols)
B09C

Documentation searched other than minimum documentation to the extent that such documents are included in the fields searched

Electronic data base consulted during the international search (name of data base and, where practicable, search terms used)
EPO-Internal

C. DOCUMENTS CONSIDERED TO BE RELEVANT

Category*	Citation of document, with indication, where appropriate, of the relevant passages	Relevant to claim No.
X	WO 2022/169859 A1 (UNIV RICE WILLIAM M [US]) 11 August 2022 (2022-08-11)	1-10, 15-20
Y	paragraphs [0025], [0026], [0144];	14
A	claims	11-13

X	WO 2021/209504 A1 (PHOTON REMEDIATION TECH N V [NL]) 21 October 2021 (2021-10-21)	19
A	figure 3	11-13

	-/--	

[x] Further documents are listed in the continuation of Box C.

[x] See patent family annex.

* Special categories of cited documents :

"A" document defining the general state of the art which is not considered to be of particular relevance

"E" earlier application or patent but published on or after the international filing date

"L" document which may throw doubts on priority claim(s) or which is cited to establish the publication date of another citation or other special reason (as specified)

"O" document referring to an oral disclosure, use, exhibition or other means

"P" document published prior to the international filing date but later than the priority date claimed

"T" later document published after the international filing date or priority date and not in conflict with the application but cited to understand the principle or theory underlying the invention

"X" document of particular relevance;; the claimed invention cannot be considered novel or cannot be considered to involve an inventive step when the document is taken alone

"Y" document of particular relevance;; the claimed invention cannot be considered to involve an inventive step when the document is combined with one or more other such documents, such combination being obvious to a person skilled in the art

"&" document member of the same patent family

Date of the actual completion of the international search	Date of mailing of the international search report
20 February 2025	07/03/2025

Name and mailing address of the ISA/	Authorized officer
European Patent Office, P.B. 5818 Patentlaan 2 NL - 2280 HV Rijswijk Tel. (+31-70) 340-2040, Fax: (+31-70) 340-3016	Tassinari, Francesca

1

Form PCT/ISA/210 (second sheet) (April 2005)

C(Continuation). DOCUMENTS CONSIDERED TO BE RELEVANT

Category*	Citation of document, with indication, where appropriate, of the relevant passages	Relevant to claim No.
Y	VARGETTE LUCAS DS ET AL: "Prospects of complete mineralization of per- and polyfluoroalkyl substances by thermal destruction methods", CURRENT OPINION IN CHEMICAL ENGINEERING, [Online] vol. 42, 5 September 2023 (2023-09-05), pages 100954-1, XP093250931, Netherlands ISSN: 2211-3398, DOI: 10.1016/j.coche.2023.100954 [retrieved on 2025-02-20]	14
A	page 5	11-13

X,P	DENG BING ET AL: "High-temperature electrothermal remediation of multi-pollutants in soil", NATURE COMMUNICATIONS, 11 October 2023 (2023-10-11), pages 6371-1, XP093250930, UK ISSN: 2041-1723, DOI: 10.1038/s41467-023-41898-z Retrieved from the Internet: URL:https://www.nature.com/articles/s41467-023-41898-z.pdf [retrieved on 2025-02-20] the whole document	16-20

X,P	CHENG YI ET AL: "Electrothermal mineralization of per- and polyfluoroalkyl substances for soil remediation", NATURE COMMUNICATIONS, 20 July 2024 (2024-07-20), pages 6117-1, XP093250928, UK ISSN: 2041-1723, DOI: 10.1038/s41467-024-49809-6 Retrieved from the Internet: URL:https://www.nature.com/articles/s41467-024-49809-6.pdf [retrieved on 2025-02-20] the whole document	1-20

	-/--	

1

INTERNATIONAL SEARCH REPORT

International application No
PCT/US2024/050478

C(Continuation). DOCUMENTS CONSIDERED TO BE RELEVANT

Category*	Citation of document, with indication, where appropriate, of the relevant passages	Relevant to claim No.
X,P	Cheng Yi ET AL: "Electrothermal mineralization of per- and polyfluoroalkyl substances (PFAS) for soil remediation", ChemRxiv, 19 October 2023 (2023-10-19), pages 1-42, XP093250929, DOI: 10.26434/chemrxiv-2023-79t7l Retrieved from the Internet: URL:https://chemrxiv.org/engage/chemrxiv/article-details/652ee76c45aaa5fdbb376715 [retrieved on 2025-02-20] the whole document	1-20
X,P	Deng Bing ET AL: "New electrothermal process rapidly removes multiple pollutants in contaminated soils", Research Communities by Springer Nature, 11 October 2023 (2023-10-11), pages 1-2, XP093250933, Retrieved from the Internet: URL:https://communities.springernature.com/posts/new-electrothermal-process-rapidly-removes-multiple-pollutants-in-contaminated-soils [retrieved on 2025-02-20] the whole document	16-20

1

INTERNATIONAL SEARCH REPORT

Information on patent family members

International application No
PCT/US2024/050478

Patent document cited in search report	Publication date	Patent family member(s)	Publication date
WO 2022169859 A1	11-08-2022	CA 3209120 A1	11-08-2022
		EP 4288225 A1	13-12-2023
		WO 2022169859 A1	11-08-2022
WO 2021209504 A1	21-10-2021	AU 2021257607 A1	03-11-2022
		CA 3171702 A1	21-10-2021
		CN 115515730 A	23-12-2022
		EP 3895817 A1	20-10-2021
		EP 4135913 A1	22-02-2023
		JP 2023521462 A	24-05-2023
		KR 20230005207 A	09-01-2023
		US 2023381842 A1	30-11-2023
		WO 2021209504 A1	21-10-2021